

ISTANBUL TECHNICAL UNIVERSITY ★ ENERGY INSTITUTE

**APPLICATION OF MESHLESS RBF COLLOCATION METHODS TO
NEUTRON DIFFUSION AND TRANSPORT**



Ph.D. THESIS

Tayfun TANBAY

Energy Science and Technology Division

Energy Science and Technology Programme

JUNE 2016

ISTANBUL TECHNICAL UNIVERSITY ★ ENERGY INSTITUTE

**APPLICATION OF MESHLESS RBF COLLOCATION METHODS TO
NEUTRON DIFFUSION AND TRANSPORT**



Ph.D. THESIS

**Tayfun TANBAY
(301092012)**

Energy Science and Technology Division

Energy Science and Technology Programme

Thesis Advisor: Prof. Dr. Bilge ÖZGENER

JUNE 2016

İSTANBUL TEKNİK ÜNİVERSİTESİ ★ ENERJİ ENSTİTÜSÜ

**AĞSIZ RBF KOLLOKASYON YÖNTEMLERİNİN NÖTRON DİFÜZYON VE
TRANSPORTUNA UYGULANMASI**

DOKTORA TEZİ

**Tayfun TANBAY
(301092012)**

Enerji Bilim ve Teknoloji Anabilim Dalı

Enerji Bilim ve Teknoloji Programı

Tez Danışmanı: Prof. Dr. Bilge ÖZGENER

HAZİRAN 2016

Tayfun Tanbay, a Ph.D. student of ITU **Energy Institute** student ID 301092012, successfully defended the **dissertation** entitled “**APPLICATION OF MESHLESS RBF COLLOCATION METHODS TO NEUTRON DIFFUSION AND TRANSPORT**”, which he prepared after fulfilling the requirements specified in the associated legislations, before the jury whose signatures are below.

Thesis Advisor : **Prof. Dr. Bilge Özgener**
Istanbul Technical University

Jury Members : **Prof.Dr. Tayfun BÜKE**
Muğla Sıtkı Koçman University

Prof. Dr. Cemal YILDIZ
Istanbul Technical University

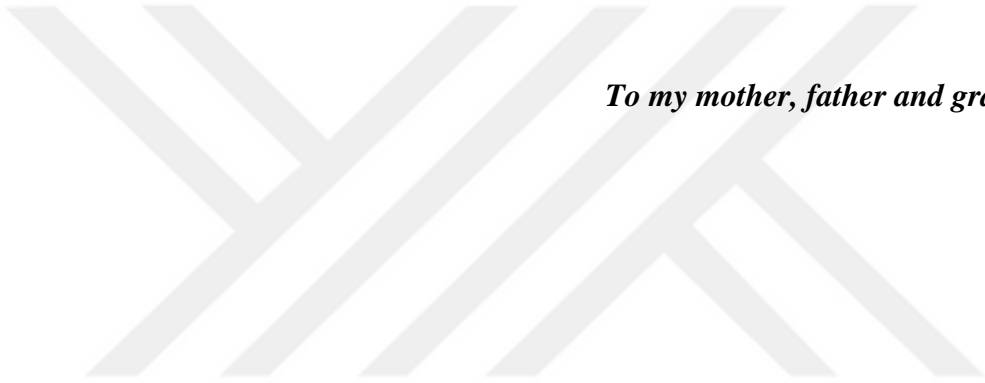
Prof. Dr. Üner ÇOLAK
Istanbul Technical University

Prof. Dr. Ayhan YILMAZER
Hacettepe University

Date of Submission : 19/04/2016

Date of Defense : 24/06/2016





To my mother, father and grandmother,



FOREWORD

I would like to express my special appreciation and thanks to my advisor professor Bilge Özgener. She has been a great mentor to me, and she has been helpful at all stages of my Ph.D. study. I would also like to thank my jury members professor Tayfun Büke and professor Cemal Yıldız for their comments and suggestions throughout this work. I am also thankful to professor Atila Özgener for his invaluable contributions since the beginning of my research.

Lastly, I especially thank my mother for her unconditional love and care. I would not have got this far without her unlimited support. She has always been there for me and I owe her everything I have achieved through all my life.

April 2016

Tayfun TANBAY
(Mechanical and chemical engineer)

TABLE OF CONTENTS

	<u>Page</u>
FOREWORD	ix
TABLE OF CONTENTS	xi
ABBREVIATIONS	xiii
SYMBOLS	xv
LIST OF TABLES	xvii
LIST OF FIGURES	xix
SUMMARY	xxiii
ÖZET	xxvii
1. INTRODUCTION	1
1.1 Purpose and Expected Outcomes of the Thesis.....	2
1.2 Literature Review	3
1.3 Outline of the Thesis	3
2. NEUTRON TRANSPORT	5
2.1 The Time-independent Neutron Transport Equation	5
2.2 The Diffusion Approximation	9
2.3 The Time-independent Multigroup Multiregion Neutron Diffusion Equation and Boundary Conditions.....	13
3. MESHLESS METHODS	15
3.1 Motivation for Meshless Methods.....	15
3.2 Weighted Residual Method, Strong and Weak Forms	16
3.3 Classification of Meshless Methods.....	18
3.4 Shape Functions	19
3.4.1 Point interpolation methods	21
3.4.2 Least squares methods	22
3.4.3 Hermite-type approximation	24
3.5 Collocation Methods	26
3.5.1 Local collocation.....	27
3.5.2 RBF collocation	30
3.5.3 Weighted RBF collocation method.....	35
4. HOMOGENEOUS NEUTRON DIFFUSION PROBLEMS	41
4.1 Numerical Formulation	41
4.2 Results and Discussion.....	46
4.2.1 External source problem	46
4.2.2 Multigroup fission source problems	58
4.3 Improving the Performance of the RBF Collocation Method.....	69
4.3.1 Increasing the precision	69
4.3.2 Exponent of the generalized multiquadric	71
4.3.3 Node number dependent shape parameter strategy.....	72
4.3.4 Singular value decomposition filtering	73
5. MODELLING OF MULTIREGION NEUTRON DIFFUSION	77

5.1 Numerical Formulation for the Weighted RBF Collocation Method.....	77
5.2 Numerical Results	89
5.2.1 One-dimensional external source problem.....	89
5.2.2 Two-dimensional problem without corner singularity	92
5.2.3 Two-dimensional problem with corner singularity	93
5.2.4 Two-dimensional problem with corner singularity and high material heterogeneity	97
5.2.5 The IAEA two-dimensional benchmark problem	98
6. NUMERICAL SOLUTION OF NEUTRON TRANSPORT PROBLEMS..	101
6.1 The One-dimensional Neutron Transport Equation and Angular Approximations	101
6.2 Even Parity Form of the Neutron Transport Equation	104
6.3 Numerical Formulations	114
6.3.1 P_3 equations.....	114
6.3.2 Even parity P_3 equations	117
6.4 Results	120
6.4.1 External source problem.....	120
6.4.2 Fission source problems	123
7. CONCLUSIONS.....	129
REFERENCES	135
CURRICULUM VITAE	143

ABBREVIATIONS

BC	: Boundary condition
BEM	: Boundary element method
CPU	: Central processing unit
DEM	: Diffuse element method
EFG	: Element-free Galerkin
FEM	: Finite element method
FPM	: Finite point method
GA	: Gaussian
GMQ	: Generalized multiquadric
IAEA	: International Atomic Energy Agency
IMQ	: Inverse multiquadric
LBE	: Linear boundary element
MLPG	: Meshless local Petrov-Galerkin
MLS	: Moving least squares
MQ	: Multiquadric
PDE	: Partial differential equation
PIM	: Point interpolation method
RBF	: Radial basis function
RMS	: Root mean square
RPIM	: Radial point interpolation method
SPH	: Smoothed particle hydrodynamics
SVD	: Singular value decomposition
WLS	: Weighted least squares



SYMBOLS

A	: Area
c	: Shape parameter
C	: Continuity
D	: Diffusion coefficient
E	: Neutron energy
F	: Fission source operator
h	: Distance between adjacent nodes
j	: Angular neutron current
J	: Neutron current
L	: Diffusion length
N	: Number of field nodes
p	: Monomial
P	: Power
r	: Spatial coordinates of neutron
s	: Neutron source
t	: Time
V	: Volume
W	: Weight function
x	: Cartesian coordinate
y	: Cartesian coordinate

Greek letters

α	: Albedo
β	: Fraction of delayed neutrons
Γ	: Boundary
δ	: Dirac's delta function
ϵ	: Error
λ	: Multiplication factor
μ	: Directional cosine
Σ	: Cross section
ν	: Number of neutrons emitted per fission
φ	: Angular neutron flux
Φ	: Shape function
ϕ	: Neutron flux
χ	: Fission spectrum
ψ	: Radial basis function
Ω	: Neutron direction

Subscripts:

a	: Absorption
b	: Boundary
col	: Collocation
crit	: Critical
Dir	: Dirichlet
ex	: External
f	: Fission
g	: Group
int	: Interpolation
iter	: Iteration
max	: Maximum
p	: Prompt
r	: Removal
R	: Reflective
rms	: Root mean square
s	: Scattering
sv	: Singular value
t	: Total
tr	: Transport
V	: Vacuum

LIST OF TABLES

	<u>Page</u>
Table 4.1 : Values of m and n in $\epsilon_{RMS} \sim O(m \exp(-n/h))$ for the constant source problem.	52
Table 4.2 : The values of the constants for the exponential fit $\epsilon_{RMS} \sim O(m \exp(-n/h))$, and algebraic fit $\epsilon_{RMS} \sim O(ph^{-r})$	54
Table 4.3 : RMS and maximum pointwise errors of RBF collocation, FEM and BEM together with optimum c^2 values for MQ, IMQ and GA for s_1 ...	55
Table 4.4 : RMS and maximum pointwise errors of RBF collocation, FEM and BEM together with optimum c^2 values for MQ, IMQ and GA for s_2 ...	55
Table 4.5 : RMS and maximum pointwise errors of RBF collocation, FEM and BEM together with optimum c^2 values for MQ, IMQ and GA for s_3 ...	56
Table 4.6 : Two-group nuclear data.	60
Table 4.7 : ϵ_{max} and ϵ_λ for the two-group problem.....	60
Table 4.8 : Three-group nuclear data..	62
Table 4.9 : ϵ_{max} and ϵ_λ for the three-group problem.....	62
Table 4.10 : Group constants for the 4-group problem.	63
Table 4.11 : Maximum and minimum ϵ_λ for MQ and IMQ.	65
Table 5.1 : Two-group parameters for the 2-D problem without corner singularity	92
Table 5.2 : The percent error in λ for weighted RBF collocation calculations.	93
Table 5.3 : The percent error in λ for RBF collocation calculations.....	93
Table 5.4 : Two-group parameters for the 2-D problem with corner singularity....	94
Table 5.5 : The one-group parameters for the IAEA two-dimensional benchmark problem.	98
Table 5.6 : Numerical λ values for the IAEA benchmark problem obtained with RBF collocation method for three values of the shape parameter.	99
Table 6.1 : S_N solutions of the Pu-239 benchmark problem with diamond difference approximation for the spatial variable.	126
Table 6.2 : S_N solutions of the Pu-239 benchmark problem with discontinuous linear finite element approximation for the spatial variable.	126
Table 6.3 : S_N solutions of the Pu-239 benchmark problem with discontinuous quadratic finite element approximation for the spatial variable.	127



LIST OF FIGURES

	<u>Page</u>
Figure 3.1 : Circular support domains of size r_s	20
Figure 3.2 : 1-D domain of problem Eqs. (3.49)-(3.51).....	28
Figure 3.3a : GMQ radial basis function with $q = 1/2$	32
Figure 3.3b : GA radial basis function.	32
Figure 3.4 : Effect of shape parameter on GMQ with $q = 1/2$	33
Figure 3.5 : A two-region problem.....	37
Figure 4.1 : A node distribution with $N_I = 4, N_B = 12$	43
Figure 4.2a : Graphical representation of the trigonometric source.....	47
Figure 4.2b : Graphical representation of the linear source.	47
Figure 4.3a : Variation of the RMS error with c in the case of s_3 for MQ.....	49
Figure 4.3b : Variation of the RMS error with c in the case of s_3 for IMQ.....	49
Figure 4.3c : Variation of the RMS error with c in the case of s_3 for GA.....	49
Figure 4.4a : Variation of the RMS error with shape parameter for s_1	50
Figure 4.4b : Variation of the RMS error with shape parameter for s_2	50
Figure 4.5a : Variation of the RMS error with fill distance for MQ in case of s_1 ..	51
Figure 4.5b : Variation of the RMS error with fill distance for IMQ in case of s_1 ..	51
Figure 4.5c : Variation of the RMS error with fill distance for GA in case of s_1 ..	51
Figure 4.6a : Comparison of the performance of MQ and IMQ collocation with FEM and BEM for s_1	53
Figure 4.6b : Comparison of the performance of MQ and IMQ collocation with FEM and BEM for s_2	53
Figure 4.6c : Comparison of the performance of MQ and IMQ collocation with FEM and BEM for s_3	53
Figure 4.7 : CPU times of the MQ collocation, FEM and BEM.	57
Figure 4.8a : Distribution of pointwise errors in the case of s_2 when $N = 40$ for MQ.	57
Figure 4.8b : Distribution of pointwise errors in the case of s_2 when $N = 40$ for IMQ.	58
Figure 4.8c : Distribution of pointwise errors in the case of s_2 when $N = 40$ for GA.	58
Figure 4.9a : Variation of ϵ_{max} with respect to N	59
Figure 4.9b : Variation of ϵ_λ with respect to N	59
Figure 4.10a : Variation of $\epsilon_{max,1}$ with respect to the shape parameter.	61
Figure 4.10b : Variation of $\epsilon_{max,2}$ with respect to the shape parameter.	61
Figure 4.11 : Variation of ϵ_λ with respect to the shape parameter.	61
Figure 4.12a : Variation of ϵ_λ with shape parameter for MQ when $N = 40$	64
Figure 4.12b : Variation of ϵ_λ with shape parameter for IMQ when $N = 40$	64
Figure 4.12c : Variation of ϵ_λ with shape parameter for GA when $N = 40$	65
Figure 4.13a : Variation of ϵ_λ with shape parameter for subcritical case when MQ is the RBF and $N = 50$	66

Figure 4.13b : Variation of ϵ_λ with shape parameter for supercritical case when MQ is the RBF and $N = 50$.	66
Figure 4.14a : Comparison of MQ, IMQ and GA for ϵ_λ .	67
Figure 4.14b : Comparison of MQ, IMQ and GA for $\epsilon_{max,3}$.	67
Figure 4.15a : Comparison of MQ collocation, FEM and BEM for ϵ_λ .	68
Figure 4.15b : Comparison of MQ collocation, FEM and BEM for $\epsilon_{max,2}$.	68
Figure 4.16 : CPU times of the MQ collocation, FEM and BEM.	69
Figure 4.17 : Comparison of double and 100 precision calculations in the RBF collocation method.	70
Figure 4.18 : Effect of the exponent on generalized multiquadric centered at the origin.	71
Figure 4.19 : RMS error with respect to N for the constant source problem.	72
Figure 4.20 : Results of node number dependent shape parameter strategy.	73
Figure 4.21 : RMS error of constant source problem with respect to c and n_{sv} .	75
Figure 5.1 : A typical two-region problem.	78
Figure 5.2a : A typical uniform node distribution for the 2-region problem with 49 domain nodes and 24 exterior nodes.	87
Figure 5.2b : Uniformly distributed interpolation and collocation nodes where $h_{int} = 2h_{col}$.	87
Figure 5.3 : A typical distribution of interpolation nodes for the 1-D problem.	89
Figure 5.4 : Analytical flux distribution for the one-dimensional problem.	90
Figure 5.5a : ϵ_{max} for machine precision and 100-precision calculations.	91
Figure 5.5b : ϵ_{rms} for machine precision and 100-precision calculations.	91
Figure 5.6 : ϵ_{rms} for the 1-D problem when $h_{int} = h_{col}$ and $h_{int} = 4h_{col}$.	91
Figure 5.7 : The geometry and boundary conditions of the 2-D problem without corner singularity.	92
Figure 5.8 : The geometry and boundary conditions of the 2-D problem with corner singularity.	94
Figure 5.9a : Variation of ϵ_λ with respect to N for the weighted RBF collocation.	95
Figure 5.9b : Variation of ϵ_λ with respect to N for the RBF collocation.	96
Figure 5.10 : The effect of the shape parameter on the performance of the RBF collocation method.	96
Figure 5.11 : Variation of ϵ_λ with respect to N for weighted and standard collocation methods.	97
Figure 5.12 : The geometry of the IAEA two-dimensional benchmark problem.	98
Figure 6.1 : Discretization of the 1-D domain with $M = 6$.	115
Figure 6.2 : Effect of the shape parameter on the RMS error for the external source problem.	120
Figure 6.3 : Effect of the number of collocation nodes on the RMS error for the external source problem.	121
Figure 6.4 : RMS errors for the external source problem when a variable shape parameter is utilized.	122
Figure 6.5 : RMS error behavior of the external source problem when the fourth order equation is directly approximated with RBFs.	122
Figure 6.6a : Error in the multiplication factor for the fission source problem for three values of the shape parameter.	123
Figure 6.6b : RMS error in the neutron flux for the fission source problem for three values of the shape parameter.	124
Figure 6.7 : Percent error in λ for the plutonium benchmark problem with isotropic scattering when $a_{crit} = 1.927538$.	125

Figure 6.8a	: The value of λ for the plutonium benchmark problem when $a_{crit} = 1.853722$ and even-parity form is considered.....	125
Figure 6.8b	: The value of λ for the plutonium benchmark problem when $a_{crit} = 1.853722$ and conventional form is considered.	126
Figure 6.9a	: The value of λ for the plutonium benchmark problem with anisotropic P_1 scattering.	128
Figure 6.9b	: The value of λ for the plutonium benchmark problem with anisotropic P_2 scattering.	128





APPLICATION OF MESHLESS RBF COLLOCATION METHODS TO NEUTRON DIFFUSION AND TRANSPORT

SUMMARY

In the last decades, meshless methods have become an alternative tool to conventional schemes, such as the finite difference method, the finite element method and the boundary element method, for modelling physical phenomena in many fields of science and engineering. With these novel techniques various types of problems governed by partial differential, integral and integrodifferential equations are solved numerically without the necessity of creating a predefined mesh.

There are several kinds of meshless methods based on different numerical formulations. Among these, the radial basis function (RBF) collocation method has some important characteristics together with its meshless nature, which makes it an ideal numerical approximation scheme for the solution of differential equations. First of all, this collocation scheme is a strong-form method, which means there is no need for numerical integration and hence a background mesh in the numerical formulation. When it is compared to the weak-form methods, the RBF collocation method is defined to be a truly meshless method. The second significant property of RBF collocation is the exponential convergence rate of the method. It is possible to obtain highly accurate solutions even when the number of nodes to represent the problem domain is low. The last feature of this collocation method worthy of attention is its ease of implementation in computer programs. The coding step of the RBF collocation method is easier than those of other meshless and conventional mesh-based methods.

The RBF collocation solution of a differential equation is actually a generalized interpolation problem. The dependent variable of the governing equations and boundary conditions, in this case the neutron flux, are interpolated by a finite series of radial basis functions. After this approximation step, the resultant equations are satisfied at the interpolation nodes, which can be uniformly or randomly distributed throughout the domain. Although numerous radial basis functions exist in the literature the generalized multiquadric, which was first proposed for surface fitting, has dominated this class of functions in both function approximation and numerical solution of differential or integral equations.

Even though the RBF collocation method has been applied to a wide range of problems, its use in heterogenous configurations is limited. Recently, a weighted version of this method is proposed to tackle multidomain problems of solid mechanics. In this method, the weights, which depend on the number of interpolation nodes and physical parameters of the media, are determined by balancing the approximation error due to the interpolation with RBFs of domains with those of the boundaries and interfaces.

Neutron diffusion and neutron transport equations are being studied for a long time to model the behavior of neutrons in a multiplying or nonmultiplying system. Although analytical solutions are given in many situations, real life examples of

nuclear technology necessitate the use of advanced numerical approximation techniques to obtain a reliable and detailed analysis of the problem in question. It is impossible to get an analytical expression for a complex multi-component nuclear system even with the simpler diffusion approximation. These equations have been solved with the finite difference, finite element and boundary element methods, and the studies in this area have gained momentum lately with the recent advances in the computational capabilities.

The purpose of this study is to solve the time-independent neutron diffusion and transport equations numerically by the RBF collocation method and therefore introduce this promising meshless method into the field of nuclear reactor physics. In this context, the two-dimensional multigroup neutron diffusion equation is approximated with RBFs in both homogeneous and heterogeneous media, while the one-speed neutron transport equation is considered in a one-dimensional configuration. The performance of the meshless collocation technique is assessed by performing numerical experiments for various cases. The accuracy, stability and convergence rate of the method are investigated through these calculations.

In case of homogeneous media, five diffusion problems are solved with the RBF collocation method. One of these is an external source example while the rest are multigroup fission source problems. The external source and four-group fission source cases are studied in detail, and the performance of the RBF collocation method is compared with the finite element and boundary element methods employing linear shape functions. Multiquadric, inverse multiquadric and Gaussian are used as the radial basis functions. The root mean square error and relative percent error in the multiplication factor have shown that the multiquadric and inverse multiquadric functions are better than the Gaussian in terms of both accuracy and stability. It was found that by carefully selecting the value of the shape parameter highly accurate solutions can be obtained with the collocation method even with a few number of interpolation nodes. Also increasing the value of the shape parameter has improved the convergence rate of the method. When the results of multiquadric collocation are compared with those of linear finite element and boundary elements it is seen that the exponentially convergent RBF collocation is superior in accurate determination of the multiplication factor while boundary element method has produced the best flux values. On the other hand the finite element method has a much better computation time than the collocation scheme.

For multidomain neutron diffusion, both the conventional and weighted forms of the RBF collocation method are used for the numerical solution. Five problems are considered. First a one-dimensional two-region external source problem is solved with RBF collocation, and it was found that extraordinary accuracies are achievable with the arbitrary precision computation feature of MATHEMATICA. Then a two-dimensional two-region problem, for which an analytical solution is available, is dealt with, and the results have revealed that both versions of the RBF collocation method are capable of yielding good accuracies. The next two problems involve corner singularities, and it was seen that, when the heterogeneity between the regions is high, the conventional form of the RBF collocation technique yield accurate results, while its weighted counterpart gave up oscillatory solutions with poor accuracy. The last example of multiregion case is a five-region International Atomic Energy Agency benchmark problem. Considering the lack of robustness of the weighted collocation method in the corner singularity problem with high heterogeneity, this benchmark is solved only with the conventional form of the RBF collocation. The numerical multiplication factor values show that the meshless

technique of this study is an effective method in solving multiregion neutron diffusion problems.

The final task of this work is the numerical solution of neutron transport equation with the RBF collocation method. The P_N approach is chosen for the angular variable, and solutions are obtained with both conventional and even-parity forms of the transport equation. Four problems are treated in this context. The external source problem can be dealt with two different approaches within the even-parity form. When the P_3 approximation is utilized, the resulting two second-order differential equations can be cast into a fourth order one, and it is found that, the numerical modelling must be made by approximating coupled second-order differential equations instead of directly interpolating the fourth-order equation. The second example is a fission source case, and the numerical experiments have shown that highly accurate solutions are obtained for both the flux distribution and multiplication factor. Finally, in the third and fourth problems Pu-239 benchmarks with isotropic and anisotropic scattering are tackled, respectively. The isotropic case is solved with both forms and identical solutions are obtained for the multiplication factor. Also the results are compared with those of discrete ordinates method utilizing finite difference and finite element method for the spatial variable, and it is seen that the P_5 collocation solutions are equivalent to the S_8 results. The anisotropic problem is solved with the conventional form of the transport equation and the RBF collocation method yield a good accuracy, even with the P_5 approximation.



AĞSIZ RBF KOLLOKASYON YÖNTEMLERİNİN NÖTRON DİFÜZYON VE TRANSPORTUNA UYGULANMASI

ÖZET

Son yıllarda ağsız yöntemler, bilim ve mühendisliğin birçok alanında fiziksel olayların modellenmesi amacıyla, sonlu farklar metodu, sonlu eleman metodu ve sınır eleman metodu gibi geleneksel yöntemlere alternatif hale gelmişlerdir. Bu yeni yöntemler sayesinde herhangi bir öntanımlı ağa ihtiyaç duymadan, kısmi diferansiyel, integral ve integrodiferansiyel denklemler tarafından betimlenen birçok problem sayısal olarak çözülmüştür.

Literatürde farklı sayısal formülasyonlara bağlı olarak çeşitli ağsız yöntemler bulmak mümkündür. Bunlar içerisinde radyal baz fonksiyonu (RBF) kollokasyon yöntemi temel karakteristiği olan ağsızlığın yanında bazı önemli özellikleriyle diferansiyel denklemlerin çözümü için ideal bir sayısal yaklaşım metodudur. Öncelikle bu yöntem bir güçlü-form yöntemidir ve bu sebeple sayısal formülasyon içerisinde bir integrasyona ve dolayısıyla bir arkaplan ağına ihtiyaç duyulmaz. Bu özellik sayesinde RBF kollokasyon yöntemi diğer zayıf-form ağsız yöntemler ile karşılaştırıldığında, gerçek anlamda ağsız bir yöntem olarak sınıflandırılır. Bu yöntemin ikinci belirgin özelliği üstel yakınsama hızıdır. Problem bölgesini temsil etmek için oluşturulan nokta sayısı az bile olsa bu yakınsama hızı ile yüksek doğruluklu çözümler elde etmek mümkündür. Yöntemin dikkate değer bir diğer özelliği ise bilgisayar programlarındaki uygulama kolaylığıdır. RBF kollokasyon yönteminin programlama aşaması diğer ağsız ve ağ temelli yöntemlerin programlanmasına göre daha kolaydır.

Bir diferansiyel denklemin RBF kollokasyonu ile sayısal çözümü aslında bir genelleştirilmiş interpolasyon problemidir. Problemi tanımlayan diferansiyel denklemin ve sınır koşullarının bağımlı değişkeni, ki bu çalışma kapsamında nötron akısı, radyal baz fonksiyonlarının sonlu bir serisi ile interpolate edilir. Daha sonra bu yaklaşımla elde edilen denklemler, problem bölgesi boyunca düzenli veya rastgele bir biçimde dağıtılmış olan interpolasyon noktalarında sağlanırlar. Her ne kadar literatürde birçok radyal baz fonksiyonu bulunsa da, ilk kez yüzey uydurma için önerilmiş olan genelleştirilmiş multikvadrik fonksiyonu, bu fonksiyon sınıfında, hem fonksiyon yaklaşımı konusunda hem de diferansiyel veya integral denklemlerin sayısal çözümünde baskın hale gelmiştir.

RBF kollokasyon yöntemi bugüne kadar birçok alanda bir çözüm aracı olarak kullanılmış olsa da bu yöntemin heterojen sistemlerin çözümündeki kullanımı kısıtlı kalmıştır. Yakın bir zamanda bu yöntemin ağırlıklı bir versiyonu, çok bölgeli katı mekaniği problemlerinin çözümü için önerilmiştir. Bu ağırlıklı yöntemde, interpolasyon noktası sayısı ve ortamın fiziksel parametrelerine bağlı olan ağırlıklar, sayısal yaklaşım sonucu iç bölgelerde ortaya çıkan hata ile sınır ve arayüzlerde açığa çıkan hatalar arasında bir dengeleme yapılarak belirlenmiştir.

Çoğaltkan veya çoğaltkan olmayan bir ortamda nötronların davranışlarının belirlenmesi amacıyla, nötron difüzyon ve transport denklemleri üzerinde uzun bir

süredir çalışılmaktadır. Bazı durumlarda analitik çözümler elde etmek mümkün olmakla birlikte nükleer teknolojinin ortaya koyduğu gerçekçi problemlerde güvenilir ve detaylı bir analiz yapabilmek için ileri seviyede sayısal yaklaşım yöntemlerine ihtiyaç duyulmaktadır. Tahmin edilebileceği gibi çok bileşenli karmaşık bir nükleer sistem için difüzyon yaklaşımı durumunda bile analitik bir çözüm elde etmek olanaksızdır. Nötron difüzyon ve transport denklemleri bugüne kadar sonlu farklar, sonlu eleman ve sınır eleman yöntemleri ile çözülmüş olup son yıllarda bilgisayarların hesaplama yeteneklerindeki gelişimle beraber bu alandaki çalışmalar yeniden hız kazanmıştır.

Bu çalışmanın amacı zamandan bağımsız nötron difüzyon ve transport denklemlerinin RBF kollokasyon yöntemi ile sayısal olarak çözülmesi ve dolayısıyla bu umut vaat eden ağsız yöntemin nükleer reaktör fiziği alanına bir çözüm yöntemi olarak dahil edilmesidir. Bu kapsamda iki boyutlu çok gruplu nötron difüzyon denklemlerine hem homojen hem de heterojen ortamlarda radyal baz fonksiyonları ile yaklaşım yapılırken transport durumunda tek enerji grubuyla temsil edilen bir boyutlu problemler ele alınmıştır. Ağsız kollokasyon yönteminin performansı farklı durumlar için yapılan sayısal deneylerle değerlendirilmiş olup bu hesaplamalarla yöntemin doğruluğu, kararlılığı ve yakınsama hızı incelenmiştir.

Homojen ortam durumunda beş difüzyon problemi RBF kollokasyonu ile çözülmüştür. Bu problemlerden bir tanesi dış kaynak probleminde diğer dördü çok gruplu fisyon kaynağı problemleridir. Dış kaynak ve dört gruplu fisyon kaynağı problemleri detaylı olarak incelenmiştir ve RBF kollokasyon yönteminin performansı lineer şekil fonksiyonlu sonlu eleman ve sınır eleman yöntemleri ile karşılaştırılmıştır. Radyal baz fonksiyonu olarak multikvadrik, ters multikvadrik ve Gauss fonksiyonları kullanılmıştır. Elde edilen ortalama karekök hatası ve çoğaltma faktöründeki yüzde bağıl hata değerleri, doğruluk ve kararlılık dikkate alındığında, multikvadrik ve ters multikvadrik fonksiyonlarının Gauss baz fonksiyonuna göre daha başarılı olduğunu göstermiştir. Şekil parametresinin ince bir şekilde ayarlanmasıyla birlikte az sayıda interpolasyon noktası kullanılması durumunda bile yüksek doğruluklu çözümler bulunabileceği anlaşılmıştır. Ayrıca, yapılan hesaplarla, bu parametrenin değerinin artırılmasıyla yöntemin yakınsama hızının geliştiği görülmüştür. Multikvadrik kollokasyon ile lineer sonlu eleman ve sınır eleman yöntemleri karşılaştırıldığında üstel yakınsama özelliğine sahip RBF kollokasyonunun çoğaltma faktörünün doğru bir biçimde belirlenmesindeki üstünlüğü ortaya konmuştur. Buna karşılık nötron akı dağılımı açısından en iyi sonuçlar sınır eleman yöntemi ile elde edilirken, sonlu eleman yöntemi ise kollokasyon yaklaşımından çok daha iyi bir hesaplama zamanına sahiptir.

Çok bölgeli nötron difüzyon problemlerinde sayısal çözüm için RBF kollokasyon yönteminin hem geleneksel hem de ağırlıklı formları kullanılmıştır. Beş problem üzerinde durulmuş olup bunlardan ilki bir boyutlu iki bölgeli bir dış kaynak problemidir. Bu problemin çözümü, MATHEMATICA'nın rastgele hassasiyetle hesaplama özelliği kullanıldığında, RBF kollokasyonu ile olağanüstü doğruluk değerlerine ulaşılabileceğini göstermiştir. Bu problemin ardından analitik olarak çözülebilen iki boyutlu, iki bölgeli bir durum ele alınmış ve RBF kollokasyonunun her iki formuyla da iyi sonuçlar elde edilmiştir. Sonraki iki problem yapılarında köşe tekiliği içermektedir ve bu problemler üzerinde yapılan incelemeler, bölgeler arasındaki heterojenitenin yüksek olması durumunda geleneksel formulla doğru sonuçlar elde edilebilirken, ağırlıklı RBF kollokasyonunun salınımlı ve hatalı sonuçlar ortaya çıkardığını göstermiştir. Çok bölgeli problemler kapsamında son olarak beş bölgeli bir Uluslararası Atom Enerjisi Komisyonu kıyaslama problemi

üzerinde çalışılmıştır. Ağırlıklı kollokasyon yöntemi durumunda, köşe tekilliği ve yüksek heterojenite içeren problemde karşılaşılan sağlamlık eksikliği dikkate alınarak bu kıyaslama problemi yalnızca geleneksel form ile çözülmüştür. Elde edilen sayısal çoğaltma faktörü değerleri, kullanılan ağırsız yöntemin çok bölgeli nötron difüzyon problemlerinin sayısal çözümü için etkin bir yöntem olduğunu göstermiştir.

Bu çalışmadaki son görev nötron transport denkleminin RBF kollokasyonu ile sayısal olarak çözülmesidir. Hesaplamalarda açısal değişken için P_N yaklaşımı kullanılmış olup transport denklemi hem geleneksel hem de çift-parite formlarında çözülmüştür. İncelemede dört problem üzerinde durulmuştur. Dış kaynak problemi, çift-parite formunda, iki farklı yaklaşımla çözülebilir. P_3 yaklaşımı kullanıldığında elde edilen iki ikinci derece diferansiyel denklem tek bir dördüncü derece denkleme indirgenebilir ve yapılan hesaplamalar, sayısal modellemenin, bağlaşıklık ikinci derece denklemler üzerinden yapılması gerektiğini göstermiştir. İkinci problemde bir fisyon kaynağı durumu ele alınmış ve hem nötron akı dağılımı hem de çoğaltma faktörü için yüksek doğruluğa sahip sonuçlar bulunmuştur. Son olarak, üçüncü ve dördüncü örneklerde sırasıyla bir Pu-239 kıyaslama problemi durumu, eşyönlü ve eşyönsüz saçılma halleri için çözülmüştür. Eşyönlü problem her iki formla da incelenmiş olup elde edilen çoğaltma faktörü değerleri birbirleriyle neredeyse aynıdır. Bu sonuçlar ayrıca uzaysal değişken için sonlu fark ve sonlu eleman yaklaşımlarının kullanıldığı ayrık ordinat çözümleriyle de karşılaştırılmış ve P_5 çözümünün S_8 sonucuna denk olduğu görülmüştür. Eşyönsüz problem transport denkleminin geleneksel formuyla çözülmüştür ve P_5 yaklaşımı altında bile RBF kollokasyon yöntemi iyi sonuçlar vermiştir.



1. INTRODUCTION

The fundamental problem of nuclear reactor physics is to determine the distribution of neutrons in a multiplying or nonmultiplying system. The equation that governs the physical processes in such a system is the neutron transport equation. This equation is also known as the linear Boltzmann equation, since it is the linear version of the famous Boltzmann equation which is used to study the kinetics of rarefied gases.

Neutron transport equation is an integrodifferential equation in seven independent variables. Its dependent variable, the angular flux, is the physical parameter that describes the spatial, angular, energy and time dependence of neutron distribution. The analytical solution of this equation is possible only for highly idealized cases, such as the Milne problem. In addition to the mathematical difficulties inherent in this complex equation, practical systems are highly heterogeneous. As an example, a nuclear reactor consists of fuel elements, moderators, control rods and structural material, and in an engineering analysis, effects of these components has to be taken into account carefully. For these reasons it is necessary to use numerical techniques in the solution of the neutron transport equation.

In early years of reactor physics, because of the lack of computational capabilities, engineers and scientists have focused on an approximate treatment of the neutron transport process, the neutron diffusion approximation. This approximation ignores the angular dependence of neutron distribution and it is analogous to other diffusion processes, such as heat and gas diffusion, encountered in physics. Mathematically, it is easier to deal with the neutron diffusion equation, but the highly heterogeneous character of practical systems stated above necessitates the use of computational methods for an accurate description.

There are two completely different strategies in computational neutron transport. In the stochastic approach a finite number of particle histories are simulated through the use of random numbers. This approach does not need any governing equation. These stochastic methods are known as Monte Carlo methods. On the other hand, in

deterministic methods, the governing equation is discretized and one ends up with an algebraic system of equations. Then this algebraic system is solved directly or iteratively by conventional methods of linear algebra. In the deterministic approach the time variable is usually discretized by implicit methods, such as the backward Euler method, since these methods have the advantage of stability. For the energy variable multigroup method is the proper choice. The angular variable can be discretized by two methods, discrete ordinates (S_N approximation) or spherical harmonics (P_N approximation).

The spatial variable of the neutron transport equation has been studied by many numerical methods. Parallel to the evolution in computational science the first method applied was the finite difference method (diamond difference). The finite element method (FEM) is another important technique that has been introduced to the field of neutron transport. It is the most widely used numerical method in science and engineering, and many commercial simulation packages are based on this scheme. These conventional methods are mesh-based approaches. The nodes that are used to discretize the governing equation are connected by a predefined mesh.

Meshless or meshfree methods are a novel class of computational tools. As their name implies, the most significant property that separates them from classical techniques is that the nodes that represent the problem domain and its boundary are not connected in a predefined manner to form a mesh. These methods were first emerged in late 1970s, and they have been applied to a wide range of partial differential and integral equations.

1.1 Purpose and Expected Outcomes of the Thesis

The purpose of this thesis is to apply the meshless methods to the time-independent multigroup neutron diffusion and transport equations. In this context, the radial basis function (RBF) collocation method and the weighted RBF collocation method are utilized for the spatial discretization of these equations. For neutron diffusion both homogeneous and multiregion problems are considered, while single domain problems are studied in the transport case. Effects of different basis functions, shape parameter strategies, and fill distance will be investigated. Accuracy and stability of these collocation methods will be determined by using problems which can be solved

analytically or numerically, and the results will be compared with those of conventional techniques.

By the completion of this thesis, it is expected that the RBF collocation technique will become an alternative tool for the spatial treatment of neutron diffusion and transport equations. It is also anticipated that these methods will be extremely useful for the analysis of safety related problems and they will dominate the classical discretization techniques.

1.2 Literature Review

The neutron transport equation and its approximation, the neutron diffusion equation are studied both analytically and numerically by many books [1-6]. Among these [1,2] present a detailed computational analysis of the neutron transport process, and [6] is a reference which contains a comprehensive application of the FEM to both equations.

As a result of the increase of computational capabilities in the last decades, the research in computational neutron transport is boosted and many papers [7-12] can be found in the literature. Meshless methods have not been applied yet to the neutron transport equation, but several works [13-15] can be found in the field of radiative transport which is governed by an equation similar to the neutron transport equation. When neutron diffusion is considered, in a recent paper [16] the element free Galerkin method is applied to the neutron diffusion equation.

Although the meshless methods have a short history, one can find an extensive literature related to this topic. Many books [17-21] are devoted to this subject. Among these [17] is a text that covers most of the methods in a well-structured way. These methods have found themselves a wide range of application area which includes structural mechanics [22-24], fluid dynamics [25-28], heat transfer [29-31], acoustics [32], quantum physics [33], and countless papers can be found in the literature.

1.3 Outline of the Thesis

This thesis consists of seven sections. In section 2 neutron transport and diffusion processes are briefly described. The meshless methods are introduced in section 3,

where special emphasis is given to the RBF collocation method. Then, numerical solution of the homogeneous neutron diffusion equation is performed in section 4, and it is followed by the modelling of multiregion problems in section 5. In section 6 the neutron transport equation is solved by the RBF collocation method. Finally, the conclusions and recommendations of this study are presented in section 7.



2. NEUTRON TRANSPORT

2.1 The Time-independent Neutron Transport Equation

The distribution of neutrons in a time-independent multiplying or nonmultiplying system is characterized by a dependent variable called the angular neutron flux. This variable can be defined as follows [3]:

$$\varphi(\mathbf{r}, E, \boldsymbol{\Omega}) dV d\Omega dE = \text{total path length traveled by neutrons,} \quad (2.1)$$

in $dV d\Omega dE$ about $(\mathbf{r}, E, \boldsymbol{\Omega})$

It can be seen from Eq. (2.1) that the angular neutron flux is a function of six independent variables: three components, (x, y and z if Cartesian coordinates are chosen), of the spatial variable, two angular variables (θ and ϕ) and one energy variable. The equation that governs the interaction of neutrons within any medium is the neutron transport equation:

$$\begin{aligned} \boldsymbol{\Omega} \cdot \nabla \varphi + \Sigma_t(\mathbf{r}, E) \varphi(\mathbf{r}, E, \boldsymbol{\Omega}) \\ = \int_{4\pi} d\boldsymbol{\Omega}' \int_0^\infty dE' \Sigma_s(E' \rightarrow E, \boldsymbol{\Omega}' \rightarrow \boldsymbol{\Omega}) \varphi(\mathbf{r}, E', \boldsymbol{\Omega}') \quad (2.2) \\ + s(\mathbf{r}, E, \boldsymbol{\Omega}) \end{aligned}$$

This equation is a linear integrodifferential equation. Here $\Sigma_t(\mathbf{r}, E)$ is the macroscopic total cross section characterizing the probability of all neutron-nuclei interactions, $\Sigma_s(E' \rightarrow E, \boldsymbol{\Omega}' \rightarrow \boldsymbol{\Omega})$ is the double differential macroscopic scattering cross section characterizing the scattering probability of a particle with energy E' and a direction $\boldsymbol{\Omega}'$ into an energy interval dE about E and into a direction $d\Omega$ about $\boldsymbol{\Omega}$ and $s(\mathbf{r}, E, \boldsymbol{\Omega})$ is a general neutron source. First term on left hand side of this equation describes the streaming of the neutrons, while the second one is the collision term. The streaming term describes the leakage of neutrons into or out of the volume and the collision term is a measure of neutron losses due to any kind of neutron-nuclei interaction. The two terms on right hand side of Eq. (2.2) express the

two gain mechanisms of neutrons. First one considers all neutrons that may scatter from any energy E' and direction $\boldsymbol{\Omega}'$ into E and $\boldsymbol{\Omega}$, and the second one is simply the source term which can be either an external source or a fission source depending on the nature of the problem.

The derivation of the neutron transport equation can be done by simply considering an arbitrary volume and taking into account the various mechanisms that add or remove a neutron from it. Although this derivation is not given here it is useful to summarize the important assumptions that lead to Eq. (2.2) [1,3]:

- 1) Particles are considered as points and their interaction can be described by classical mechanics.
- 2) Particles travel in straight lines between collisions.
- 3) Particle-particle interactions are neglected since the particle densities are small compared with atomic densities in many applications.
- 4) The transport process is assumed to be Markovian.
- 5) The neutron transport equation deals with expected or mean neutron population.

It is obvious from Eq. (2.2) that one needs boundary conditions to complete the mathematical statement of the neutron transport problem. The boundary condition depends on the configuration of the problem. In general there are two kinds of boundary conditions: explicit and implicit [1]. For explicit boundary conditions the angular neutron flux is explicitly known. As an example, the commonly used vacuum boundary condition is an explicit one:

$$\varphi(\mathbf{r}_s, E, \boldsymbol{\Omega}) = 0, \quad \boldsymbol{\Omega} \cdot \mathbf{n} < 0, \quad \mathbf{r}_s \in \Gamma \quad (2.3)$$

Here Γ represents the boundary of the problem domain, \mathbf{n} is the unit outward normal vector to Γ , and subscript s is used to denote surface. Implicit boundary conditions are conditions that relate incoming and outgoing fluxes. The albedo boundary condition is an example to this class

$$\varphi(\mathbf{r}_s, E, \boldsymbol{\Omega}) = \alpha(E)\varphi(\mathbf{r}_s, E, \boldsymbol{\Omega}'), \quad \boldsymbol{\Omega} \cdot \mathbf{n} < 0, \quad \mathbf{r}_s \in \Gamma \quad (2.4)$$

where the reflection angle $\boldsymbol{\Omega}$ and the incidence angle $\boldsymbol{\Omega}'$ are related by:

$$\boldsymbol{\Omega} \cdot \mathbf{n} = -\boldsymbol{\Omega}' \cdot \mathbf{n}, \quad (\boldsymbol{\Omega} \times \boldsymbol{\Omega}') \cdot \mathbf{n} = 0 \quad (2.5)$$

Note that for the special case of $\alpha(E) = 1$, Eq. (2.4) is the reflective boundary condition.

Although Eq. (2.2) with boundary conditions is enough to fully describe the transport problem mathematically, the source term has to be expressed explicitly. In the most general case one can write:

$$s(\mathbf{r}, E, \boldsymbol{\Omega}) = s_{ex}(\mathbf{r}, E, \boldsymbol{\Omega}) + s_f(\mathbf{r}, E) \quad (2.6)$$

In this relation $s_{ex}(\mathbf{r}, E, \boldsymbol{\Omega})$ denotes the external neutron source while $s_f(\mathbf{r}, E)$ is the fission source which characterizes the fission event when there is a fissionable material in the problem considered. If all the neutrons are assumed to be born instantaneously (prompt neutrons) then the fission source takes the following form:

$$s_f(\mathbf{r}, E) = \frac{\chi(E)}{4\pi} \int_{4\pi} d\boldsymbol{\Omega}' \int_0^{\infty} dE' v(E') \Sigma_f(E') \varphi(\mathbf{r}, E', \boldsymbol{\Omega}') \quad (2.7)$$

Here $\Sigma_f(E)$ is the macroscopic fission cross section characterizing the fission probability of a fissionable isotope, $v(E)$ is the number of neutrons per fission and $\chi(E)$ is the fission spectrum.

For a complete analysis, the influence of delayed neutrons has to be considered. In this case one has to work with a set of equations which are known as neutron kinetics equations. But since the focus of this work is time-independent problems, the details will be omitted and the final form of the time-independent neutron transport equation will be given

$$\begin{aligned} & \boldsymbol{\Omega} \cdot \nabla \varphi + \Sigma_t(\mathbf{r}, E) \varphi(\mathbf{r}, E, \boldsymbol{\Omega}) \\ &= \int_{4\pi} d\boldsymbol{\Omega}' \int_0^{\infty} dE' \Sigma_s(E' \rightarrow E, \boldsymbol{\Omega}' \rightarrow \boldsymbol{\Omega}) \varphi(\mathbf{r}, E', \boldsymbol{\Omega}') \\ &+ \frac{\chi(E)}{4\pi} \int_{4\pi} d\boldsymbol{\Omega}' \int_0^{\infty} dE' v(E') \Sigma_f(E') \varphi(\mathbf{r}, E', \boldsymbol{\Omega}') \\ &+ s_{ex}(\mathbf{r}, E, \boldsymbol{\Omega}) \end{aligned} \quad (2.8)$$

where the fission spectrum is expressed by

$$\chi(E) = \chi_p(E)(1 - \beta) + \sum_{m=1}^6 \chi_m(E)\beta_m \quad (2.9)$$

In Eq.(2.9) $\chi_p(E)$ is the prompt fission spectrum, β is the fraction of delayed neutrons, and $\chi_m(E)$ and β_m are the fission spectrum and fraction of the m th delayed neutron group, respectively. β and β_m are related by

$$\sum_{m=1}^6 \beta_m = \beta \quad (2.10)$$

It is well known from basic reactor physics that a time-independent solution can be obtained in two cases. One must either have a nonmultiplying system with external sources or a multiplying system without any external source. For the nonmultiplying case, i.e. $\Sigma_f = 0$

$$\begin{aligned} & \boldsymbol{\Omega} \cdot \nabla \varphi + \Sigma_t(\mathbf{r}, E)\varphi(\mathbf{r}, E, \boldsymbol{\Omega}) \\ &= \int_{4\pi} d\boldsymbol{\Omega}' \int_0^\infty dE' \Sigma_s(E' \rightarrow E, \boldsymbol{\Omega}' \rightarrow \boldsymbol{\Omega})\varphi(\mathbf{r}, E', \boldsymbol{\Omega}') + s_{ex}(\mathbf{r}, E, \boldsymbol{\Omega}) \end{aligned} \quad (2.11)$$

The situation is more complicated for source-free, multiplying system problem which is governed by:

$$\begin{aligned} & \boldsymbol{\Omega} \cdot \nabla \varphi + \Sigma_t(\mathbf{r}, E)\varphi(\mathbf{r}, E, \boldsymbol{\Omega}) \\ &= \int_{4\pi} d\boldsymbol{\Omega}' \int_0^\infty dE' \Sigma_s(E' \rightarrow E, \boldsymbol{\Omega}' \rightarrow \boldsymbol{\Omega})\varphi(\mathbf{r}, E', \boldsymbol{\Omega}') \\ &+ \frac{\chi(E)}{4\pi} \int_{4\pi} d\boldsymbol{\Omega}' \int_0^\infty dE' \nu(E')\Sigma_f(E')\varphi(\mathbf{r}, E', \boldsymbol{\Omega}') \end{aligned} \quad (2.12)$$

The complexity of this problem comes from the fact that, to obtain a time-independent chain reacting (critical) system, fine adjustments in composition and/or geometry have to be performed. The practical solution to this issue is to convert the equation into an eigenvalue problem. The most common formulation is the λ -eigenvalue formulation, which can be achieved by simply replacing ν by ν/λ . By doing this replacement, the number of neutrons per fission is “magically” adjusted to

yield a time-independent solution. λ is a parameter that measures how far the system is away from criticality. If $\lambda > 1$, one has a supercritical system and if $\lambda < 1$ the system is said to be subcritical.

Now some important properties of the solutions of the neutron transport equation can be given. An important feature of the angular neutron flux is its smoothness, since it has major implications in the accuracy of numerical methods, significant results will be summarized here [3]:

- For planar geometry transport problems if one has vacuum boundary conditions and isotropic sources then the flux has C^1 smoothness in both x and μ where $\mu = \cos \theta$ except at outer boundaries and material interfaces.
- For multidimensional problems with vacuum boundaries generally the flux has C^0 smoothness.
- If the boundary fluxes are not smooth, then the solution is non-smooth throughout the problem domain.

2.2 The Diffusion Approximation

The complexity of the neutron transport equation can be reduced by assuming that the flux is weakly-dependent on the angular variable Ω . Although information on the behavior of neutron distribution is lost, the equation that governs the angle-independent system can be solved much more easily than the transport equation.

In order to derive the diffusion approximation, two fundamental concepts, the angle-integrated or total flux and the neutron current must be defined. The total flux can be obtained by just integrating the angular flux over all directions:

$$\phi(\mathbf{r}, E) = \int_{4\pi} d\Omega \varphi(\mathbf{r}, E, \Omega) \quad (2.13)$$

A closely related dependent variable to the angular flux is the angular neutron current vector:

$$\mathbf{j}(\mathbf{r}, E, \Omega) \equiv \Omega \varphi(\mathbf{r}, E, \Omega) \quad (2.14)$$

This variable has the following physical interpretation [4]:

$$\mathbf{j}(\mathbf{r}, E, \boldsymbol{\Omega}) \cdot dA dE d\boldsymbol{\Omega} \equiv \text{expected number of neutrons passing} \\ \text{through an area } dA \text{ per unit time with} \quad (2.15) \\ \text{energy } E \text{ in } dE, \text{ direction } \boldsymbol{\Omega} \text{ in } d\boldsymbol{\Omega}$$

The angle-independent current vector can be defined in a similar way that was used to define the total flux:

$$\mathbf{J}(\mathbf{r}, E) = \int_{4\pi} d\boldsymbol{\Omega} \mathbf{j}(\mathbf{r}, E, \boldsymbol{\Omega}) \quad (2.16)$$

The first step in the derivation of the diffusion approximation is to integrate the neutron transport equation, Eq. (2.2), over all directions:

$$\int_{4\pi} d\boldsymbol{\Omega} \cdot \nabla \varphi + \int_{4\pi} d\boldsymbol{\Omega} \Sigma_t(\mathbf{r}, E) \varphi(\mathbf{r}, E, \boldsymbol{\Omega},) \\ = \int_{4\pi} d\boldsymbol{\Omega} \int_{4\pi} d\boldsymbol{\Omega}' \int_0^\infty dE' \Sigma_s(E' \rightarrow E, \boldsymbol{\Omega}' \rightarrow \boldsymbol{\Omega}) \varphi(\mathbf{r}, E', \boldsymbol{\Omega}') \quad (2.17) \\ + \int_{4\pi} d\boldsymbol{\Omega} s(\mathbf{r}, E, \boldsymbol{\Omega})$$

All terms, except the first term on right hand side of this equation can be treated in a straightforward manner by using Eqs. (2.13) and (2.14). To evaluate the exceptional inscattering term it has to be assumed that the double differential scattering cross section depends only on $\mu_0 = \boldsymbol{\Omega}' \cdot \boldsymbol{\Omega}$, which is a frequent case. This assumption reduces this cross section to a single differential scattering cross section. Hence:

$$\int_{4\pi} d\boldsymbol{\Omega} \int_{4\pi} d\boldsymbol{\Omega}' \int_0^\infty dE' \Sigma_s(E' \rightarrow E, \boldsymbol{\Omega}' \rightarrow \boldsymbol{\Omega}) \varphi(\mathbf{r}, E', \boldsymbol{\Omega}') = \\ \int_{4\pi} d\boldsymbol{\Omega}' \int_0^\infty dE' \left[\int_{4\pi} d\boldsymbol{\Omega} \Sigma_s(E' \rightarrow E, \boldsymbol{\Omega}' \rightarrow \boldsymbol{\Omega}) \right] \varphi(\mathbf{r}, E', \boldsymbol{\Omega}') = \quad (2.18) \\ \int_0^\infty dE' \Sigma_s(E' \rightarrow E) \int_{4\pi} d\boldsymbol{\Omega}' \varphi(\mathbf{r}, E', \boldsymbol{\Omega}') = \int_0^\infty dE' \Sigma_s(E' \rightarrow E) \phi(\mathbf{r}, E')$$

The equation that comes out of this operation of integrating over all directions is known as the neutron continuity equation:

$$\nabla \cdot \mathbf{J}(\mathbf{r}, E) + \Sigma_t(\mathbf{r}, E)\phi(\mathbf{r}, E) = \int_0^\infty dE' \Sigma_s(E' \rightarrow E)\phi(\mathbf{r}, E') + S(\mathbf{r}, E) \quad (2.19)$$

Notice that Eq. (2.19) contains two unknowns, $\phi(\mathbf{r}, E)$ and $\mathbf{J}(\mathbf{r}, E)$. The abovementioned procedure can be repeated and the following equation can be obtained for the current vector [4]:

$$\begin{aligned} & \nabla \cdot \int_{4\pi} d\Omega \mathbf{\Omega} \mathbf{\Omega} \phi(\mathbf{r}, E, \mathbf{\Omega}) + \Sigma_t(\mathbf{r}, E)\mathbf{J}(\mathbf{r}, E) \\ &= \int_0^\infty dE' \Sigma_{s_1}(E' \rightarrow E)\mathbf{J}(\mathbf{r}, E') + S_1(\mathbf{r}, E) \end{aligned} \quad (2.20)$$

where

$$\Sigma_{s_1}(E' \rightarrow E) = 2\pi \int_{-1}^1 d\mu_0 \mu_0 \Sigma_s(E' \rightarrow E, \mu_0) \quad (2.21)$$

$$S_1(\mathbf{r}, E) = \int_{4\pi} d\Omega \mathbf{\Omega} s(\mathbf{r}, E, \mathbf{\Omega}) \quad (2.22)$$

To make life simple let's consider the case where all neutrons are characterized by the same energy. This is known as the one-speed approximation. The key assumption in obtaining the diffusion approximation is that the angular flux is only weakly dependent on angle, so that it is linearly anisotropic. This means one has to expand the angular flux in angle and neglect all the terms that have an order higher than linear order in $\mathbf{\Omega}$:

$$\varphi(\mathbf{r}, \mathbf{\Omega}) \cong \frac{1}{4\pi} \phi(\mathbf{r}) + \frac{3}{4\pi} \mathbf{J} \cdot \mathbf{\Omega} \quad (2.23)$$

By using this relation to evaluate the first term of Eq. (2.20) and taking into account the one-speed approximation [4]:

$$\frac{1}{3}\nabla\phi + \Sigma_{tr}(\mathbf{r})\mathbf{J}(\mathbf{r}) = S_1(\mathbf{r}) \quad (2.24)$$

The one-speed form of Eq. (2.19) is also needed:

$$\nabla \cdot \mathbf{J} + \Sigma_a(\mathbf{r})\phi(\mathbf{r}) = S(\mathbf{r}) \quad (2.25)$$

Here, Σ_a and Σ_{tr} are the macroscopic absorption and transport cross sections, respectively. Now there are two equations for two unknowns. These two equations can be simplified further by assuming that the neutron source term is isotropic i.e., $S_1(\mathbf{r}) = 0$. From Eq. (2.24) it follows that

$$\mathbf{J}(\mathbf{r}) = -\frac{1}{3\Sigma_{tr}(\mathbf{r})}\nabla\phi(\mathbf{r}, t) \quad (2.26)$$

Now, defining the neutron diffusion coefficient by

$$D(\mathbf{r}) = \frac{1}{3\Sigma_{tr}(\mathbf{r})} \quad (2.27)$$

and substituting (2.26) into (2.25) the familiar one-speed neutron diffusion equation can be obtained:

$$-\nabla \cdot D(\mathbf{r})\nabla\phi + \Sigma_a(\mathbf{r})\phi(\mathbf{r}) = S(\mathbf{r}) \quad (2.28)$$

In summary, Eq. (2.28) is a consequence of three approximations:

- Linear anisotropy
- Energy-independency
- Isotropic sources

As stated above the most important assumption in the derivation of the neutron diffusion equation is the weak independence of neutron flux on Ω . This assumption is violated near boundaries and localized sources. It also loses validity in strongly absorbing media and when material properties change dramatically over a small distance. In these situations one has to work with the neutron transport equation to get more accurate results.

2.3 The Time-independent Multigroup Multiregion Neutron Diffusion Equation and Boundary Conditions

Although the one-speed single region neutron diffusion equation is instructive, the modelling and design of nuclear reactors necessitates the use of a much detailed approximation. The time-independent multigroup multiregion neutron diffusion equation represents the heterogeneous structure of such systems, and it can provide a better approach for the energy variable:

$$-D_g^i \nabla^2 \phi_g^{i,(n)} + \Sigma_{r,g}^i \phi_g^{i,(n)} - \sum_{g'=1}^{g-1} \Sigma_{s,g' \rightarrow g}^i \phi_{g'}^{i,(n)} = Q_g^i \quad (2.29)$$

$$Q_g^i = \begin{cases} \frac{1}{\lambda^{(n-1)}} \chi_g^i F^{i,(n-1)} \\ S_{g,ex}^i \end{cases}$$

where $g = 1, \dots, G$ and $i = 1, \dots, M$. In Eq. (2.29), g and i denote the energy group and material number, respectively, and $\Sigma_r \equiv \Sigma_a - \Sigma_{s,g \rightarrow g}$ is the removal cross section. It has been assumed that the fission source iteration is employed for the determination of λ , the effective multiplication factor, and n denotes the iteration number [4]. The fission source is defined by

$$F^i \equiv \sum_{g'=1}^G v_{g'}^i \Sigma_{f,g'}^i \phi_{g'}^i \quad (2.30)$$

where v_g^i is the number of neutrons emitted per fission of group g and $\Sigma_{f,g}^i$ is the group fission cross section.

In the fission source case the system of partial differential equations (PDEs) in Eq. (2.29) is solved iteratively. The iterative algorithm, known as fission source iteration, starts by making a guess for the fission source and the multiplication factor as $F^i \sim F^{i,(0)}$ and $\lambda \sim \lambda^{(0)}$, which gives $\phi_1^{i,(1)}$. Then, $\phi_g^{i,(1)}, g = 2, \dots, G$ are found successively and a new fission source and multiplication factor are determined by

$$F^{i,(1)} = \sum_{g'=1}^G v_{g'}^i \Sigma_{f,g'}^i \phi_{g'}^{i,(1)}, \quad \lambda^{(1)} = \lambda^{(0)} \frac{\int dAF^{i,(1)}}{\int dAF^{i,(0)}} \quad (2.31)$$

where dA is the area element. This iterative algorithm is terminated when a predetermined convergence criterion is satisfied

$$\left| \frac{\lambda^{(n+1)} - \lambda^{(n)}}{\lambda^{(n+1)}} \right| < \xi \quad (2.32)$$

On the other hand if an external source term is present, then Eq. (2.29) can be solved directly.

To complete the description of the problem boundary and interface conditions are needed. In general there are three types of boundary conditions (BCs):

$$\begin{aligned} \phi_g^i &= 0 && \text{(Vacuum BC)} \\ J &\equiv \frac{\partial \phi_g^i}{\partial n} = 0 && \text{(Neumann type reflective BC)} \\ J^- &\equiv \frac{1}{4} \phi_g^i + \frac{D}{2} \frac{\partial \phi_g^i}{\partial n} = 0 && \text{(Robin type vacuum BC)} \end{aligned} \quad (2.33)$$

Finally, at material interfaces the neutron flux and its first derivative should be continuous:

$$\begin{aligned} \phi_g^i &= \phi_g^{i+1} \\ \frac{\partial \phi_g^i}{\partial n} &= \frac{\partial \phi_g^{i+1}}{\partial n} \end{aligned} \quad (2.34)$$

3. MESHLESS METHODS

Meshless methods are a novel class of computational tools. As their name implies, they have the significant property that they do not need a mesh for the simulation of the problem considered. The domain and its boundary are represented by nodes and these nodes do not have to satisfy any relation in a predefined manner to form a mesh. The nodes can be distributed uniformly or randomly. By using these nodes one can first create shape functions to approximate the field variable and then solve the resulting algebraic system of equations by standard techniques of linear algebra.

One of the first meshless method was proposed in late 1970's. It was called the smoothed particle hydrodynamics (SPH) and dealt with astrophysical problems [34]. In the last decades there has been a growing interest in this field and today many meshless schemes are proposed to tackle various problems of science and engineering.

3.1 Motivation for Meshless Methods

The motivation behind meshless methods was to eliminate the difficulties encountered in classical mesh-based techniques. The need for meshless methods can best be understood by comparing it with the most widely used technique in science and engineering, the FEM. In [18] a detailed comparison is given based on the problems of structural mechanics, and these observations will be summarized here:

- 1) Mesh creation is a requirement in FEM packages and the analyst have to spend much of his or her time on this operation.
- 2) The stresses, calculated by FEM are discontinuous and less accurate.
- 3) It is difficult to simulate problems where the material integrity is lost partially or totally such as large deformations, crack growth, phase transformations and fracture.
- 4) Re-meshing is a solution for fracture mechanics problems, but one needs complex mesh generation processors which increases the computational cost for 3-D problems.

3.2 Weighted Residual Method, Strong and Weak Forms

Today, a huge number of meshless methods can be found in the literature, and it is intuitive to categorize them. This categorization can be done with respect to the formulation procedure of the problem or function approximation scheme [17]. In the next section a classification based on the formulation procedure will be presented, but first the ideas of weighted residual method, strong-form and weak-form have to be introduced.

Now consider the following problem:

$$L(u) + f = 0, \quad u \in \Omega \quad (3.1)$$

$$B(u) = g \quad u \in \Gamma \quad (3.2)$$

Here u is the field variable, f and g are known functions that drive the system, and L and B are differential operators. The problem domain and its boundary are denoted by Ω and Γ , respectively.

In most of the practical situations it is generally not possible to obtain an analytical solution for the problem considered. Then, it is a natural choice to try to obtain a numerical solution, and one first approximates the field variable in the following form

$$u^a(\mathbf{r}) = \sum_{i=1}^n a_i \Phi_i(\mathbf{r}) \quad (3.3)$$

where Φ_i are called the trial or shape functions, a_i are unknown coefficients and $\mathbf{r} = (x, y, z)$ are Cartesian coordinates. The trial functions, of course, must satisfy some admissibility conditions to minimize the error introduced by the last equation. By substituting Eq. (3.3) into Eqs. (3.1) and (3.2) the following residuals can be obtained

$$R_s = L(u^a) + f \quad (3.4)$$

$$R_b = B(u^a) - g \quad (3.5)$$

Then the procedure continues with multiplying these residuals with weight or test functions and integrating over the problem domain to minimize the error in an average sense:

$$\int_{\Omega} W_i R_s d\Omega + \int_{\Gamma} V_i R_b d\Gamma = 0, \quad i = 1, \dots, n \quad (3.6)$$

Here W_i and V_i are weight functions and one can choose $W_i = V_i$. This is known as the weighted residual method, and it is the starting point of many numerical procedures.

If Eqs. (3.4) and (3.5) are substituted into Eq. (3.6)

$$\int_{\Omega} W_i \left[L \left(\sum_{i=1}^n a_i \Phi_i(\mathbf{r}) \right) + f \right] d\Omega + \int_{\Gamma} V_i \left[B \left(\sum_{i=1}^n a_i \Phi_i(\mathbf{r}) \right) - g \right] d\Gamma = 0 \quad (3.7)$$

where $i = 1, \dots, n$ or explicitly:

$$\begin{aligned} \int_{\Omega} W_1 \left[L \left(\sum_{i=1}^n a_i \Phi_i(\mathbf{r}) \right) + f \right] d\Omega + \int_{\Gamma} V_1 \left[B \left(\sum_{i=1}^n a_i \Phi_i(\mathbf{r}) \right) - g \right] d\Gamma &= 0 \\ \int_{\Omega} W_2 \left[L \left(\sum_{i=1}^n a_i \Phi_i(\mathbf{r}) \right) + f \right] d\Omega + \int_{\Gamma} V_2 \left[B \left(\sum_{i=1}^n a_i \Phi_i(\mathbf{r}) \right) - g \right] d\Gamma &= 0 \\ \vdots & \\ \int_{\Omega} W_n \left[L \left(\sum_{i=1}^n a_i \Phi_i(\mathbf{r}) \right) + f \right] d\Omega + \int_{\Gamma} V_n \left[B \left(\sum_{i=1}^n a_i \Phi_i(\mathbf{r}) \right) - g \right] d\Gamma &= 0 \end{aligned} \quad (3.8)$$

By performing the integrations in Eq. (3.8) a system of algebraic equations can be obtained. Solution of this system will yield the unknown constants a_i and hence the numerical solution u^a .

The integration operation in the weighted residual method has a key role in the formulation of the numerical scheme. The original statement of the problem, whether it is an ordinary or partial differential equation, is also called the strong-form. As stated above, the trial functions should satisfy some criteria. Suppose that the governing equation is a differential equation of second order. In this case the trial function must be at least C^2 smooth. But as an alternative, integration by parts can be used (Green's identity for multidimensional problems) to weaken the smoothness requirements of the trial functions. Therefore, the methods which directly deal with the original statement of the problem are called strong-form methods, and the

methods which work on analytically integrated expressions are called weak-form methods.

Different choices of trial and weight functions will lead to different numerical methods. As an example one can use the Dirac's delta function, $\delta(x - x_i)$, as the weight function to satisfy the differential equation at certain nodes. If this is the choice then from Eq. (3.7) it is easy to show that

$$\left[L \left(\sum_{i=1}^n a_i \Phi_i(\mathbf{r}_i) \right) + f \right] + \left[B \left(\sum_{i=1}^n a_i \Phi_i(\mathbf{r}_i) \right) - g \right] = 0 \quad (3.9)$$

by using the fundamental property of Dirac's delta function:

$$f(x_i) = \int f(x) \delta(x - x_i) dx \quad (3.10)$$

The method, defined by Eq. (3.9) is known as the collocation method. It is obvious that this is a strong-form method since the approximation function is directly substituted into the differential equation and its boundary conditions.

Another well known technique is the least squares method that uses the following weight functions:

$$W_i = \frac{\partial R_s}{\partial a_i} \quad V_i = \frac{\partial R_b}{\partial a_i} \quad (3.11)$$

If the trial and weight functions are chosen to be the same then the resulting approach is of the Bubnov-Galerkin type. This weak-form scheme has the advantage that the resultant system matrix is symmetric. But, if different functions are preferred for trial and weight functions, then the procedure is called the Petrov-Galerkin method.

3.3 Classification of Meshless Methods

Meshless methods fall into three categories according to their formulation procedures:

1) Weak-form methods: These methods are based on the weak-form of the governing differential equations. The first weak-form method was the diffuse element method (DEM) which is a generalization of the FEM [35]. Two years later another method, the element-free Galerkin (EFG) method was proposed [36]. These two methods use

the moving least squares (MLS) approximation in shape function construction. Another method that uses the MLS is the meshless local Petrov-Galerkin (MLPG) method [37]. MLPG differs from DEM and EFG in the way that numerical integrations are performed locally. The last example to this class is the radial point interpolation method (RPIM) which utilizes a different approach in shape function construction [17]. This interpolation based scheme can be employed both locally and globally.

2) Strong-form methods: In these methods the original form of the governing equation is satisfied at particular nodes of the domain. The most significant strong-form method is the radial basis function collocation method in which RBFs are used as trial functions [38]. Another important strong-form scheme is the finite point method (FPM), which is based on weighted least squares interpolation [39].

3) Hybrid methods: Weak-form methods can deal with Neumann type boundary conditions easily since these conditions came up naturally in the problem formulation, but Dirichlet boundary conditions need special treatments. For strong form methods the opposite is true, in which the error caused by Neumann boundary conditions diffuse through the problem domain. Although there are special techniques to overcome these problems one can also use weak and strong forms together to get more accurate results. In [40] such a method has been proposed.

3.4 Shape Functions

After determining the nodes in the domain and on the boundary, the second step of solution for meshless methods is the construction of shape functions by using these nodes. Most meshless techniques use the concept of support domain. Hence, before introducing various strategies to build up shape functions it is necessary to define the support domain.

Support domain is a region with any shape and any size that is used to determine the number of nodes in the construction of shape functions. It determines the order of coupling and therefore the order of sparseness of the final system matrix. If one uses a support domain with a small size relative to the size of the problem domain then the result will be a sparse matrix. In Figure 3.1, circular support domains are illustrated as an example.

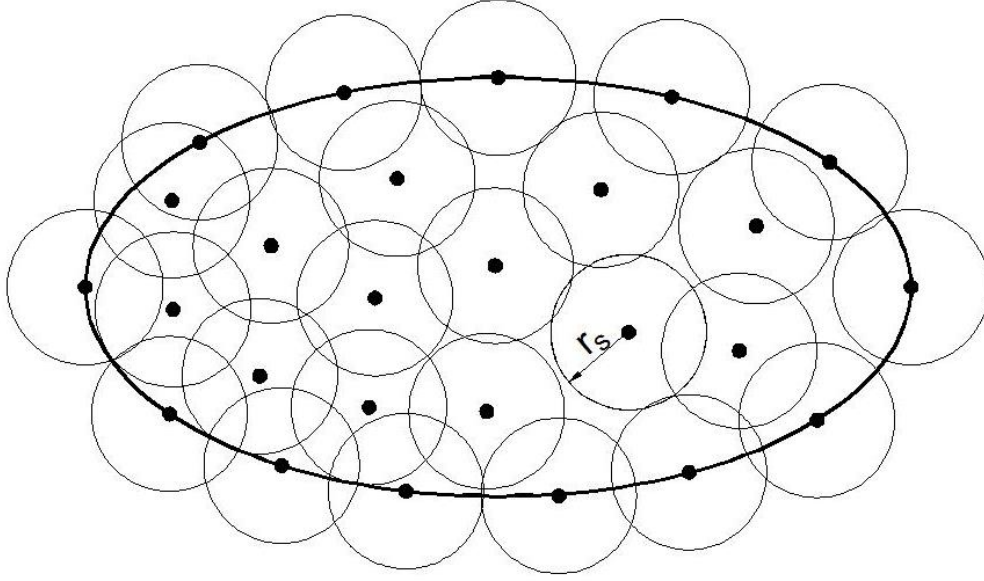


Figure 3.1: Circular support domains of size r_s .

For any point, the size of the support domain, d_s , can be determined by a simple relation;

$$d_s = \alpha_s d_c \quad (3.12)$$

where α_s is a dimensionless parameter determined by the analyst and d_c is the average nodal spacing. α_s should be chosen in an optimal way to give accurate solutions with low computational cost. If uniformly scattered nodes are used, then d_c is simply the spacing between neighboring nodes, but if randomly distributed nodes are used then one has to follow the procedure below [17]:

- i) The value of the support domain is estimated and denoted by D_s .
- ii) The nodes enclosed by D_s , n_{D_s} , are counted.
- iii) For an n-dimensional domain d_c is found from:

$$d_c = \frac{D_s^{1/n}}{n_{D_s}^{1/n} - 1} \quad (3.13)$$

- iv) d_s is found from Eq. (3.12).

Now that the concept of support domain is defined, the construction of shape functions can be introduced. Although there are various approaches to build up these functions, only the most widely used techniques will be presented in this section.

These techniques result from two different strategies, point interpolation and least squares approximation. A detailed discussion can be found in [18].

3.4.1 Point interpolation methods (PIM)

Interpolation is an approximation technique in which one tries to find a function, f_a , to fit a collection of data, y_i , where

$$f_a(x_i) = y_i \quad (3.14)$$

Here x_i are data points (field nodes for meshless methods).

The first step in building up a shape function is to approximate the field variable, $u(\mathbf{x})$ by a series

$$u^a(\mathbf{r}) = \sum_{i=1}^m a_i \Phi_i(\mathbf{r}) \quad (3.15)$$

where a_i are unknown coefficients, $\Phi_i(\mathbf{r})$ are shape functions and m is the number of shape functions. For interpolation, the number of nodes in support domain is chosen as $n = m$ since the shape function has to pass through the function values at every node.

In the polynomial point interpolation method the shape functions are chosen as monomials:

$$u^a(\mathbf{r}) = \sum_{i=1}^m p_i(\mathbf{r}) a_i = \mathbf{p}^T(\mathbf{r}) \mathbf{a} \quad (3.16)$$

Here $p_i(\mathbf{r})$ are monomials and \mathbf{p} and \mathbf{a} are the vectors that collect the monomials and unknown coefficients, respectively. The monomials can be built using Pascal's triangles. As an example if quadratic basis functions are needed for a 2-D problem, then:

$$\mathbf{p}^T(\mathbf{r}) = \{1 \quad x \quad y \quad x^2 \quad xy \quad y^2\} \quad (3.17)$$

The coefficients a_i can be determined by enforcing $u(\mathbf{r})$ to pass through the n nodes in the support domain. This operation yields n equations which can be written in compact form as follows

$$\mathbf{U} = \mathbf{P}_m \mathbf{a} \quad (3.18)$$

where \mathbf{U} and \mathbf{a} are the vectors that collect the nodal values and unknown coefficients respectively and

$$\mathbf{P}_m = \begin{bmatrix} 1 & x_1 & y_1 & x_1 y_1 & \cdots & p_m(\mathbf{r}_1) \\ 1 & x_2 & y_2 & x_2 y_2 & \cdots & p_m(\mathbf{r}_2) \\ 1 & x_3 & y_3 & x_3 y_3 & \cdots & p_m(\mathbf{r}_3) \\ \vdots & \vdots & \vdots & \vdots & \ddots & \vdots \\ 1 & x_n & y_n & x_n y_n & \cdots & p_m(\mathbf{r}_n) \end{bmatrix} \quad (3.19)$$

is called the moment matrix [17]. Notice that \mathbf{P}_m is a square matrix since $n = m$. From Eqs. (3.18) and (3.16) it is easy to obtain

$$u(\mathbf{r}) = \mathbf{p}^T(\mathbf{r}) \mathbf{P}_m^{-1} \mathbf{U} = \mathbf{\Psi}^T(\mathbf{r}) \mathbf{U} \quad (3.20)$$

where $\mathbf{\Psi}^T(\mathbf{r})$ is the vector of shape functions:

$$\mathbf{\Phi}^T(\mathbf{r}) = \{\Phi_1(\mathbf{r}) \quad \Phi_2(\mathbf{r}) \quad \cdots \quad \Phi_n(\mathbf{r})\} \quad (3.21)$$

Point interpolation with monomials is a simple method to construct shape functions, but it has an important defect. The moment matrix, \mathbf{P}_m , can become singular. There are several strategies to avoid this issue. One of them is to use radial basis functions instead of monomials. These functions will be presented in the next section.

3.4.2 Least squares methods

Least squares technique is a well-known approximation method and it can also be used in shape function creation for meshless methods.

The first method that will be introduced is the weighted least squares (WLS) approximation. Once again, the field variable is represented with a finite series of polynomial basis functions:

$$u^a(\mathbf{r}) = \sum_{i=1}^m a_i p_i(\mathbf{r}) = \mathbf{p}^T \mathbf{a} \quad (3.22)$$

To determine the coefficients this series is satisfied at the n approximation nodes, but this time $n > m$ and therefore the resultant moment matrix \mathbf{P}_m is a rectangular one. In general the weighted least squares problem is solved by minimizing

$$J = \sum_{i=1}^n W_i [u^a(\mathbf{r}_i) - u(\mathbf{r}_i)]^2 \quad (3.23)$$

where W_i ($i = 1, 2, \dots, n$) is the weight coefficient for the i th node. To minimize J one must have

$$\frac{\partial J}{\partial \mathbf{a}} = 0 \quad (3.24)$$

which leads to

$$\mathbf{P}_m^T \mathbf{W} \mathbf{P}_m \mathbf{a} = \mathbf{P}_m^T \mathbf{W} \mathbf{U} \quad (3.25)$$

where:

$$\mathbf{W} = \begin{bmatrix} W_1 & \cdots & 0 \\ \vdots & \ddots & \vdots \\ 0 & \cdots & W_n \end{bmatrix} \quad (3.26)$$

For data fitting problems the weights are usually chosen as the standard deviation to decrease the effects of possible measurement errors in experiments. In case of meshless methods one can use the following weight

$$W_i = W(\mathbf{x}_i) = \frac{e^{-\left(\frac{r}{c}\right)^2} - e^{-\left(\frac{r_s}{c}\right)^2}}{1 - e^{-\left(\frac{r_s}{c}\right)^2}} \quad (3.27)$$

where r_s is the size of support domain, c is a constant to be determined by the analyst and

$$r = \sqrt{(x - x_i)^2 + (y - y_i)^2} \quad (3.28)$$

The WLS shape functions can be obtained by letting

$$\mathbf{A} = \mathbf{P}_m^T \mathbf{W} \mathbf{P}_m \quad (3.29)$$

$$\mathbf{B} = \mathbf{P}_m^T \mathbf{W} \quad (3.30)$$

This leads us to:

$$\Phi^T = \mathbf{p}^T(\mathbf{r})\mathbf{A}^{-1}\mathbf{B} \quad (3.31)$$

The second least squares based technique in shape function construction is the moving least squares approximation. This method is similar to WLS approach and in fact WLS is just a special case of MLS. In this method the field variable is approximated by:

$$u^a(\mathbf{x}) = \sum_{j=1}^m p_j(\mathbf{r})a_j(\mathbf{r}) = \mathbf{p}^T(\mathbf{r})\mathbf{a}(\mathbf{r}) \quad (3.32)$$

From Eq. (3.32) it is easy to see the difference between MLS and WLS; the coefficients are functions of the independent variable \mathbf{r} in the MLS case. To obtain the shape functions of MLS the following functional has to be minimized:

$$J = \sum_{i=1}^n W(\mathbf{r} - \mathbf{r}_i)[\mathbf{p}^T(\mathbf{r}_i)\mathbf{a}(\mathbf{r}) - u_i]^2 \quad (3.33)$$

The MLS shape functions can be obtained by a similar procedure that was used to obtain WLS shape functions:

$$\Phi^T(\mathbf{r}) = \mathbf{p}^T(\mathbf{r})\mathbf{A}^{-1}(\mathbf{r})\mathbf{B}(\mathbf{r}) \quad (3.34)$$

3.4.3 Hermite-type approximation

Treatment of Neumann type boundary conditions is an important issue if a strong-form method is preferred to solve a problem with these type of conditions. If one uses the abovementioned shape functions directly then there will be a significant loss in accuracy. Fortunately there are strategies to prevent this issue and in this subsection, one of them, the Hermite-type approximation, will be introduced. This method can be applied to any shape function discussed above. A brief description for WLS approach will be presented and its detailed version can be found in [17].

Suppose that in addition to n interior and Dirichlet type nodes, n_{NB} Neumann type nodes are created. The field variable is again represented by a series:

$$u^a(\mathbf{r}) = \sum_{i=1}^m p_i(\mathbf{r})a_i = \mathbf{p}^T \mathbf{a} \quad (3.35)$$

To determine the coefficients this series has to be satisfied at the interpolation nodes.

This operation leads to

$$\mathbf{U} = \mathbf{P}_m \mathbf{a} \quad (3.36)$$

for interior and Dirichlet type nodes, as before. For Neumann type nodes

$$\frac{\partial u(\mathbf{r}_i^{NB})}{\partial \mathbf{n}} = l_{xi} \frac{\partial u(\mathbf{r}_i^{NB})}{\partial x} + l_{yi} \frac{\partial u(\mathbf{r}_i^{NB})}{\partial y} \quad (3.37)$$

where \mathbf{n} is the normal vector, and l_{xi} and l_{yi} are the direction cosines. Utilizing (3.37) for all NB nodes

$$\mathbf{U}' = \mathbf{P}_D \mathbf{a} \quad (3.38)$$

where

$$\mathbf{U}'^T = \left\{ \frac{\partial u(\mathbf{r}_1^{DB})}{\partial \mathbf{n}}, \frac{\partial u(\mathbf{r}_2^{DB})}{\partial \mathbf{n}}, \dots, \frac{\partial u(\mathbf{r}_{n_{DB}}^{DB})}{\partial \mathbf{n}} \right\} \quad (3.39)$$

and

$$\mathbf{P}_D = \begin{bmatrix} 0 & l_{x1} & l_{y1} & \dots & l_{x1} \frac{\partial p_m(\mathbf{r}_1^{NB})}{\partial x} + l_{y1} \frac{\partial p_m(\mathbf{r}_1^{NB})}{\partial y} \\ 0 & l_{x2} & l_{y2} & \dots & l_{x2} \frac{\partial p_m(\mathbf{r}_2^{NB})}{\partial x} + l_{y2} \frac{\partial p_m(\mathbf{r}_2^{NB})}{\partial y} \\ \vdots & \vdots & \vdots & \dots & \vdots \\ 0 & l_{xn_{NB}} & l_{yn_{NB}} & \dots & l_{xn_{NB}} \frac{\partial p_m(\mathbf{r}_{n_{NB}}^{NB})}{\partial x} + l_{yn_{NB}} \frac{\partial p_m(\mathbf{r}_{n_{NB}}^{NB})}{\partial y} \end{bmatrix} \quad (3.40)$$

Next, Eqs. (3.36) and (3.38) are combined to get;

$$\mathbf{U}^D = \mathbf{P} \mathbf{a} = \begin{Bmatrix} \mathbf{P}_m \\ \mathbf{P}_D \end{Bmatrix} \mathbf{a} \quad (3.41)$$

where

$$\mathbf{U}^D = \left\{ u(\mathbf{r}_1) \quad \dots \quad u(\mathbf{r}_n) \quad \frac{\partial u(\mathbf{r}_1^{NB})}{\partial \mathbf{n}} \quad \dots \quad \frac{\partial u(\mathbf{r}_{n_{NB}}^{NB})}{\partial \mathbf{n}} \right\}^T \quad (3.42)$$

To obtain the shape functions the following functional is minimized

$$J = \sum_{i=1}^n W_i [u^a(\mathbf{r}_i) - u(\mathbf{r}_i)]^2 + \sum_{j=1}^{n_{NB}} W_j^{NB} \left[\frac{\partial u^a(\mathbf{r}_j^{NB})}{\partial \mathbf{n}} - \frac{\partial u(\mathbf{r}_j^{NB})}{\partial \mathbf{n}} \right]^2 \quad (3.43)$$

which again leads to

$$\mathbf{P}^T \mathbf{W} \mathbf{P} \mathbf{a} = \mathbf{P}^T \mathbf{W} \mathbf{U}^D \quad (3.44)$$

where

$$\mathbf{W} = \begin{bmatrix} \mathbf{W}_0 & \mathbf{0} \\ \mathbf{0} & \mathbf{W}_D \end{bmatrix} \quad (3.45)$$

Here \mathbf{W}_0 and \mathbf{W}_D are again diagonal matrices and same weight functions can be chosen for both Neumann type nodes and other nodes. Now letting

$$\mathbf{A} = (\mathbf{P}^T \mathbf{W} \mathbf{P}) = (\mathbf{P}_m^T \mathbf{W}_0 \mathbf{P}_m) + (\mathbf{P}_D^T \mathbf{W}_D \mathbf{P}_D) \quad (3.46)$$

$$\mathbf{B} = (\mathbf{P}^T \mathbf{W}) = (\mathbf{P}_m^T \mathbf{W}_0) + (\mathbf{P}_D^T \mathbf{W}_D) \quad (3.47)$$

the Hermite type WLS functions can be found as follows:

$$\boldsymbol{\Phi}^T = \mathbf{p}^T \mathbf{A}^{-1} \mathbf{B} \quad (3.48)$$

3.5 Collocation Methods

As discussed at the beginning of this section collocation methods are strong-form techniques in which the approximation proposed for the field variable is directly substituted into the governing differential equation. The global system matrix is formed by collocating the equation at every node in the problem domain and its boundary.

There are two main approaches in the utilization of collocation methods. The first choice is to use a support domain and collocate only with the neighboring nodes. This strategy will yield a sparse matrix. Suppose that there is a 1-D problem and the support domain is arranged so that it only covers the two neighboring points. Then the resultant global system matrix will be a sparse and banded (three-diagonal) one. The other alternative is to use all the nodes to form the matrix. This approach, in which the RBFs are chosen as trial functions, leads to a full system matrix. Although

the RBF collocation technique has a higher computational cost because of its resultant matrix there is a growing interest in this method due to the flexibility of radial basis functions and methods developed to deal with populated matrices.

Collocation methods, whether they result in a full or a sparse matrix, have some significant advantages. First of all they are straightforward since trial functions are directly substituted into the problem. The programming of these methods is easier than those of weak-form methods since there is no need for numerical integration. Also, for the same reason these methods are truly meshless. On the other hand, collocation techniques are not without disadvantages. Weak-form methods are more stable, and when RBF collocation is considered, the ill-conditioning problem of the global system matrix becomes an important issue if the number of nodes is increased. Finally, treatment of Neumann type boundary conditions has to be performed carefully in collocation methods, but weak-form methods have a similar disadvantage when a Dirichlet boundary condition is present.

3.5.1 Local collocation

First, the collocation method with support domains will be briefly presented. To separate it from the RBF collocation, which will be described in the next subsection, this method will be called the local collocation method since support domains localize the calculations.

Application of collocation method is the same whether one deals with a simple ordinary differential equation or a complex system of partial differential equations. For simplicity consider the following boundary value problem defined over a 1-D domain

$$\frac{d^2u}{dx^2} + u = f(x) \quad (3.49)$$

$$u|_{x=a} = g(x) \quad (3.50)$$

$$\left. \frac{du}{dx} \right|_{x=b} = h(x) \quad (3.51)$$

where $f(x)$, $g(x)$ and $h(x)$ are known functions. As shown in Figure 3.2 the domain is represented by N field nodes.

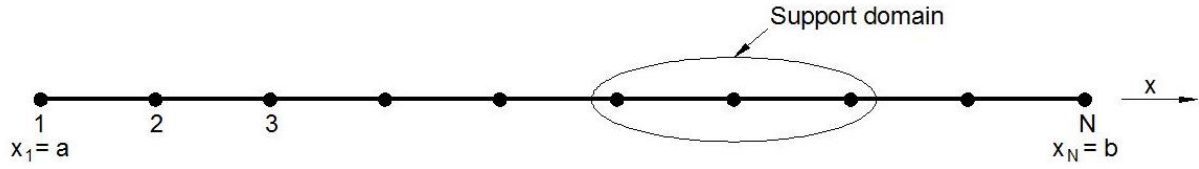


Figure 3.2: 1-D domain of problem Eqs. (3.49)-(3.51).

The first step is to introduce the shape functions (built up by n nodes in the support domain) which yields

$$u_I^a = u^a(x_I) = \Phi^T \mathbf{u} \quad (3.52)$$

$$\frac{\partial u_I^a}{\partial x} = \frac{\partial \Phi^T}{\partial x} \mathbf{u} \quad (3.53)$$

$$\frac{\partial^2 u_I^a}{\partial x^2} = \frac{\partial^2 \Phi^T}{\partial x^2} \mathbf{u} \quad (3.54)$$

where:

$$\Phi^T = \{\phi_1 \quad \phi_2 \quad \cdots \quad \phi_n\} \quad (3.55)$$

$$\mathbf{u}^T = \{u_1 \quad u_2 \quad \cdots \quad u_n\} \quad (3.56)$$

In practice any shape function construction method demonstrated in section 3.4 can be used. For an internal node at x_I

$$\left(\frac{d^2 \Phi^T}{dx^2} + \Phi^T \right) \mathbf{u} = f(x_I) \quad (3.57)$$

or in matrix form:

$$\mathbf{K}_I \mathbf{u} = \mathbf{f}_I \quad (3.58)$$

Here

$$\mathbf{K}_I = \frac{d^2 \Phi^T}{dx^2} + \Phi^T = \left\{ \frac{d^2 \phi_1}{dx^2} + \phi_1 \quad \cdots \quad \frac{d^2 \phi_n}{dx^2} + \phi_n \right\} \quad (3.59)$$

$$\mathbf{f}_I = f(x_I) \quad (3.60)$$

Treatment of Dirichlet boundary conditions is easy:

$$\mathbf{K}_1 \mathbf{u} = g(x_1) \quad (3.61)$$

where

$$\mathbf{K}_1 = \mathbf{\Phi}^T = \{\phi_1 \quad \phi_2 \quad \cdots \quad \phi_n\} \quad (3.62)$$

There are several approaches to impose Neumann type boundary conditions and some of them are presented below [17]:

- 1) The direct collocation method: No special treatment is applied, but there will be a significant decrease in accuracy.
- 2) The method using fictitious points: Additional set of nodes are added outside and/or on the Neumann type boundary.
- 3) The Hermite-type collocation method: Additional derivative variables for the Neumann type boundary nodes are used to enforce the derivative boundary conditions.
- 4) The method using regular grids: Finite difference method is used for the Neumann boundary conditions.
- 5) Hybrid method: A weak-form formulation can be used for the nodes on Neumann type boundary.

Let us illustrate the second approach, in which a fictitious point is added outside the domain to impose the derivative boundary condition. Coordinate of this point is:

$$x_{N+1} = x_N + h \quad (3.63)$$

With this approach an additional degree of freedom, u_{N+1} , is added to the global system matrix

$$\mathbf{K}_{(N+1) \times (N+1)} \mathbf{U}_{(N+1) \times 1} = \mathbf{F}_{(N+1) \times 1} \quad (3.64)$$

where:

$$\mathbf{K}_{(N+1) \times (N+1)} = \begin{bmatrix} K_{11} & K_{12} & \cdots & K_{1N} & K_{1(N+1)} \\ K_{21} & K_{22} & \cdots & K_{2N} & K_{2(N+1)} \\ \vdots & \vdots & \ddots & \vdots & \vdots \\ K_{N1} & K_{N1} & \cdots & K_{NN} & K_{N(N+1)} \\ K_{(N+1)1} & K_{(N+1)2} & \cdots & K_{(N+1)N} & K_{(N+1)(N+1)} \end{bmatrix} \quad (3.65)$$

$$\mathbf{U}_{(N+1) \times 1} = \{u_1 \quad \cdots \quad u_{N-1} \quad u_N \quad u_{N+1}\} \quad (3.66)$$

$$\mathbf{F}_{(N+1) \times 1} = \{g(x_1) \quad f(x_2) \quad \cdots \quad f(x_N) \quad h(x_N)\} \quad (3.67)$$

The first and last rows of the matrix in Eq. (3.65) are related to Dirichlet and Neumann boundary conditions, respectively, and the other rows are associated with the differential equation. Since f , g and h are known functions of x , the unknown coefficients, u_n $n = 1, \dots, N + 1$ can be found from Eq. (3.64) and the numerical solution can be found in a piecewise manner since the nodes are localized by support domains:

$$u^a(x) = \sum_{i=1}^n u_i \phi_i \quad (3.68)$$

3.5.2 RBF collocation

The RBF collocation technique was proposed by Kansa in 1990 to solve fluid dynamics problems [38]. Since that day there is a growing interest in this method and it has been applied to various fields to deal with different kinds of differential, integral and integrodifferential equations.

The solution procedure is similar to that of the local collocation method, and it is even simpler since there are no support domains. Absence of such local domains simplifies the method and also the programming especially for randomly distributed nodes because there is no need to control whether a node is possessed by a specific support domain or not.

In the RBF collocation method, the field variable is simply expanded by a finite set of RBFs and then by using this approximation, the differential equation and its boundary conditions are collocated by utilizing a uniformly or randomly distributed set of nodes. Kansa's method is also known as the asymmetric RBF collocation method because of its asymmetric collocation matrix. In [41] a symmetric version of RBF collocation has been proposed which is based on the Hermite-Birkhoff interpolation.

One of the main concerns of the RBF collocation method is that it results in a full matrix which becomes ill-conditioned as the number of collocation points increases. There are several approaches to overcome the ill-conditioning problem of the collocation matrix such as affine space decomposition [42], matrix preconditioning

[43] and optimization of the shape parameter of the RBF [44]. These techniques come with their computational costs, but they also improve the accuracy of the numerical results.

As for the mathematical background, in [45] it is shown that a general proof for the nonsingularity of the collocation matrix is impossible, but based on numerical evidence it is also stated that singularity happens in rare situations. In [46] the RBF collocation method is compared with Galerkin method using RBFs theoretically and found that the condition number of the global matrix for the collocation method is greater than the Galerkin based technique by one order of magnitude. The situation is worse if the method is compared with the FEM in which the basis functions have local influence resulting in a sparse global solution matrix, but the spectral convergence properties of RBFs that cannot be achieved even with super-convergent adaptive $h - p$ FEM schemes, motivate the use of RBF collocation method.

It has been shown numerically [47] that the RBF collocation method is very accurate, even with a small number of scattered nodes. There are also papers [48,49] which show that the RBF collocation has an higher order of accuracy than the spectral methods and the FEM with linear trial functions.

Before explaining the RBF collocation method it will be useful to give some information on radial basis functions. These functions are being used widely for both function approximation and in the solution of PDEs. There is a wide class of RBFs with different properties and their theoretical background is well established [50,51].

A radial function ψ is a function with the following property [19]:

$$\|\mathbf{r}_1\| = \|\mathbf{r}_2\| \Rightarrow \psi(\mathbf{r}_1) = \psi(\mathbf{r}_2) \quad \mathbf{r}_1, \mathbf{r}_2 \in R^s \quad (3.69)$$

Here $\|\cdot\|$ is some norm on R^s .

Although there are several RBFs in the literature the most well-known and widely used RBFs are the generalized multiquadric (GMQ) and the Gaussian (GA). These globally supported functions are as follows

$$\begin{aligned} \psi_j &= (r^2 + c^2)^q && (GMQ) \\ \psi_j &= \exp(-r^2/c^2) && (GA) \end{aligned} \quad (3.70)$$

where, r is the distance between the nodes, $r = \|\mathbf{x} - \mathbf{x}_j\|_2$, the constant c is called the shape parameter, and q is the exponent of GMQ. These functions are shown in Figures 3.3a and 3.3b, respectively, where $c = 0.1$ and, for the GMQ, the exponent is chosen as $1/2$.

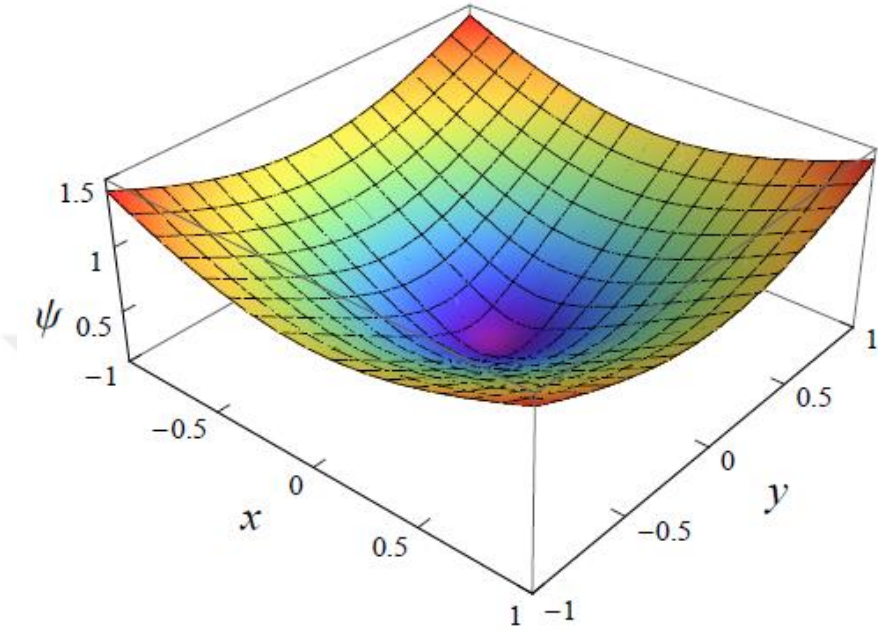


Figure 3.3a: GMQ radial basis function with $q = 1/2$.

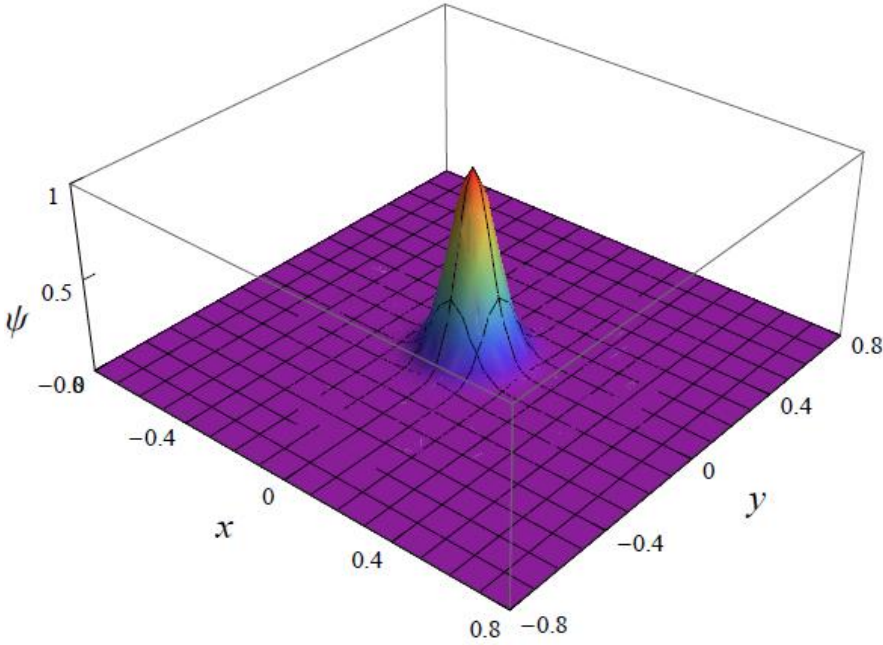


Figure 3.3b: GA radial basis function.

The shape parameter determines the shape of the RBF. As c gets larger the function gets flatter and also its sensitivity to the variation of r decreases. Besides this geometric influence, increasing the value of c improves the accuracy of the approximation and theoretically as $c \rightarrow \infty$, the approximation error vanishes [52]. However, this promising behavior would be possible if one has the chance to perform infinite precision computation. In practice as $c \rightarrow \infty$, the accuracy increases, but the interpolation matrix becomes more and more ill-conditioned and at some point the solution breaks down. This trade-off between accuracy and stability has been explained by Schaback’s “uncertainty principle” [53]. There have been many efforts to treat the ill-conditioning problem caused by the increment of c which includes matrix preconditioning [54], utilizing variable shape parameter strategy [55] and analytical treatment in the $c \rightarrow \infty$ limit [56]. The effect of the shape parameter on the GMQ with $q = 1/2$ is illustrated for one-dimensional case in Figure 3.4.

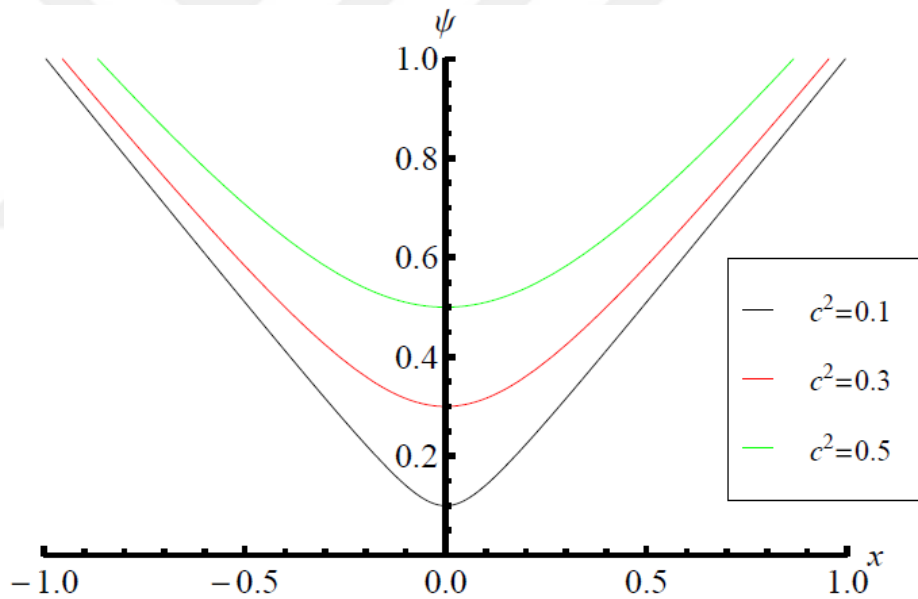


Figure 3.4: Effect of shape parameter on GMQ with $q = 1/2$.

The exponent of the GMQ has an effect similar to that of the shape parameter. Larger q increases the accuracy of the method, but it also results with a less stable algorithm. For the widely-utilized multiquadric (MQ) and inverse multiquadric (IMQ), q takes on the values of $1/2$ and $-1/2$, respectively.

Positive definiteness is a significant property for RBFs since positive definite functions generate positive definite matrices in interpolation, which is important, especially for stable computation. By Micchelli’s theorem [57], the IMQ and GA are

positive definite functions whereas the MQ is conditionally positive definite of order one. The conditional positive definiteness of MQ means that, it is necessary to augment this function by first order monomials as

$$u^a(\mathbf{r}) = \sum_{j=1}^n a_j \psi_j(\mathbf{r}) + \sum_{j=1}^m b_j p_j(\mathbf{r}) \quad (3.71)$$

Now since there are $n + m$ variables an additional set of m equations are needed to obtain a determined system. These can be obtained by

$$\sum_{j=1}^n a_j p_i(\mathbf{r}_j) = 0, \quad i = 1, 2, \dots, m \quad (3.72)$$

Besides this theoretical issue, in numerical experiments it was observed that this augmentation did not improve the results while increasing the condition number [58].

The meshless RBF collocation method is a strong-form method in which the field variable is approximated by a finite series of RBFs. This finite series is directly substituted into the governing PDE and BCs. As stated earlier the critical point in the implementation of the method is the treatment of BCs. When the BCs are of the Neumann or mixed type, the numerical solution is contaminated by the inaccuracy introduced via collocation at the nodes near the boundary of the problem domain. This situation is pointed out by numerical studies [58,59], and Fedoseyev et al. [60] have formulated an improved version of the method. They have added an additional set of nodes and an additional set of collocation equations by collocating the PDE also on the boundary.

Let's now consider the following partial differential equation to describe the RBF collocation method:

$$\nabla^2 u + u = f(x, y) \quad (3.73)$$

$$u(a, y) = u(x, b) = 0 \quad (3.74)$$

$$\frac{\partial u(0, y)}{\partial x} = \frac{\partial u(x, 0)}{\partial y} = 0 \quad (3.75)$$

The domain is represented by N_i internal, N_b boundary and N_{ex} external nodes. Note that external nodes are used because there are Neumann type boundary conditions.

The solution procedure starts with representation of the field variable by a finite series of RBFs

$$u(x, y) = \sum_{j=1}^N a_j \psi_j(x, y) \quad (3.76)$$

where $N = N_i + N_b + N_{ex}$. Substituting Eq. (3.76) into (3.73)-(3.75)

$$\sum_{j=1}^N a_j \left[\frac{\partial^2 \psi_j(x, y)}{\partial x^2} + \frac{\partial^2 \psi_j(x, y)}{\partial y^2} + \psi_j(x, y) \right] = f(x, y) \quad (3.77)$$

$$\sum_{j=1}^N a_j \psi_j(a, y) = \sum_{j=1}^N a_j \psi_j(x, b) = 0 \quad (3.78)$$

$$\sum_{j=1}^N a_j \frac{\partial \psi_j(0, y)}{\partial x} = \sum_{j=1}^N a_j \frac{\partial \psi_j(x, 0)}{\partial y} = 0 \quad (3.79)$$

Collocating Eqs. (3.77)-(3.79)

$$\sum_{j=1}^N a_j \left[\frac{\partial^2 \psi_j(x_i, y_i)}{\partial x^2} + \frac{\partial^2 \psi_j(x_i, y_i)}{\partial y^2} + \psi_j(x_i, y_i) \right] = f_i, \quad i = 1, \dots, N_i \quad (3.80)$$

$$\sum_{j=1}^N a_j \psi_j(a, y_i) = \sum_{j=1}^N a_j \psi_j(x_i, b) = 0, \quad i = N_i + 1, \dots, N_i + N_{b,Dir} \quad (3.81)$$

$$\sum_{j=1}^N a_j \frac{\partial \psi_j(0, y_i)}{\partial x} = \sum_{j=1}^N a_j \frac{\partial \psi_j(x_i, 0)}{\partial y} = 0, \quad i = N_i + N_{b,Dir}, \dots, N_i + N_b \quad (3.82)$$

where $f_i \equiv f(x_i, y_i)$ and the subscript ‘‘Dir’’ stands for Dirichlet BCs. These collocation equations can be expressed in matrix form as

$$\mathbf{Ka} = \mathbf{f} \quad (3.83)$$

Since $f(x, y)$ is a known function, the unknown coefficients can be found from Eq. (3.83), and substituting these into Eq. (3.76) the numerical solution can be obtained.

3.5.3 Weighted RBF collocation method

Although the RBF collocation method has become a popular tool for solving partial differential equations, much of the work deals with single-region problems. There

exist a few papers dealing with more complex heterogeneous media problems. In [61], the subdomain RBF collocation method was used to solve multiregion elasticity problems. According to this study the imposition of interface conditions, in the case of neutron diffusion continuity of flux and current, is necessary and it has an important effect on both the accuracy and convergence of the collocation technique. It is pointed out that to achieve a good accuracy, the number of collocation points should be larger than that of the interpolation points and the numerical solution of the problems is performed in a weighted least squares sense. The weights of the collocation matrix are determined via an error analysis, and it was found that the exponential convergence characteristic of the RBF collocation method can be preserved for multiregion problems if the weights are chosen properly.

The weighted RBF collocation method was introduced by Hu et al. [62]. The Poisson equation and elasticity problems were treated with this method where the overdetermined system is treated with the least squares approximation. This study has shown that the least-squares residual method is an approximation of the direct strong form collocation method. As a heat transfer application, in [63], this weighted collocation method was used to determine the temperature distribution in biological tissues.

The least squares approximation is a useful approach in solving PDEs with the advantage of possessing a positive definite and symmetric matrix. Also, when the finite element literature is considered, the least squares finite element method propounds a uniform solution procedure as compared with the ad hoc treatments of Galerkin methods [64]. On the other hand, least squares approximation has an important drawback when stability is taken into account as a result of quadratically increasing the condition number [65].

To illustrate the method, consider a two-region problem as shown in Figure 3.5, where S_1 and S_2 are two domains with different properties, Γ_V is the vacuum (Dirichlet) boundary, Γ_R is the reflective (Neumann) boundary and Γ_0 is the interface of the two regions. In operator form, the problem can be expressed as

$$L_i \phi_i(\mathbf{r}) = q_i(\mathbf{r}), \quad \mathbf{r} \in S_i, \quad i = 1,2 \quad (3.84)$$

$$\phi_i(\mathbf{r}) = 0, \quad \mathbf{r} \in \Gamma_V, \quad i = 1,2 \quad (3.85)$$

$$\begin{aligned}
\frac{\partial \phi_i(\mathbf{r})}{\partial n} &= 0, \quad \mathbf{r} \in \Gamma_R, \quad i = 1, 2 \\
\phi_1(\mathbf{r}) &= \phi_2(\mathbf{r}), \quad \mathbf{r} \in \Gamma_0 \\
D_1 \frac{\partial \phi_1(\mathbf{r})}{\partial n} &= D_2 \frac{\partial \phi_2(\mathbf{r})}{\partial n}, \quad \mathbf{r} \in \Gamma_0
\end{aligned} \tag{3.86}$$

where q_i is the source term and L_i is some differential operator.

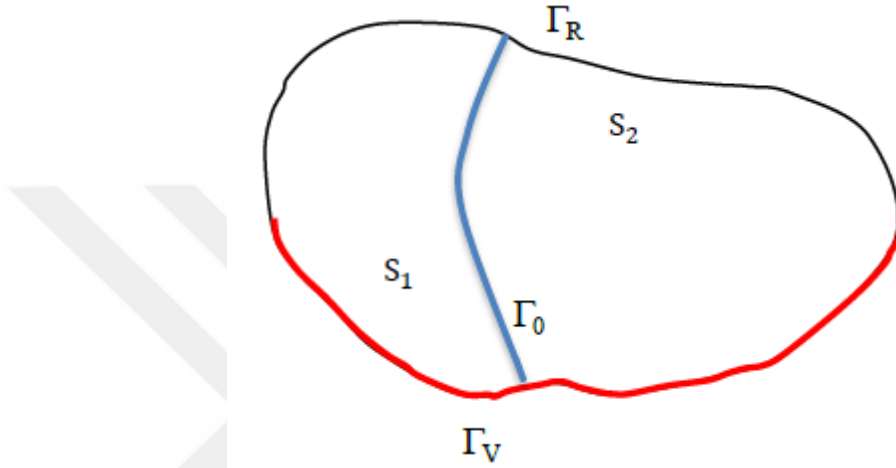


Figure 3.5: A two-region problem.

Formulation of the method starts by defining the weighted least-squares functional

$$\begin{aligned}
I[u_i] &= \frac{1}{2} \left\{ \iint_{S_i} (L_i u_i - q_i)^2 dS + \bar{w}_V \int_{\Gamma_0} (u_1 - u_2)^2 d\Gamma \right. \\
&\quad \left. + \bar{w}_R \int_{\Gamma_0} \left(D_1 \frac{\partial u_1}{\partial n} - D_2 \frac{\partial u_2}{\partial n} \right)^2 d\Gamma + w_{V,i} \int_{\Gamma_V} u_i^2 d\Gamma + w_{R,i} \int_{\Gamma_R} \left(D_i \frac{\partial u_i}{\partial n} \right)^2 d\Gamma \right\}
\end{aligned} \tag{3.87}$$

The weights, $\bar{w}_V, \bar{w}_R, w_{V,i}$ and $w_{R,i}$ give different importance on the interface, vacuum and reflective boundary conditions and hence they provide additional freedom in the choice of the numerical solution [66].

In the least-squares approximation one seeks a solution, ϕ_i , which minimizes the functional in Eq. (3.87):

$$I[\phi_i] = \min_{u_i \in U} I[u_i] \tag{3.88}$$

This procedure, which will be given in detail for the one-group neutron diffusion equation later in Section 5, leads to the bilinear form of Eqs. (3.84)-(3.86):

$$a(\phi, v) = f(v) \quad (3.89)$$

where

$$\begin{aligned} a(\phi, v) \equiv & \iint_{S_i} L_i \phi_i L_i v_i dS + w_{R,i} D_i^2 \int_{\Gamma_R} \frac{\partial \phi_i}{\partial n} \frac{\partial v_i}{\partial n} d\Gamma + w_{V,i} \int_{\Gamma_V} \phi_i v_i d\Gamma \\ & + \bar{w}_R \int_{\Gamma_0} \left(D_1 \frac{\partial \phi_1}{\partial n} - D_2 \frac{\partial \phi_2}{\partial n} \right) \left(D_1 \frac{\partial v_1}{\partial n} - D_2 \frac{\partial v_2}{\partial n} \right) d\Gamma \\ & + \bar{w}_V \int_{\Gamma_0} (\phi_1 - \phi_2)(v_1 - v_2) d\Gamma \\ f(v) \equiv & \iint_{S_i} q_i L_i v_i dS \end{aligned} \quad (3.90)$$

$$f(v) \equiv \iint_{S_i} q_i L_i v_i dS \quad (3.91)$$

Taking into account of the fact that the least-squares residual method is an approximation of the direct strong-form collocation method, the collocation matrix of this least-squares approach is

$$\begin{bmatrix} \mathbf{K}_1 & \mathbf{0} \\ w_{V,1} \mathbf{K}_{d,1} & \mathbf{0} \\ w_{R,1} \mathbf{K}_{n,1} & \mathbf{0} \\ \bar{w}_V \mathbf{I}_{d,1} & \bar{w}_V \mathbf{I}_{d,2} \\ \bar{w}_R \mathbf{I}_{n,1} & \bar{w}_R \mathbf{I}_{n,2} \\ \mathbf{0} & \mathbf{K}_2 \\ \mathbf{0} & w_{V,2} \mathbf{K}_{d,2} \\ \mathbf{0} & w_{R,2} \mathbf{K}_{n,2} \end{bmatrix} \mathbf{a} = \begin{bmatrix} \mathbf{Q}_1 \\ \mathbf{0} \\ \mathbf{0} \\ \mathbf{0} \\ \mathbf{0} \\ \mathbf{Q}_2 \\ \mathbf{0} \\ \mathbf{0} \end{bmatrix} \quad (3.92)$$

Here \mathbf{K}_1 and \mathbf{K}_2 are related to the PDEs, while $\mathbf{K}_{d,i}$ and $\mathbf{K}_{n,i}$ are the collocation matrices of the Dirichlet and Neumann BCs, respectively, and $\mathbf{I}_{d,i}$ and $\mathbf{I}_{n,i}$ are the matrices for the interface conditions.

The success of the weighted RBF collocation method depends on the proper choice of weights appearing in Eq. (3.92). To accomplish this task, first a weighted norm is defined

$$\begin{aligned}
\|v\|_H = & \left\{ \|v\|_{1,S_1}^2 + \|v\|_{1,S_2}^2 + \|Lv\|_{0,S_1}^2 + \|Lv\|_{0,S_2}^2 + w_{V,1}\|v\|_{0,\Gamma_{V,1}}^2 \right. \\
& + w_{V,2}\|v\|_{0,\Gamma_{V,2}}^2 + w_{R,1}\|v\|_{0,\Gamma_{R,1}}^2 + w_{R,2}\|v\|_{0,\Gamma_{R,2}}^2 \\
& \left. + \bar{w}_V\|v_1 - v_2\|_{0,\Gamma_0}^2 + \bar{w}_R \left\| D_1 \frac{\partial v_1}{\partial n} - D_2 \frac{\partial v_2}{\partial n} \right\|_{0,\Gamma_0}^2 \right\}^{1/2}
\end{aligned} \tag{3.93}$$

where the norms on the right hand side of Eq. (3.93) are Sobolev norms. According to [61,62,67-69] if the bilinear form of Eq. (3.89) is continuous, i.e.,

$$a(\phi, v) \leq C \|\phi\|_H \|v\|_H, \quad \forall v \in V \tag{3.94}$$

and coercive, i.e.,

$$a(v, v) \geq C_0 \|v\|_H^2, \quad \forall v \in V \tag{3.95}$$

where V is the space of admissible functions, then the weighted collocation method has the following error bound

$$\|\phi - \phi_h\|_H \leq M \inf_{v \in V} \|\phi - v\|_H \tag{3.96}$$

It should be noted that in [67,68] collocation is performed in a Galerkin sense where the weights are chosen to be the weights of quadrature formula for the integral terms. Inequalities in Eqs. (3.94) and (3.95) form the basis of the Lax-Milgram lemma, and convergence analysis of finite element and spectral collocation methods with the estimate of Eq. (3.96) is presented in [70].

The weights are determined based on Eq. (3.96), and it is obvious that they depend on the differential equation and boundary conditions that govern the problem considered. For the neutron diffusion equation these weights are derived in Section 5.



4. HOMOGENEOUS NEUTRON DIFFUSION PROBLEMS

In this chapter, the numerical solution of the homogeneous neutron diffusion problems in 2-D Cartesian geometry by the meshless RBF collocation method is presented. In this context, first the numerical formulation of the method is given. Both external source and multigroup criticality problems are studied, and the results are discussed in the second section. Finally, some techniques to improve the performance of the RBF collocation method are evaluated.

4.1 Numerical Formulation

When the problem consists of a single square region Eqs. (2.29)-(2.31) reduce to

$$-D_g \nabla^2 \phi_g^{(n)} + \Sigma_{r,g} \phi_g^{(n)} - \sum_{g'=1}^{g-1} \Sigma_{s,g' \rightarrow g} \phi_{g'}^{(n)} = Q_g \quad (4.1)$$

$$Q_g = \begin{cases} 1 \\ \lambda^{(n-1)} \chi_g F^{(n-1)} \\ S_{g,ex} \end{cases}$$

$$F \equiv \sum_{g'=1}^G v_{g'} \Sigma_{f,g'} \phi_{g'} \quad (4.2)$$

$$F^{(1)} = \sum_{g'=1}^G v_{g'} \Sigma_{f,g'} \phi_{g'}^{(1)}, \quad \lambda^{(1)} = \lambda^{(0)} \frac{\int dAF^{(1)}}{\int dAF^{(0)}} \quad (4.3)$$

where $0 \leq x, y \leq a$. Neumann type reflective boundary conditions at the bottom and left sides and vacuum boundary conditions at the right and top sides are considered

$$\begin{aligned} \frac{\partial \phi_g}{\partial y}(x, 0) &= 0, & 0 \leq x < a \\ \phi_g(a, y) &= 0, & 0 \leq y < a \\ \phi_g(x, a) &= 0, & 0 < x \leq a \\ \frac{\partial \phi_g}{\partial x}(0, y) &= 0, & 0 < y \leq a \end{aligned} \quad (4.4)$$

When the medium is nonmultiplying and a one-group energy representation is chosen only the external source terms in Eq. (4.1) exists and one has the Helmholtz equation:

$$-D\nabla^2\phi + \Sigma_a\phi = s_{ex} \quad (4.5)$$

where Σ_a is the absorption cross section.

The numerical formulation of the RBF collocation method starts by introducing a set of internal nodes with N_I members such that

$$I = \{(x_i, y_i): 0 < x < a, 0 < y < a, 1 \leq i \leq N_I\} \quad (4.6)$$

Then a set of reflective boundary nodes with $N_B/2$ members are introduced such that

$$B_R = B_{RB} \cup B_{RL} \quad (4.7)$$

where B_{RB} represent a set of reflective boundary nodes on the bottom side while B_{RL} represent a set of reflective boundary nodes on the left side, that is

$$\begin{aligned} B_{RB} &= \left\{ (x_i, 0): 0 \leq x_i < a, N_I < i \leq N_I + \frac{N_B}{4} \right\} \\ B_{RL} &= \left\{ (0, y_i): 0 < y_i \leq a, N_I + \frac{3N_B}{4} < i \leq N_I + N_B \right\} \end{aligned} \quad (4.8)$$

Also a set of vacuum boundary nodes with $N_B/2$ members such that

$$B_V = B_{VR} \cup B_{VT} \quad (4.9)$$

where B_{VR} represent a set of vacuum boundary nodes on the right side while B_{VT} represent a set of vacuum boundary nodes on the top side. That is:

$$\begin{aligned} B_{VR} &= \left\{ (0, y_i): 0 \leq y_i < a, N_I + \frac{N_B}{4} < i \leq N_I + \frac{N_B}{2} \right\} \\ B_{VT} &= \left\{ (x_i, 0): 0 < x_i \leq a, N_I + \frac{N_B}{2} < i \leq N_I + \frac{3N_B}{4} \right\} \end{aligned} \quad (4.10)$$

Then, the set of boundary nodes B is

$$B = B_R \cup B_V = (B_{RB} \cup B_{RL}) \cup (B_{VR} \cup B_{VT}) \quad (4.11)$$

The set of domain nodes, D is defined as

$$D = I \cup B \quad (4.12)$$

which represents a set with $N_D = N_I + N_B$ members.

Secondly, a set of external nodes, E is introduced. For the purpose of preserving the nonsingularity of the coefficient matrix, the number of members of E has to be equal to N_B . That is:

$$E = \{(x_i, y_i): [(x_i < 0) \vee (x_i > a)] \wedge [(y_i < 0) \vee (y_i > a)], \\ N_D < i \leq N_D + N_B\} \quad (4.13)$$

A typical distribution of nodes with $N_I = 4$ and $N_B = 12$ members is presented in Figure 4.1.

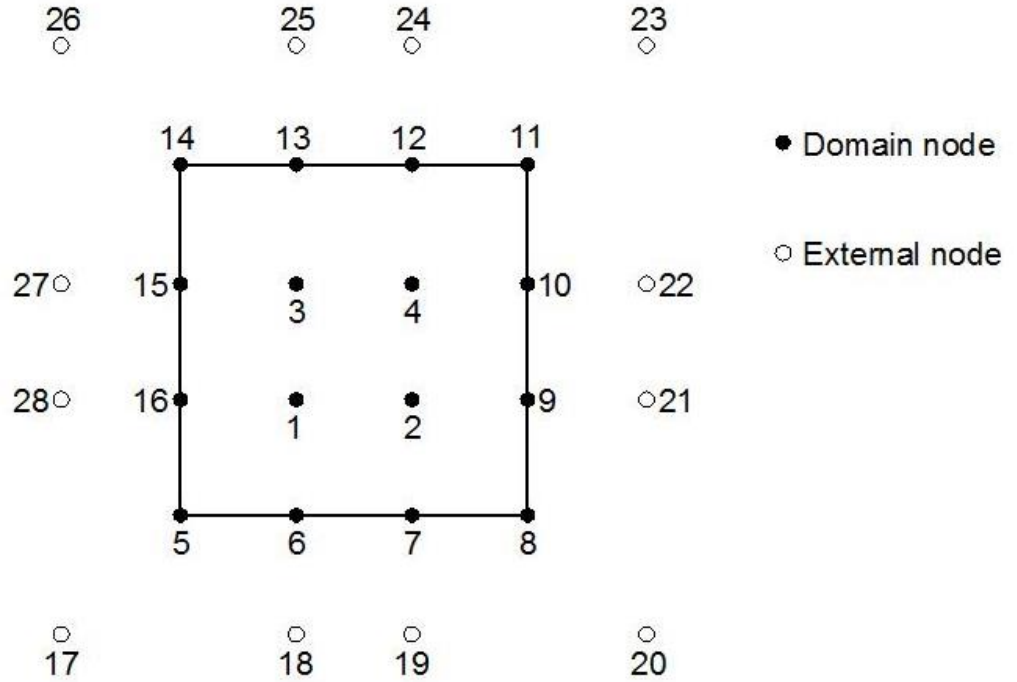


Figure 4.1: A node distribution with $N_I = 4$, $N_B = 12$.

The neutron flux is to be approximated by

$$\tilde{\phi}_g(x, y) \approx \sum_{j=1}^{N_D+N_B} a_{j,g} \psi_j(x, y) \quad (4.14)$$

where $\psi_j(x, y)$ is the radial basis function.

For the first part of the collocation process, the neutron diffusion equation is required to hold for (x_i, y_i) such that $1 \leq i \leq N_D$. Then:

$$\begin{aligned} \sum_{j=1}^{N_D} k_{ij,g}^{DD} a_{j,g}^{D,(n)} - \sum_{j=1}^{N_D} S_{ij,g' \rightarrow g}^{DD} a_{j,g}^{D,(n)} &= \frac{\chi_g F^{(n-1)}}{\lambda^{(n-1)}} + S_{g,ex} \\ \sum_{j=1}^{N_B} k_{ij,g}^{DE} a_{j,g}^{E,(n)} - \sum_{j=1}^{N_B} S_{ij,g' \rightarrow g}^{DE} a_{j,g}^{E,(n)} &= \frac{\chi_g F^{(n-1)}}{\lambda^{(n-1)}} + S_{g,ex} \end{aligned} \quad (4.15)$$

Here

$$\begin{aligned} k_{ij,g}^{DD} &= -D_g \nabla^2 \psi_j(x_i, y_i) + \Sigma_{r,g} \psi_j(x_i, y_i), & 1 \leq j \leq N_D \\ k_{ij,g}^{DE} &= -D_g \nabla^2 \psi_{j+N_D}(x_i, y_i) + \Sigma_{r,g} \psi_{j+N_D}(x_i, y_i), & 1 \leq j \leq N_B \\ S_{ij,g' \rightarrow g}^{DD} &= \Sigma_{s,g' \rightarrow g} \psi_j(x_i, y_i), & 1 \leq j \leq N_D \\ S_{ij,g' \rightarrow g}^{DE} &= \Sigma_{s,g' \rightarrow g} \psi_{j+N_D}(x_i, y_i), & 1 \leq j \leq N_B \\ a_{j,g}^{D,(n)} &= a_{j,g}^{(n)}, & 1 \leq j \leq N_D \\ a_{j,g}^{E,(n)} &= a_{j+N_D,g}^{(n)}, & 1 \leq j \leq N_B \\ S_{g,ext} &= S_{g,ext}(x_i, y_i), \end{aligned} \quad (4.16)$$

where $1 \leq i \leq N_D$.

The collocation is completed by requiring the reflective and vacuum boundary conditions to hold for points (x_i, y_i) which are members of B_R and B_V respectively.

That is:

$$\sum_{j=1}^{N_D} k_{ij}^{BD} a_{j,g}^{D,(n)} + \sum_{j=1}^{N_B} k_{ij}^{BE} a_{j,g}^{E,(n)} = 0, \quad 1 \leq i \leq N_B \quad (4.17)$$

where

$$k_{ij}^{BD} = \begin{cases} \frac{\partial \psi_j}{\partial y}(x_{i+N_I}, y_{i+N_I}), & 1 \leq i \leq \frac{N_B}{4} \\ \frac{\partial \psi_j}{\partial x}(x_{i+N_I}, y_{i+N_I}), & \frac{3N_B}{4} < i \leq N_B \\ \psi_j(x_{i+N_I}, y_{i+N_I}), & \frac{N_B}{4} < i \leq \frac{3N_B}{4} \end{cases} \quad (4.18)$$

for $1 \leq j \leq N_D$ and

$$k_{ij}^{BE} = \begin{cases} \frac{\partial \psi_{j+N_D}}{\partial y}(x_{i+N_I}, y_{i+N_I}), & 1 \leq i \leq \frac{N_B}{4} \\ \frac{\partial \psi_{j+N_D}}{\partial x}(x_{i+N_I}, y_{i+N_I}), & \frac{3N_B}{4} < i \leq N_B \\ \psi_{j+N_D}(x_{i+N_I}, y_{i+N_I}), & \frac{N_B}{4} < i \leq \frac{3N_B}{4} \end{cases} \quad (4.19)$$

for $1 \leq j \leq N_B$.

The collocation equations, Eqs. (4.15) and (4.17), can be combined and written in the block-matrix form:

$$\begin{bmatrix} \mathbf{K}_1 & \mathbf{0} & \mathbf{0} & \mathbf{0} \\ -\mathbf{S}_{1 \rightarrow 2} & \mathbf{K}_2 & \mathbf{0} & \mathbf{0} \\ \vdots & \vdots & \ddots & \mathbf{0} \\ -\mathbf{S}_{1 \rightarrow G} & -\mathbf{S}_{2 \rightarrow G} & \cdots & \mathbf{K}_G \end{bmatrix} \begin{bmatrix} \mathbf{a}_1^{(n)} \\ \mathbf{a}_2^{(n)} \\ \vdots \\ \mathbf{a}_G^{(n)} \end{bmatrix} = \begin{bmatrix} \mathbf{Q}_1 \\ \mathbf{Q}_2 \\ \vdots \\ \mathbf{Q}_G \end{bmatrix} \quad (4.20)$$

The lower triangular structure of the collocation matrix in Eq. (4.20) is a consequence of the no upscattering assumption (i.e., neutrons do not gain energy in scattering reactions).

In Eq. (4.20), the elements of the global system matrix are block matrices themselves. For every energy group an $(N_D + N_B) \times (N_D + N_B)$ system of equations has to be solved. As an example for the first group one has to deal with

$$\begin{bmatrix} \mathbf{K}_1^{DD} & \mathbf{K}_1^{DE} \\ \mathbf{K}_1^{BD} & \mathbf{K}_1^{BE} \end{bmatrix} \begin{bmatrix} \mathbf{a}_1^{D,(n)} \\ \mathbf{a}_1^{E,(n)} \end{bmatrix} = \begin{bmatrix} \mathbf{Q}_1 \\ \mathbf{0} \end{bmatrix} \quad (4.21)$$

where \mathbf{K}_1^{DD} and \mathbf{K}_1^{BE} are square matrices of dimension N_D and N_B respectively. The matrix \mathbf{K}_1^{BD} is rectangular with dimensions $N_B \times N_D$, while \mathbf{K}_1^{DE} is again rectangular with dimensions $N_D \times N_B$. $\mathbf{a}_1^{D,(n)}$ and \mathbf{Q}_1 vectors are N_D dimensional while the vector $\mathbf{a}_1^{E,(n)}$ is N_B dimensional. Solution of Eq. (4.21) yields $\mathbf{a}_1^{D,(n)}$ and hence the numerical result.

The linear system in block-matrix form can be subjected to block-LU decomposition by:

$$\begin{bmatrix} \mathbf{K}^{DD} & \mathbf{K}^{DE} \\ \mathbf{K}^{BD} & \mathbf{K}^{BE} \end{bmatrix} = \begin{bmatrix} \mathbf{K}^{DD} & \mathbf{0}^{DE} \\ \mathbf{K}^{BD} & \mathbf{L}^{BE} \end{bmatrix} \begin{bmatrix} \mathbf{I}^{DD} & \mathbf{U}^{DE} \\ \mathbf{0}^{BD} & \mathbf{I}^{BE} \end{bmatrix} \quad (4.22)$$

Here $\mathbf{0}^{DE}$ and $\mathbf{0}^{BD}$ are rectangular matrices consisting of zero entries which are $N_D \times N_B$ and $N_B \times N_D$ dimensional, respectively, and the subscript g is omitted to simplify the notation. The identity matrices, \mathbf{I}^{DD} and \mathbf{I}^{BE} are N_D and N_B dimensional, respectively. From the matrix equality, it follows:

$$\begin{aligned}\mathbf{U}^{DE} &= (\mathbf{K}^{DD})^{-1} \mathbf{K}^{DE} \\ \mathbf{L}^{BE} &= \mathbf{K}^{BE} - \mathbf{K}^{BD} \mathbf{U}^{DE}\end{aligned}\quad (4.23)$$

The determination of \mathbf{U}^{DE} requires the solution of N_B linear systems of dimension N_D . Since the coefficient matrix \mathbf{K}^{DD} does not change, an LU decomposition of \mathbf{K}^{DD} for once is sufficient for the solution of the N_B linear systems.

Once \mathbf{U}^{DE} and \mathbf{L}^{BE} are determined, the algorithm

$$\begin{aligned}\mathbf{y}^{D,(n)} &= (\mathbf{K}^{DD})^{-1} (\mathbf{F}^{D,(n-1)} + \mathbf{Q}) \\ \mathbf{y}^{B,(n)} &= -(\mathbf{L}^{BE})^{-1} \mathbf{K}^{BD} \mathbf{y}^{D,(n)} \\ \mathbf{a}^{E,(n)} &= \mathbf{y}^{B,(n)} \\ \mathbf{a}^{D,(n)} &= \mathbf{y}^{D,(n)} - \mathbf{U}^{DE} \mathbf{a}^{E,(n)}\end{aligned}\quad (4.24)$$

yields the desired solution.

4.2 Results and Discussion

In order to assess the performance of the meshless RBF collocation method several examples are considered. First, a 1-group external source case is studied, which is followed by 1-,2-,3- and 4-group fission source problems. For the external source and 4- group fission source problems, the RBF collocation method is compared with finite element [71] and boundary element [72] methods. All calculations are performed in FORTRAN with double precision.

4.2.1 External source problem

For the external source problem three types of sources are treated:

$$\begin{aligned}s_1(x, y) &= S_0 & 0 \leq x \leq a, \quad 0 \leq y \leq a \\ s_2(x, y) &= \cos\left(\frac{\pi x}{2a}\right) \cos\left(\frac{\pi y}{2a}\right) & 0 \leq x \leq a, \quad 0 \leq y \leq a \\ s_3(x, y) &= \begin{cases} 1 - \frac{x}{a} & 0 \leq y \leq x \leq a \\ 1 - \frac{y}{a} & 0 \leq x \leq y \leq a \end{cases}\end{aligned}\quad (4.25)$$

The trigonometric and linear sources are presented in Figure 4.2. The analytical solutions corresponding to these sources are as follows [73]

$$\begin{aligned}
 \varphi_1(x, y) &= \left(\frac{4}{\pi}\right)^2 \frac{S_0}{\Sigma_a} \sum_{\substack{n=1 \\ n \text{ odd}}}^{\infty} \sum_{\substack{m=1 \\ m \text{ odd}}}^{\infty} \frac{(-1)^{\frac{n+m}{2}+1}}{nm} \frac{\cos\left(\frac{n\pi x}{\tilde{a}}\right) \cos\left(\frac{m\pi y}{\tilde{a}}\right)}{1 + L^2 \left[\left(\frac{n\pi}{\tilde{a}}\right)^2 + \left(\frac{m\pi}{\tilde{a}}\right)^2 \right]} \\
 \varphi_2(x, y) &= \frac{1}{\Sigma_a \left[1 + 2L^2 \left(\frac{\pi}{\tilde{a}}\right)^2 \right]} \cos\left(\frac{\pi x}{\tilde{a}}\right) \cos\left(\frac{\pi y}{\tilde{a}}\right) \\
 \varphi_3(x, y) &= \frac{8}{\pi^2 \Sigma_a} \sum_{\substack{n=1 \\ n \text{ odd}}}^{\infty} \frac{\cos\left(\frac{n\pi x}{\tilde{a}}\right) \cos\left(\frac{m\pi y}{\tilde{a}}\right)}{n^2 \left[1 + 2L^2 \left(\frac{n\pi}{\tilde{a}}\right)^2 \right]}
 \end{aligned} \tag{4.26}$$

where $\tilde{a} = 2a$ and $L = \sqrt{D/\Sigma_a}$ is the diffusion length.

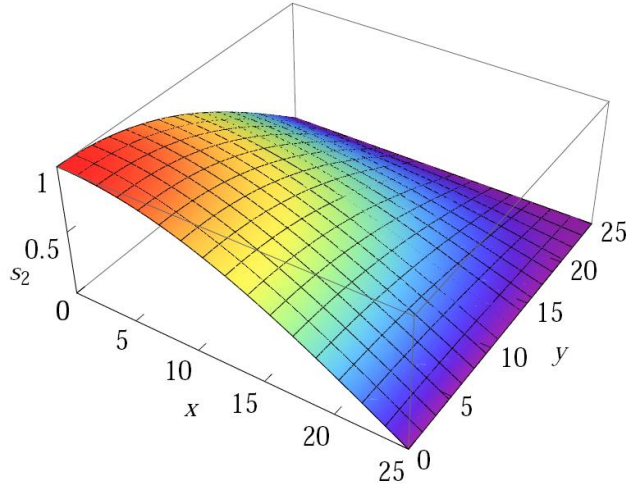


Figure 4.2a: Graphical representation of the trigonometric source.

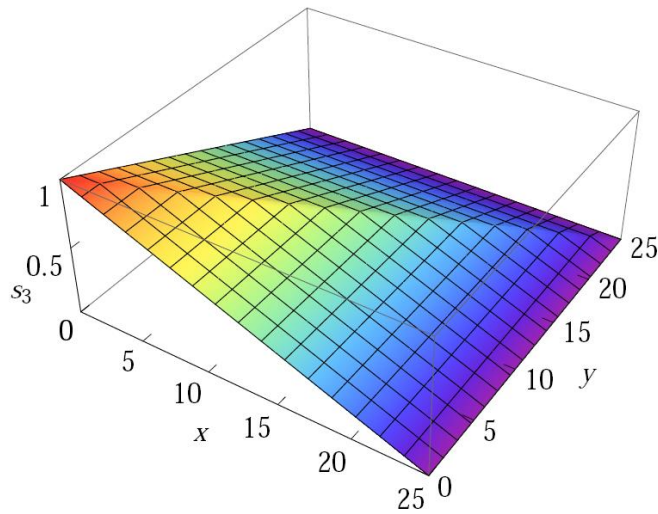


Figure 4.2b: Graphical representation of the linear source.

The diffusion constant and the diffusion length are chosen as 1.77764 cm and, 11.1232 cm respectively. For the constant source problem the source rate is taken to be $S_0 = 1 \text{ n/cm}^3\text{s}$. Accuracy of the methods is tested via calculating the root mean square (RMS) and pointwise percent errors, which are defined as

$$\epsilon_{rms} = \sqrt{\frac{1}{N_D} \sum_{i=1}^{N_D} [\phi_s(x_i, y_i) - \tilde{\phi}_s(x_i, y_i)]^2} \quad (4.27)$$

$$\epsilon_{max} = \max_{1 \leq i \leq N_D} [|\phi_s(x_i, y_i) - \tilde{\phi}_s(x_i, y_i)| \times 100 / \phi_s(x_i, y_i)] \quad (4.28)$$

where $\tilde{\phi}_s$ is the numerical solution and, $s = 1, 2, 3$ corresponds to constant, trigonometric and linear sources respectively.

The infinite series of the analytical solutions for constant and linear sources are approximated by setting the upper limits of series to 250. In all tests uniformly scattered sets of nodes with different fill distances, h , are utilized. The nodes that are outside the domain are located by a distance of h to the nearest boundary node.

The RBF collocation method is invariant under uniform scaling [74] and computations are carried out on a domain scaled to $[0, 1]^2$. This is done by simply multiplying the elements of \mathbf{K}^{DD} by $1/a^2$. In all tests a is chosen to be 25 cm.

First, the effect of the shape parameter, c , on the accuracy and stability of the RBF collocation method is examined. In Figure 4.3 (a)-(c) the variation of RMS errors with the shape parameter in case of linear source, s_3 , when $N = 40$ for MQ, IMQ and GA, respectively, where N is the inverse of the fill distance is presented. It can be inferred from this figure that there is an optimum shape parameter value for all basis functions, and as c increases the RMS error first decreases and then at some point it starts to oscillate and the accuracy decreases sharply if one continues to increase the shape parameter. This result is expected since as c increases the solution matrix becomes singular. It is seen from this figure that the MQ and IMQ results in a better performance than the GA. Also the GA has a narrower range of maneuvering for the shape parameter. This sensitivity of GA to c has also been reported by Cheng et al. [47].

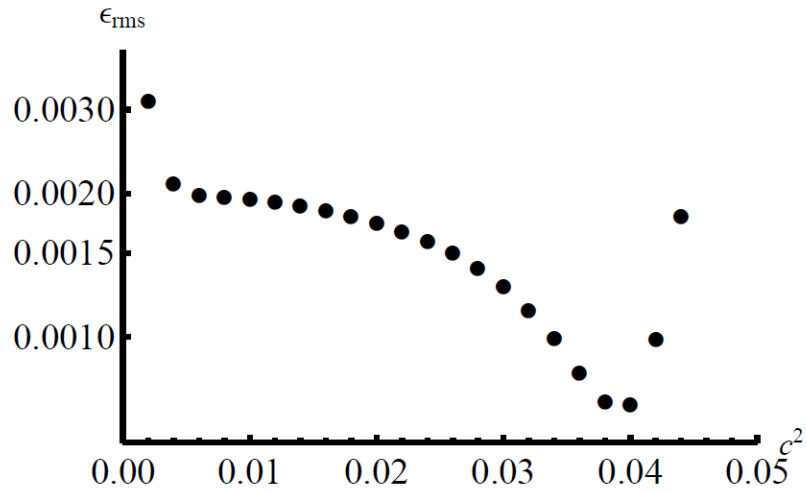


Figure 4.3a: Variation of the RMS error with c in the case of s_3 for MQ.

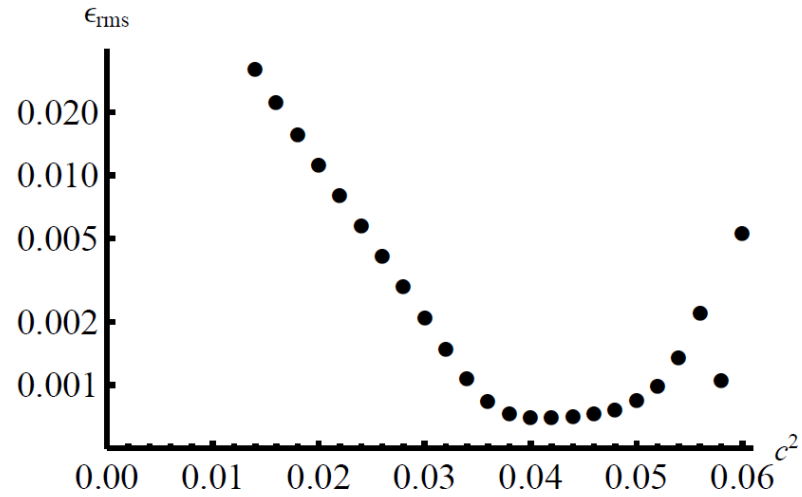


Figure 4.3b: Variation of the RMS error with c in the case of s_3 for IMQ.

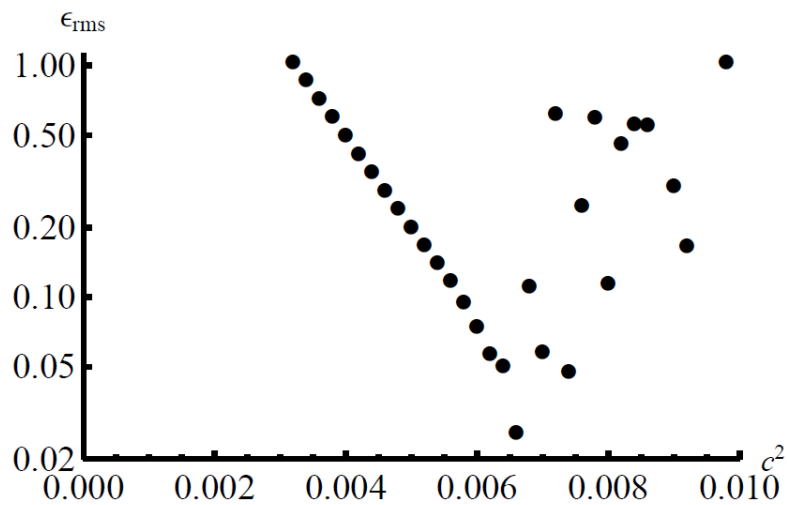


Figure 4.3c: Variation of the RMS error with c in the case of s_3 for GA.

The shape parameter dependence of RMS errors were also studied for constant and trigonometric sources, and the results are given in Figure 4.4 where $N = 40$. Once again, for all basis functions considered, there exists a minimum RMS error with respect to the shape parameter, and the MQ and IMQ are superior to the GA in terms of both accuracy and stable range of computation.

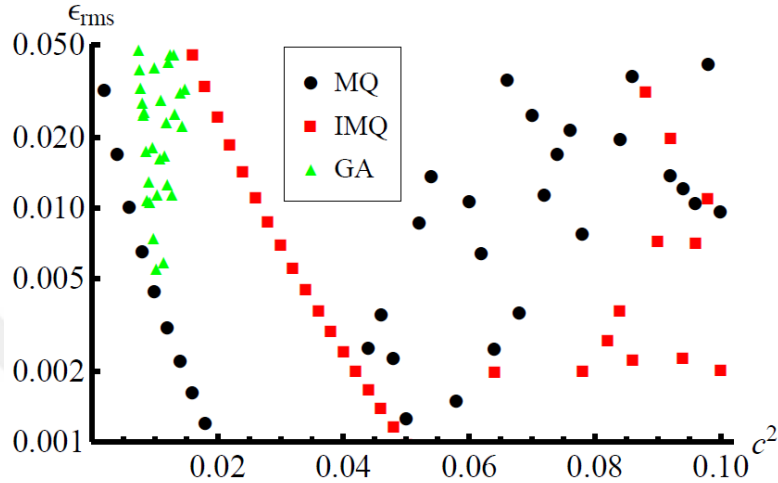


Figure 4.4a: Variation of the RMS error with shape parameter for s_1 .

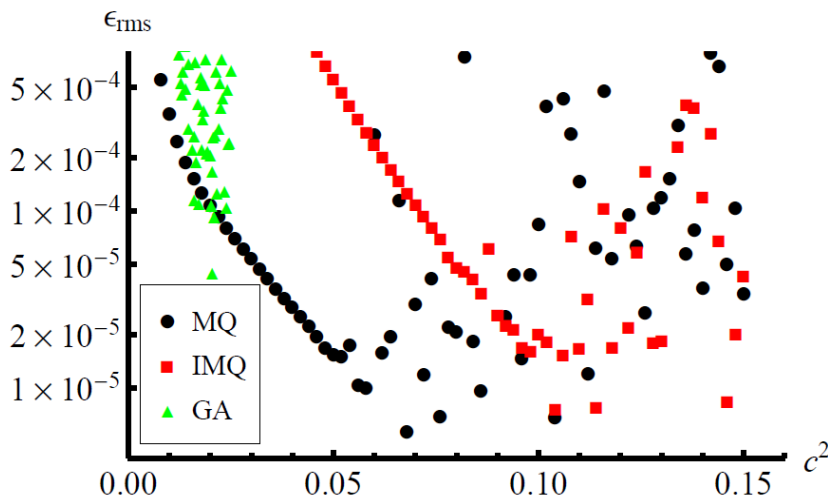


Figure 4.4b: Variation of the RMS error with shape parameter for s_2 .

The shape parameter has an important effect on the convergence rate of the RBF collocation method. In Figure 4.5 (a)-(c) the variation of RMS errors with N for the MQ, IMQ and GA, respectively, in the case of the constant source, s_1 , for three values of c in semi-log scale is shown. Continuous lines are obtained by fitting the RMS error data in the form of $\epsilon_{RMS} \sim O(m \exp(-n/h))$. The constants m and n are given in Table 4.1. It is clear from this figure that there exists an exponential

convergence rate and the accuracy of solution increases with increasing shape parameter, which also enhances the convergence rate, for all basis functions. It can also be observed from Figure 4.5 that the GA has performed poorly for sparse sets of nodes where MQ and IMQ gave a reasonable accuracy.

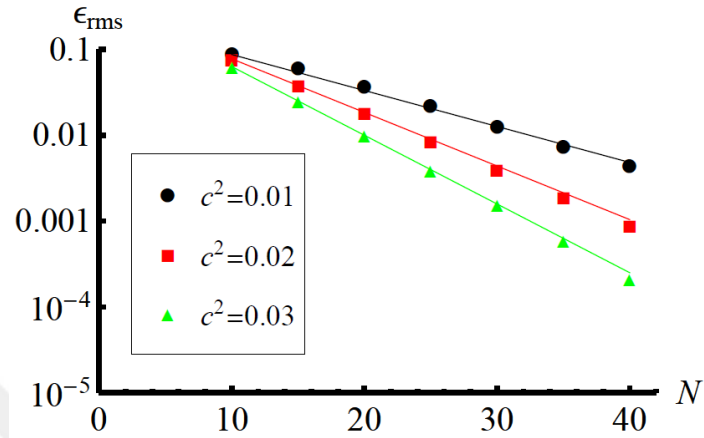


Figure 4.5a: Variation of the RMS error with fill distance for MQ in case of s_1 .

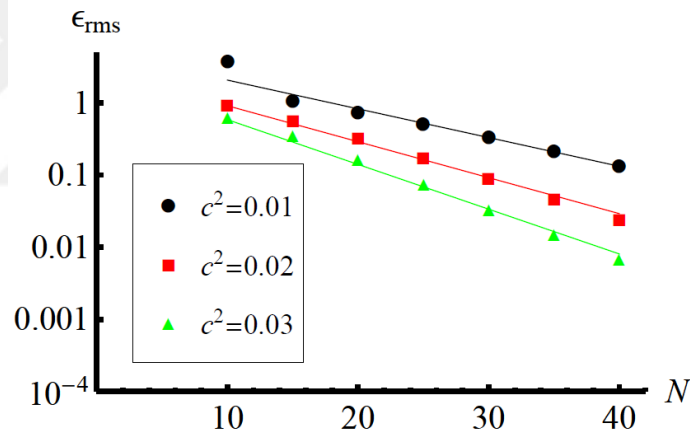


Figure 4.5b: Variation of the RMS error with fill distance for IMQ in case of s_1 .

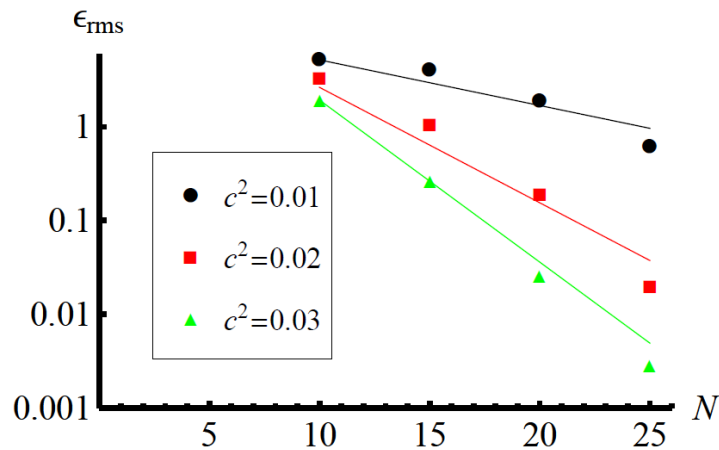


Figure 4.5c: Variation of the RMS error with fill distance for GA in case of s_1 .

Table 4.1: Values of m and n in $\epsilon_{RMS} \sim O(m \exp(-n/h))$ for the constant source problem.

	MQ			IMQ			GA		
c^2	0.01	0.02	0.03	0.01	0.02	0.03	0.01	0.02	0.03
m	0.227	0.325	0.396	5.169	2.874	2.442	15.90	45.05	103.7
n	0.096	0.144	0.184	0.092	0.115	0.143	0.112	0.284	0.398

A noticeable result of Table 4.1 is the much higher m values of the GA than MQ and IMQ. Huang et al. [75] have reported exponential convergence rates of $\epsilon \sim O(\exp(bc^{3/2}) \Lambda^{c^{1/2}/h})$ and $\epsilon \sim O(\exp bc^4 \Lambda^{c/h})$ for IMQ and GA, respectively, where $0 < \Lambda < 1$ and $b > 0$, for the solution of the Poisson equation. Since c has a larger exponent for the convergence rate of GA, the m values of Table 4.1 are in well agreement with the estimates of [75].

The results of RMS errors with fill distance, when trigonometric and linear sources are considered, are similar to those presented in Figure 4.5 and Table 4.1. The RMS errors diminish exponentially with increasing N and the shape parameter improves both accuracy and convergence rate of the method. GA produces less accurate results for sparse sets of nodes.

In Figure 4.6 (a)-(c) the convergence curves of the RBF collocation method with MQ and IMQ are plotted together with the FEM and BEM (boundary element method) for the constant, trigonometric and linear sources, respectively. For collocation, the shape parameter is chosen as $c^2 = 0.1$ for both MQ and IMQ. FEM is employed by discretizing the 2D domain with linear triangular elements, while BEM utilizes linear elements for the discretization along the system boundary. First of all, it is observed from this figure that the collocation method converges faster than FEM and BEM for all cases. MQ collocation provided more accurate results than both FEM and BEM for s_1 and s_2 . When $N = 20$, the RMS error of MQ is better by at least one order of magnitude. In the case of linear source, s_3 , to obtain a more accurate solution than FEM and BEM, the MQ collocation should have $N > 20$.

To observe the effect of source type on convergence rate, the data presented in Figure 4.6 is fitted exponentially for MQ and IMQ in the form of $\epsilon_{RMS} \sim O(m \exp(-n/h))$, and algebraically for FEM and BEM in the form of $\epsilon_{RMS} \sim O(ph^{-r})$. The values of the constants m , n , p and r are given Table 4.2. This

table shows that, when RBF collocation and BEM are used the fastest convergence rate is found for the constant source problem, while FEM has the best rate for the trigonometric source.

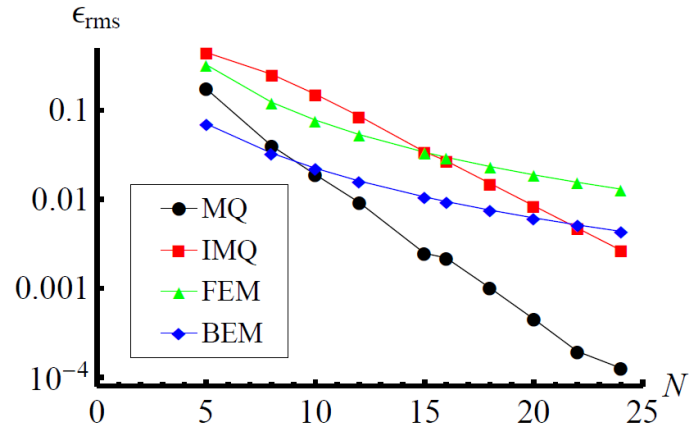


Figure 4.6a: Comparison of the performance of MQ and IMQ collocation with FEM and BEM for s_1 .

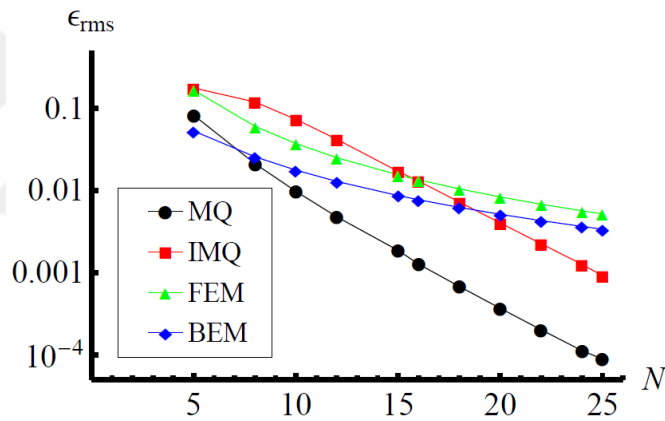


Figure 4.6b: Comparison of the performance of MQ and IMQ collocation with FEM and BEM for s_2 .

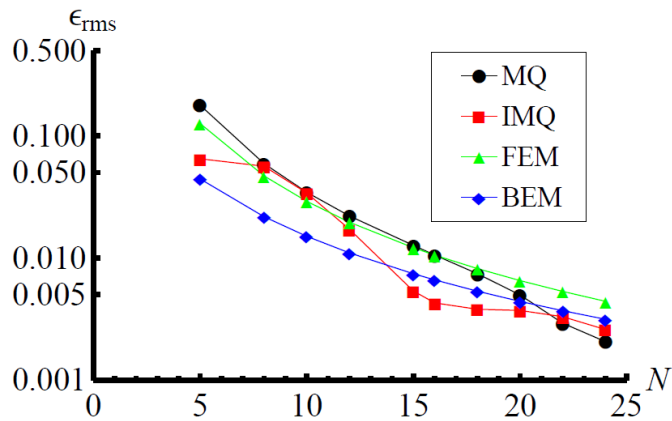


Figure 4.6c: Comparison of the performance of MQ and IMQ collocation with FEM and BEM for s_3 .

Table 4.2: The values of the constants for the exponential fit $\epsilon_{RMS} \sim O(m \exp(-n/h))$, and algebraic fit $\epsilon_{RMS} \sim O(ph^{-r})$.

Source type	MQ		IMQ		FEM		BEM	
	m	n	m	n	p	r	p	r
s_1	1.831	0.420	1.427	0.257	9.025	2.063	1.102	1.703
s_2	0.729	0.377	0.502	0.241	5.310	2.156	0.736	1.634
s_3	0.508	0.235	0.173	0.202	3.844	2.122	0.560	1.613

Despite the better accuracy and convergence characteristics of the collocation method, FEM and BEM have a significant advantage, when stability is considered, owing to their weak-form formulation and local approximation nature. As an example, the MQ collocation becomes unstable for $N \geq 30$ when $c^2 = 0.1$, while FEM and BEM preserve their stability. The instability of the MQ collocation can be treated by decreasing the value of c , but this results in less accurate solutions. There is a trade-off, that is, if one increases the value of c indefinitely for the sake of accuracy, it results with the loss of stability.

A simple strategy to improve the accuracy of RBF collocation without causing instability is to select an optimum value of c . In Tables 4.3-4.5 the optimum shape parameter values with corresponding RMS and maximum pointwise percent errors for constant, trigonometric and linear sources are presented, respectively. These calculations are carried out with three fill distances. The optimum shape parameters are the ones that result in minimum RMS errors. In these tables the FEM and BEM solutions to the problems considered are also given.

It is observed from Tables 4.3-4.5 that the MQ, IMQ and GA RBFs have exhibited a good performance in the numerical solution of the neutron diffusion equation and yield highly accurate numerical solutions, when the shape parameter is optimized. For the constant and linear sources, MQ and IMQ gave better results than the GA, especially as N increases. The MQ solution is better than the GA solution by two orders of magnitude for the constant source when $N = 50$. In the case of trigonometric source, the performance of RBFs is similar, and the best solution was obtained by the GA when $N = 25$. It is also seen that the value of the optimum c^2 decreases as the fill distance decreases, except the MQ for the linear source and GA for the trigonometric source.

Table 4.3: RMS and maximum pointwise errors of RBF collocation, FEM and BEM together with optimum c^2 values for MQ, IMQ and GA for s_1 .

N	Method	c^2	ϵ_{max}	ϵ_{rms}
10	MQ	0.8843	7.35×10^{-2}	1.07×10^{-3}
	IMQ	1.1042	7.11×10^{-2}	9.53×10^{-4}
	GA	0.2152	9.42×10^{-2}	1.73×10^{-3}
	FEM	-	1.68	7.78×10^{-2}
	BEM	-	3.62×10^{-1}	2.24×10^{-2}
25	MQ	0.0790	1.03×10^{-1}	1.39×10^{-4}
	IMQ	0.1685	7.15×10^{-2}	1.20×10^{-4}
	GA	0.0269	1.19×10^{-1}	2.01×10^{-3}
	FEM	-	1.29	1.20×10^{-2}
	BEM	-	1.69×10^{-1}	4.04×10^{-3}
50	MQ	0.0258	3.77×10^{-2}	4.93×10^{-5}
	IMQ	0.0470	4.43×10^{-2}	1.62×10^{-4}
	GA	0.0109	2.66×10^{-1}	4.87×10^{-3}
	FEM	-	9.96×10^{-1}	2.96×10^{-3}
	BEM	-	1.88×10^{-1}	1.04×10^{-3}

Table 4.4: RMS and maximum pointwise errors of RBF collocation, FEM and BEM together with optimum c^2 values for MQ, IMQ and GA for s_2 .

N	Method	c^2	ϵ_{max}	ϵ_{rms}
10	MQ	2.4473	3.78×10^{-4}	3.39×10^{-6}
	IMQ	3.3799	1.42×10^{-4}	2.24×10^{-6}
	GA	0.4551	3.28×10^{-5}	5.42×10^{-7}
	FEM	-	7.87×10^{-1}	3.71×10^{-2}
	BEM	-	1.68×10^{-1}	1.76×10^{-2}
25	MQ	0.2773	6.30×10^{-4}	2.66×10^{-6}
	IMQ	0.2872	9.45×10^{-4}	1.04×10^{-6}
	GA	1.1450	6.96×10^{-3}	4.44×10^{-6}
	FEM	-	1.65×10^{-1}	5.16×10^{-3}
	BEM	-	3.36×10^{-2}	3.37×10^{-3}
50	MQ	0.0382	8.44×10^{-3}	1.57×10^{-6}
	IMQ	0.0782	2.82×10^{-2}	3.92×10^{-6}
	GA	0.2250	5.24×10^{-2}	8.06×10^{-6}
	FEM	-	4.85×10^{-2}	1.21×10^{-3}
	BEM	-	9.20×10^{-3}	8.97×10^{-4}

Table 4.5: RMS and maximum pointwise errors of RBF collocation, FEM and BEM together with optimum c^2 values for MQ, IMQ and GA for s_3 .

N	Method	c^2	ϵ_{max}	ϵ_{rms}
10	MQ	0.0068	9.08×10^{-1}	8.99×10^{-3}
	IMQ	0.6016	7.84×10^{-1}	1.06×10^{-2}
	GA	0.0875	1.42	1.08×10^{-2}
	FEM	-	8.13×10^{-1}	2.91×10^{-2}
	BEM	-	1.96×10^{-1}	1.50×10^{-2}
25	MQ	0.0902	2.28×10^{-1}	1.79×10^{-3}
	IMQ	0.0660	4.73×10^{-1}	1.72×10^{-3}
	GA	0.0177	7.59×10^{-1}	5.90×10^{-3}
	FEM	-	1.83×10^{-1}	4.05×10^{-3}
	BEM	-	4.24×10^{-2}	2.92×10^{-3}
50	MQ	0.0261	6.70×10^{-1}	4.14×10^{-4}
	IMQ	0.0304	1.16×10^{-1}	5.44×10^{-4}
	GA	0.0043	8.53	3.78×10^{-2}
	FEM	-	5.60×10^{-2}	9.39×10^{-4}
	BEM	-	1.41×10^{-2}	7.82×10^{-4}

When the performance of FEM and BEM is compared with those of RBF collocation, it is seen that for all sources considered the RBF collocation method with MQ and IMQ give better performance than both FEM and BEM at all values of N . For the constant source, when $N = 50$, the MQ results with a solution that is two orders of magnitude more accurate than FEM and BEM, and the GA becomes less accurate than these mesh-based methods. For the trigonometric source it is observed that RBF collocation outperforms both FEM and BEM, especially for sparse sets of nodes. In all cases collocation solutions are better than the solutions of FEM and BEM by at least two orders of magnitude. RBFs have also worked well for the linear source problem, but the GA performed poorly for the linear source when $N = 50$ yielding a result two orders of magnitude less accurate than all other methods.

The results of Tables 4.3-4.5 point out the importance of shape parameter optimization for the collocation method. By carefully selecting the value of c , highly accurate results can be obtained even with low N . Optimization also helps to increase N in a stable manner without utilizing algorithms such as domain decomposition and matrix preconditioning.

Next, the central processing unit (CPU) time of the RBF collocation method is compared with those of FEM and BEM. In Figure 4.7, the CPU times of MQ

collocation together with FEM and BEM in the case of constant source is presented in semi-log scale. The shape parameter, which does not affect the computation time, is chosen as $c^2 = 0.01$. It is clear from this figure that the FEM is superior to the RBF collocation method when the CPU time is taken into account, and the collocation method is more efficient than the BEM. The superiority of FEM is due to the sparse and symmetric nature of the resulting coefficient matrix. It should be noted that similar results are obtained for other source types and RBFs.

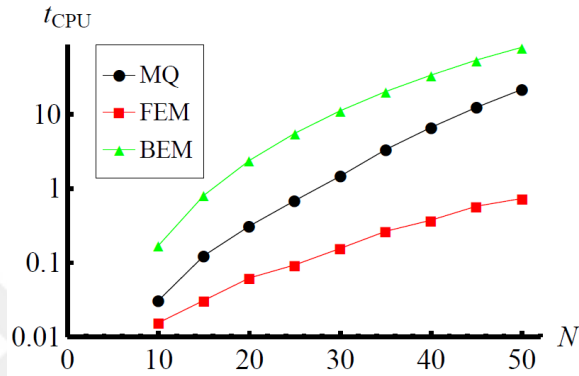


Figure 4.7: CPU times of the MQ collocation, FEM and BEM.

As a last study for the external source problem, in Figure 4.8 the distribution of pointwise errors, ϵ_φ , in the case of trigonometric source is illustrated for all basis functions. The shape parameter is chosen as $c^2 = 0.1$ and $N = 40$ for all RBFs. It can be seen from this figure that the errors tend to increase near the boundaries of the domain. This was expected, even though external nodes are used to enhance the performance of RBF collocation, due to the so-called Runge phenomenon [55]. According to this phenomenon, oscillation is observed around the edges when interpolation is deployed with a uniformly distributed set of nodes in a finite domain.

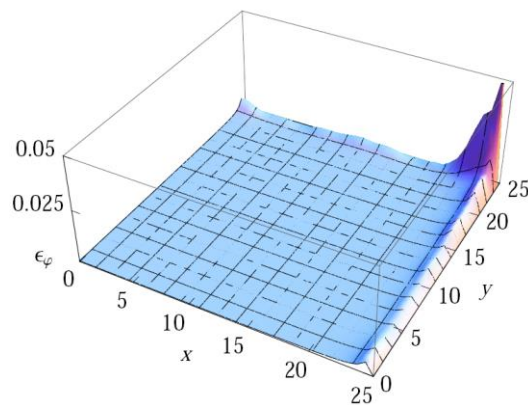


Figure 4.8a: Distribution of pointwise errors in the case of s_2 when $N = 40$ for MQ.

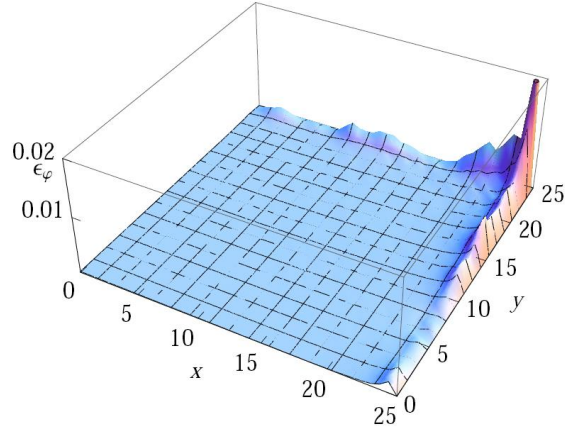


Figure 4.8b: Distribution of pointwise errors in the case of s_2 when $N = 40$ for IMQ.

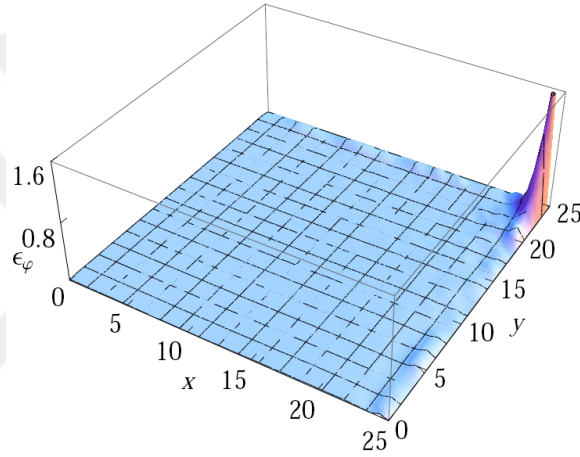


Figure 4.8c: Distribution of pointwise errors in the case of s_2 when $N = 40$ for GA.

4.2.2 Multigroup fission source problems

To investigate the performance of the RBF collocation method for multigroup fission source problems, 1-, 2-, 3- and 4-group cases are considered. The analytical solutions for 1-, 2- and 3-group problems can be found in [5]. For the calculation of flux values the power is selected as 16 kW/cm for the first three problems and 25 kW/cm for the 4-group case. The convergence criterion is chosen as 10^{-6} for all problems. Accuracy of the method is examined via calculating the error in λ and maximum errors in group fluxes

$$\epsilon_\lambda = |\lambda - \tilde{\lambda}| \times 100/\lambda \quad (4.29)$$

$$\epsilon_{max,g} = \max_{1 \leq i \leq N_D} [|\phi_g(x_i, y_i) - \tilde{\phi}_g(x_i, y_i)| \times 100/\phi_g(x_i, y_i)] \quad (4.30)$$

where $g = 1,2,3,4$, and $\tilde{\lambda}$ and $\tilde{\phi}_g$ are the numerical effective multiplication factor and group flux, respectively.

In the first problem the one-group case is studied. The length of the square domain is taken as $a = 50 \text{ cm}$, while $D = 1.77764 \text{ cm}$, $\Sigma_f = 0.0104869 \text{ cm}^{-1}$, $\nu = 2.5$, $\Sigma_r = 0.0143676 \text{ cm}^{-1}$ and $\chi = 1$. The analytical value of λ is 1.46657782. Figure 4.9 shows the variation of ϵ_{max} and ϵ_λ with respect to N , where $c^2 = 0.06$. It is observed from this figure that ϵ_{max} decreases continuously with decreasing value of the fill distance. It has its minimum value of 5.642×10^{-3} when $N = 36$. Highly accurate λ values are obtained above $N = 22$ and, the percent error has decreased to its minimum of 4.091×10^{-6} when $N = 32$.

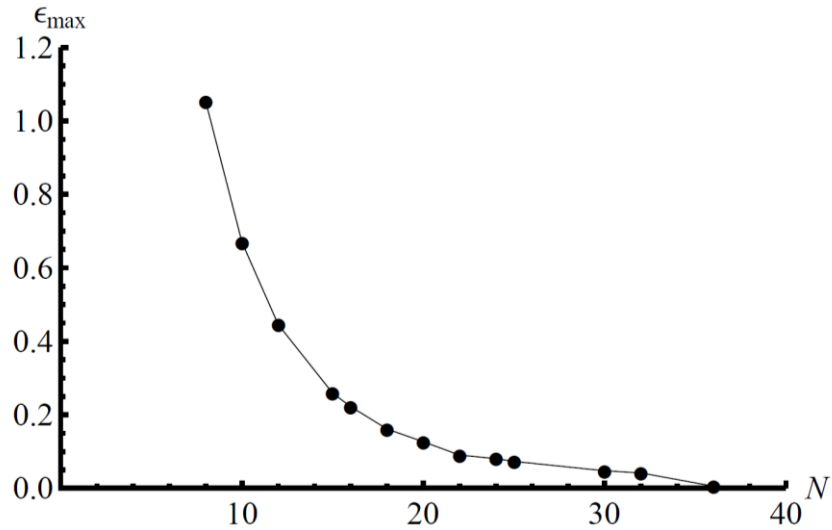


Figure 4.9a: Variation of ϵ_{max} with respect to N .

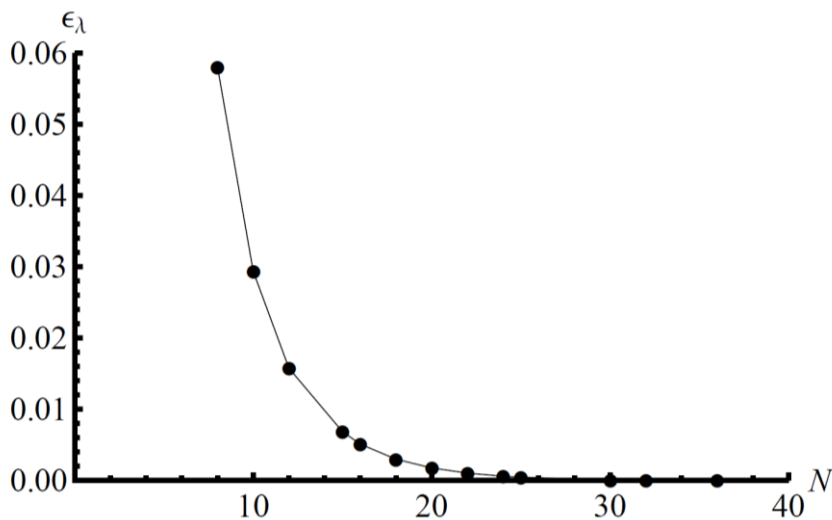


Figure 4.9b: Variation of ϵ_λ with respect to N .

In the second problem the number of energy groups is two and $a = 25$ cm. The nuclear data is given in Table 4.6. Diffusion constants are given in units of centimeters and all cross sections have units of inverse centimeters in Table 4.6 and later on in Table 4.8 and Table 4.10. For this problem $\lambda_a = 1.96293774$.

Table 4.6: Two-group nuclear data.

Group	D	ν	Σ_f	Σ_r	$\Sigma_{s,g \rightarrow g+1}$	χ
1	1.2245	2.65	0.063	0.13552	0.0676	0.575
2	1.2245	2.55	0.06776	0.08228	-	0.425

The numerical results of the two-group problem are summarized in Table 4.7, where $c^2 = 0.06$. It is seen that the maximum errors in group fluxes are similar and decrease with decreasing fill distance value. For the multiplication factor, a very high level of accuracy is obtained above $N = 16$. It is also observed from this table that the number of iterations increases by one when $N = 32$.

Table 4.7: ϵ_{max} and ϵ_λ for the two-group problem.

N	n_{iter}	$\epsilon_{max,1}$	$\epsilon_{max,2}$	ϵ_λ
8	29	1.040	1.060	3.221×10^{-2}
12	29	4.429×10^{-1}	4.478×10^{-1}	8.663×10^{-3}
16	29	2.222×10^{-1}	2.236×10^{-1}	2.691×10^{-3}
20	29	1.274×10^{-1}	1.277×10^{-1}	8.238×10^{-4}
24	29	8.173×10^{-2}	8.161×10^{-2}	1.722×10^{-4}
28	29	5.550×10^{-2}	5.502×10^{-2}	7.132×10^{-5}
32	30	4.361×10^{-2}	4.298×10^{-2}	9.730×10^{-5}
36	30	8.136×10^{-3}	7.384×10^{-3}	1.365×10^{-4}

In Figure 4.10 the variation of $\epsilon_{max,1}$ and $\epsilon_{max,2}$ with the shape parameter of the multiquadric is illustrated where $N = 25$ is chosen. The maximum pointwise errors in flux for both groups decrease continuously with increasing shape parameter up to $c^2 \cong 0.12$. Beyond this value the errors start to oscillate and the numerical solution breaks down except for $c^2 = 0.149$. This is expected since as the shape parameter increases the collocation matrix becomes more and more ill-conditioned.

The error in multiplication factor is shown in Figure 4.11 where, again $N = 25$. It is seen that the error increases with the shape parameter at first up to $c^2 = 0.015$ and then starts to decrease until $c^2 = 0.072$ where the analytical solution is reproduced.

Above this value it increases again, and similar to the pointwise errors in group fluxes the numerical solution oscillates and breaks down above $c^2 \cong 0.12$.

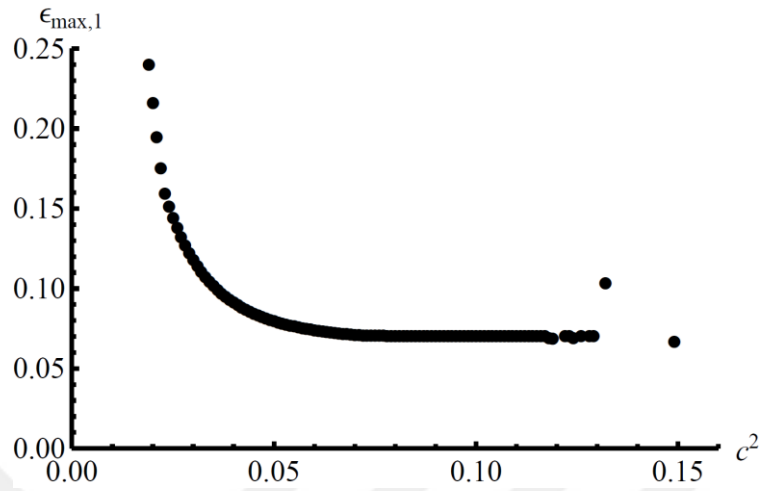


Figure 4.10a: Variation of $\epsilon_{max,1}$ with respect to the shape parameter.

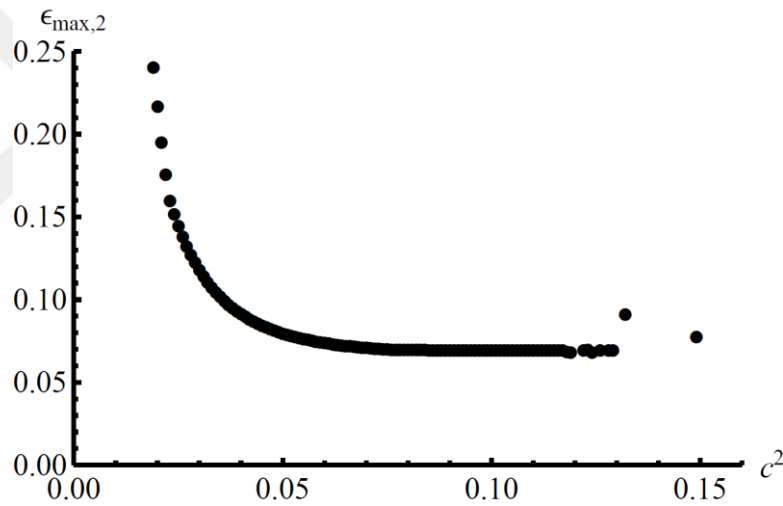


Figure 4.10b: Variation of $\epsilon_{max,2}$ with respect to the shape parameter.

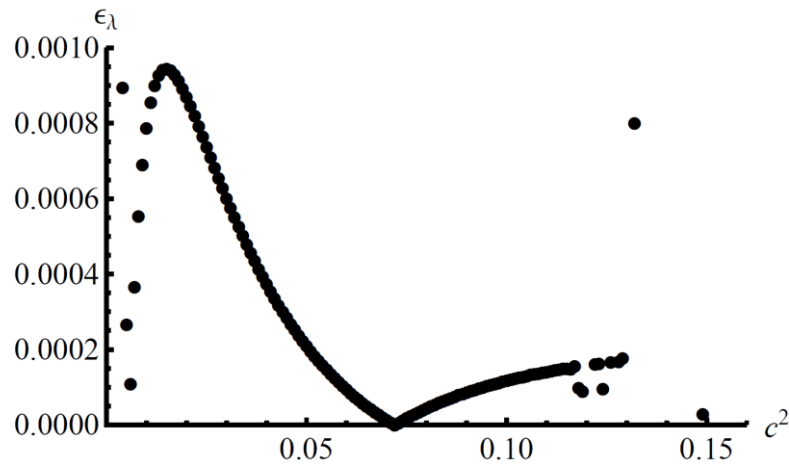


Figure 4.11: Variation of ϵ_λ with respect to the shape parameter.

It should also be noted that the change of errors in flux and multiplication factor with the shape parameter is found to be similar for the one and three-group problems.

The third problem deals with the solution of the three-group neutron diffusion equation where a is assumed to be 25 cm. The nuclear data characterizing a three-group structure is given in Table 4.8 and the analytical value of λ is 0.75024241 for this problem.

Table 4.8: Three-group nuclear data.

Group	D	ν	Σ_f	Σ_r	$\Sigma_{s,g \rightarrow g+1}$	$\Sigma_{s,g \rightarrow g+2}$	χ
1	3.0034	2.65	0.0131267	0.05286	0.02705	0.01181	0.575
2	2.2297	2.53	0.006102	0.016704	0.00822	-	0.326
3	1.4627	2.47	0.008317	0.01414	-	-	0.099

The number of iterations, maximum pointwise errors for the three group fluxes and the error in λ is given in Table 4.9 for different N values where $c^2 = 0.06$. Once again, it is found that the errors in group fluxes and multiplication factor decrease with decreasing value of the fill distance. Highly accurate λ values are obtained when $N = 20$ or higher. It is also observed that the number of iterations does not depend on the choice of N .

Table 4.9: ϵ_{max} and ϵ_λ for the three-group problem.

N	n_{iter}	$\epsilon_{max,1}$	$\epsilon_{max,2}$	$\epsilon_{max,3}$	ϵ_λ
8	12	9.715×10^{-1}	1.068	1.116	1.702×10^{-1}
12	12	4.232×10^{-1}	4.494×10^{-1}	4.624×10^{-1}	4.649×10^{-2}
16	12	2.149×10^{-1}	2.234×10^{-1}	2.276×10^{-1}	1.519×10^{-2}
20	12	1.239×10^{-1}	1.270×10^{-1}	1.285×10^{-1}	5.428×10^{-3}
24	12	7.958×10^{-2}	8.072×10^{-2}	8.128×10^{-2}	2.037×10^{-3}
28	12	5.363×10^{-2}	5.406×10^{-2}	5.427×10^{-2}	7.811×10^{-4}
32	12	4.149×10^{-2}	4.168×10^{-2}	4.172×10^{-2}	2.972×10^{-4}
36	12	8.572×10^{-3}	5.375×10^{-3}	5.329×10^{-3}	9.197×10^{-5}

As the final example, the 4-group fission source problem is studied. In this case, since the analytical solution does not exist in the literature, it will be given first. The group flux distributions have the following form

$$\phi_g(x, y) = H_g A_4 \cos\left(\frac{\pi x}{\tilde{a}}\right) \cos\left(\frac{\pi y}{\tilde{a}}\right), \quad g = 1, 2, 3, 4 \quad (4.31)$$

where $\tilde{a} = 2a$, $H_g = A_g/A_4$, $g = 1,2,3,4$ and A_4 is a factor dependening on the power (P) and size of the system, and fission cross sections

$$H_1 = \frac{a_1}{\frac{\chi_4}{\chi_1} + \frac{1}{D_1 B_g^2 + \Sigma_{r,1}} [\Sigma_{s,1 \rightarrow 4} + \Sigma_{s,2 \rightarrow 4} a_2 + \Sigma_{s,3 \rightarrow 4} a_3]} \quad (4.32)$$

$$H_2 = H_1 a_2 \quad (4.33)$$

$$H_3 = H_1 a_3 \quad (4.34)$$

$$A_4 = \frac{P \pi^2}{w_f (H_1 \Sigma_{f,1} + H_2 \Sigma_{f,2} + H_3 \Sigma_{f,3} + \Sigma_{f,4}) a^2} \quad (4.35)$$

where $B_g^2 = 0.5 \times (\pi/a)^2$ is the geometric buckling and

$$a_1 = \frac{D_4 B_g^2 + \Sigma_{r,4}}{D_1 B_g^2 + \Sigma_{r,1}} \quad (4.36)$$

$$a_2 = \frac{\frac{\chi_2}{\chi_1} + \frac{\Sigma_{s,1 \rightarrow 2}}{D_1 B_g^2 + \Sigma_{r,1}}}{\frac{D_2 B_g^2 + \Sigma_{r,2}}{D_1 B_g^2 + \Sigma_{r,1}}} \quad (4.37)$$

$$a_3 = \frac{\frac{\chi_3}{\chi_1} + \frac{\Sigma_{s,1 \rightarrow 3}}{D_1 B_g^2 + \Sigma_{r,1}} + \frac{\Sigma_{s,2 \rightarrow 3} \left(\frac{\chi_2}{\chi_1} + \frac{\Sigma_{s,1 \rightarrow 2}}{D_1 B_g^2 + \Sigma_{r,1}} \right)}{D_2 B_g^2 + \Sigma_{r,2}}}{\frac{D_3 B_g^2 + \Sigma_{r,3}}{D_1 B_g^2 + \Sigma_{r,1}}} \quad (4.38)$$

The nuclear data representing a four-group structure is presented in Table 4.10. Length of the square domain is chosen to be $a = 50$ cm. These data yield a subcritical (i.e., $\lambda < 1$) system with an analytical multiplication factor of $\lambda = 0.87227$.

Table 4.10: Group constants for the 4-group problem.

g	D	$v\Sigma_f$	Σ_r	$\Sigma_{s,g \rightarrow g+1}$	$\Sigma_{s,g \rightarrow g+2}$	$\Sigma_{s,g \rightarrow g+3}$	χ
1	2.876787	0.0118781	0.028204	0.023597	4.079×10^{-6}	4.449×10^{-8}	0.768
2	1.570845	0.0053251	0.005275	0.001615	4.231×10^{-8}	-	0.232
3	0.722486	0.0104709	0.017612	0.004684	-	-	0
4	0.964199	0.0266109	0.026546	-	-	-	0

The effect of shape parameter on ϵ_λ is illustrated in Figure 4.12a-c for MQ, IMQ and GA, respectively, when $N = 40$. This figure shows that the error in λ decreases with

c for IMQ and GA, until the iterative algorithm becomes divergent as a result of ill-conditioning of the collocation matrix. On the other hand, an interesting trend is observed when MQ is utilized. Before going into the unstable region, ϵ_λ passes through a maximum value of 4.71×10^{-4} at $c^2 = 0.014$. Figure 4.12 also shows that MQ and IMQ are superior to GA in terms of both accuracy and stability. The stable region of GA is narrower than MQ and IMQ, and a convergent solution exists for a limited number of c values.

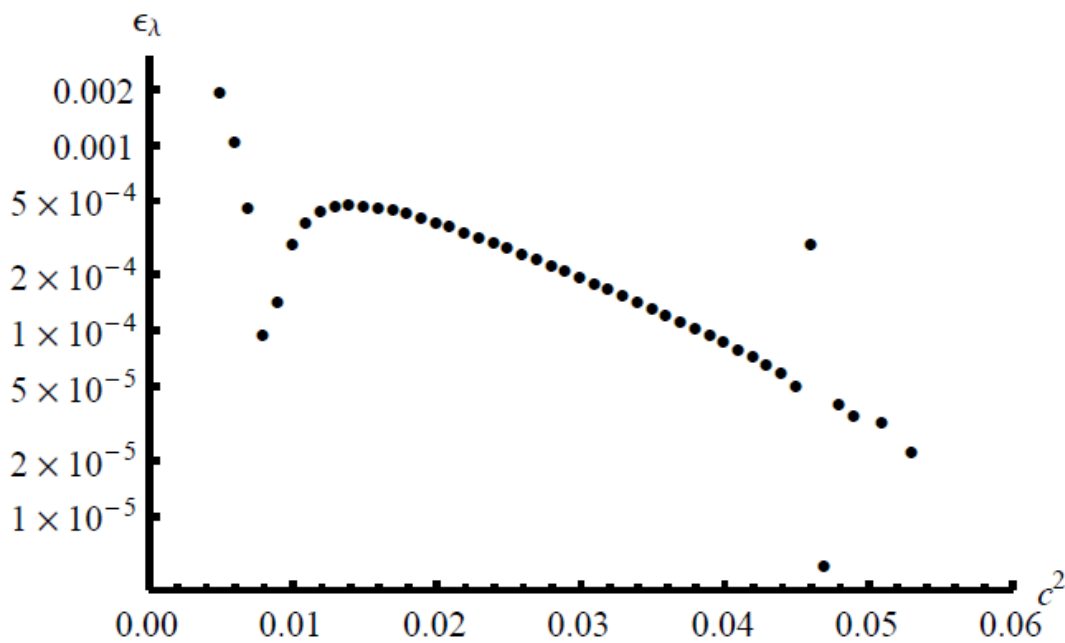


Figure 4.12a: Variation of ϵ_λ with shape parameter for MQ when $N = 40$.

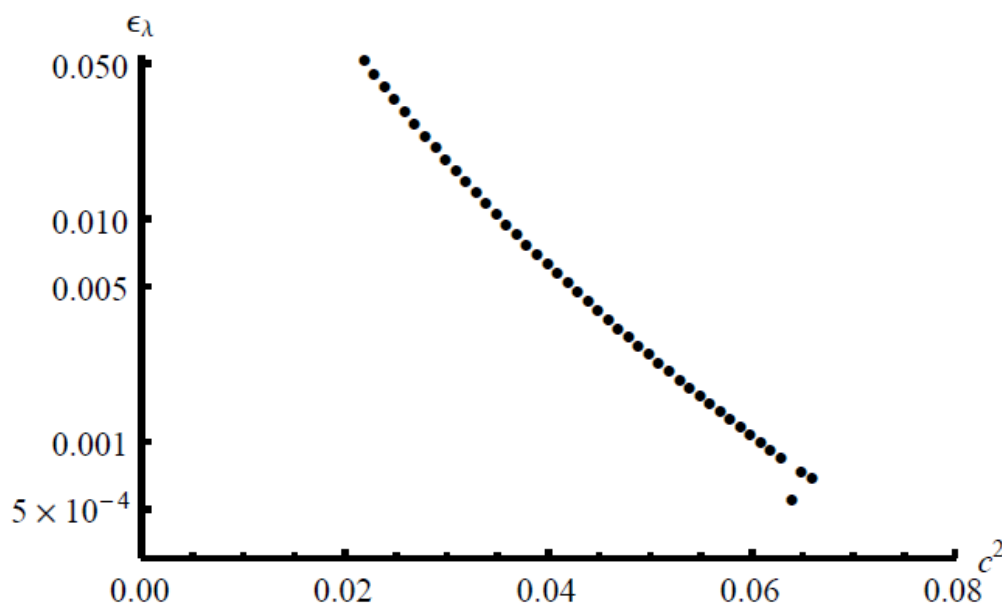


Figure 4.12b: Variation of ϵ_λ with shape parameter for IMQ when $N = 40$.

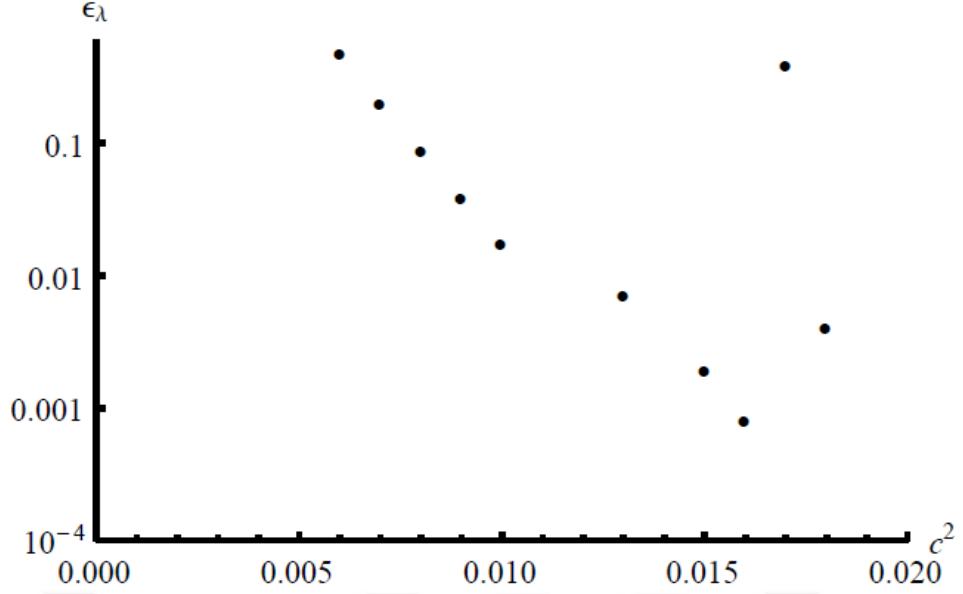


Figure 4.12c: Variation of ϵ_λ with shape parameter for GA when $N = 40$.

The abovementioned calculations are carried out for $N = 10, 15, \dots, 50$. The maximum error behavior is observed at all N values for MQ, while it is encountered only at $N = 10$ and 15 for IMQ, and never seen for GA. The maximum and minimum errors with corresponding shape parameter values are tabulated in Table 4.11 for MQ and IMQ. The results show that highly accurate results can be obtained by the RBF collocation method even with low N and thus propound the importance of shape parameter optimization. Also, in cases where there is a maximum error in λ , the multiplication factor corresponding to that error is indeed a good approximation to the analytical value.

Table 4.11: Maximum and minimum ϵ_λ for MQ and IMQ.

N	MQ				IMQ			
	c_{max}^2	$\epsilon_{\lambda,max}$	c_{min}^2	$\epsilon_{\lambda,min}$	c_{max}^2	$\epsilon_{\lambda,max}$	c_{min}^2	$\epsilon_{\lambda,min}$
10	0.022	8.81×10^{-2}	1.203	4.17×10^{-6}	0.516	2.65×10^{-3}	1.694	1.03×10^{-6}
20	0.013	1.05×10^{-2}	0.231	5.52×10^{-5}	-	-	0.314	3.24×10^{-5}
30	0.015	1.94×10^{-3}	0.096	4.06×10^{-5}	-	-	0.120	4.02×10^{-4}
40	0.014	4.71×10^{-4}	0.047	5.32×10^{-6}	-	-	0.064	5.48×10^{-4}
50	0.013	1.15×10^{-4}	0.009	2.89×10^{-6}	-	-	0.040	1.11×10^{-3}

To see whether the criticality has an influence on the solution, the calculations are repeated for $a = 100$ cm which yields a supercritical (i.e., $\lambda > 1$) system with $\lambda = 1.23984$. In Figures 4.13a and 4.13b the effect of criticality on the c dependence of ϵ_λ is demonstrated where MQ is chosen as the RBF and $N = 50$, for the

subcritical and supercritical cases, respectively. These figures show that an increase in λ has resulted with the disappearance of maximum error behavior. These numerical tests are also done with $N = 10, 15, \dots, 50$ for MQ, IMQ and GA. It was found that the stable computation region with respect to c is narrowed down with an increase in λ . In addition, the results show that, when there is a maximum error in stable region, the corresponding c value is independent of the criticality.

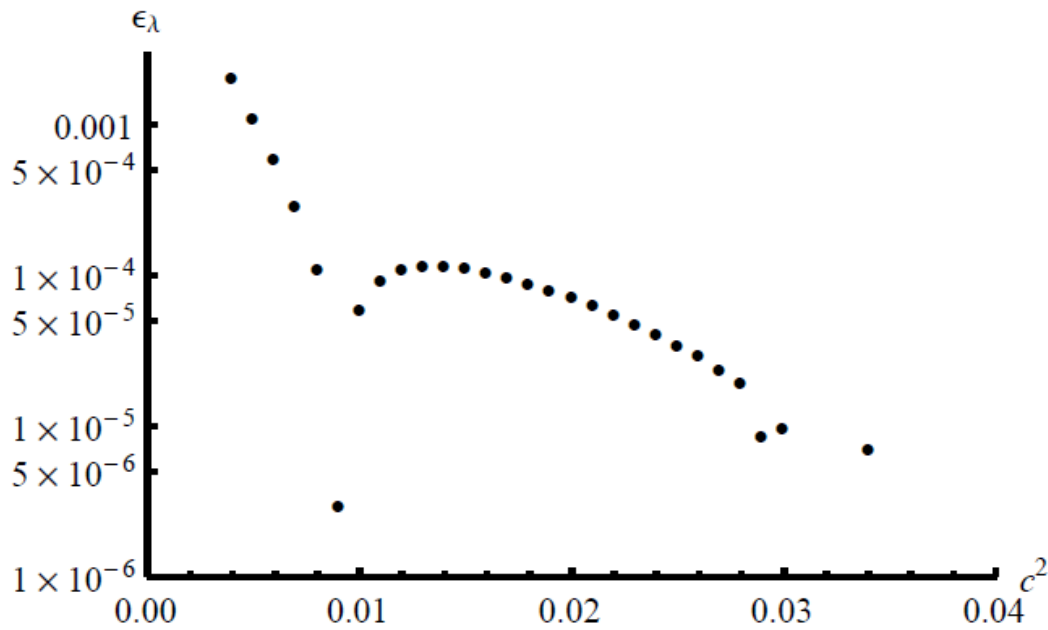


Figure 4.13a: Variation of ϵ_λ with shape parameter for subcritical case when MQ is the RBF and $N = 50$.

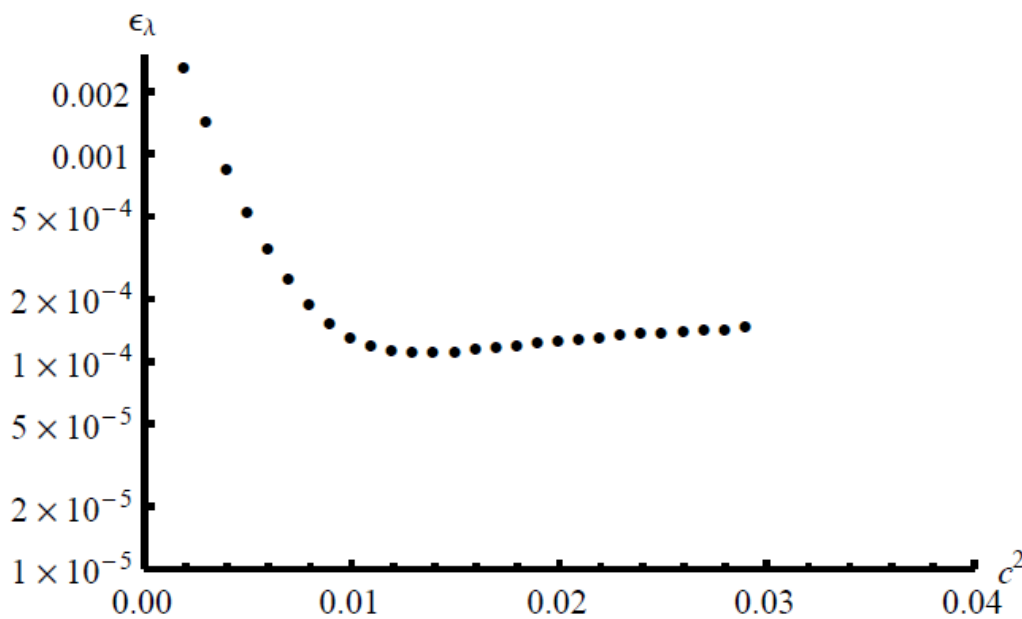


Figure 4.13b: Variation of ϵ_λ with shape parameter for supercritical case when MQ is the RBF and $N = 50$.

The variations of ϵ_λ and $\epsilon_{max,3}$ with respect to N , for the three RBFs, are plotted in Figures 4.14a and 4.14b, respectively where $c^2 = 0.02$ and $\lambda = 0.87227$. The relative maximum percent error in group flux is presented only for the third group, since it follows a similar path for $g = 1,2,4$. It is clear from this figure that GA converges faster than both MQ and IMQ, but it performs poorly for low N . Another disadvantage of GA is its stability. At $N = 40$, MQ and IMQ produces ϵ_λ values of 3.82×10^{-4} and 6.86×10^{-2} , respectively, while iteration diverges due to instability for the GA. These results show that, MQ is the proper choice, when accuracy and stability are taken into account together.

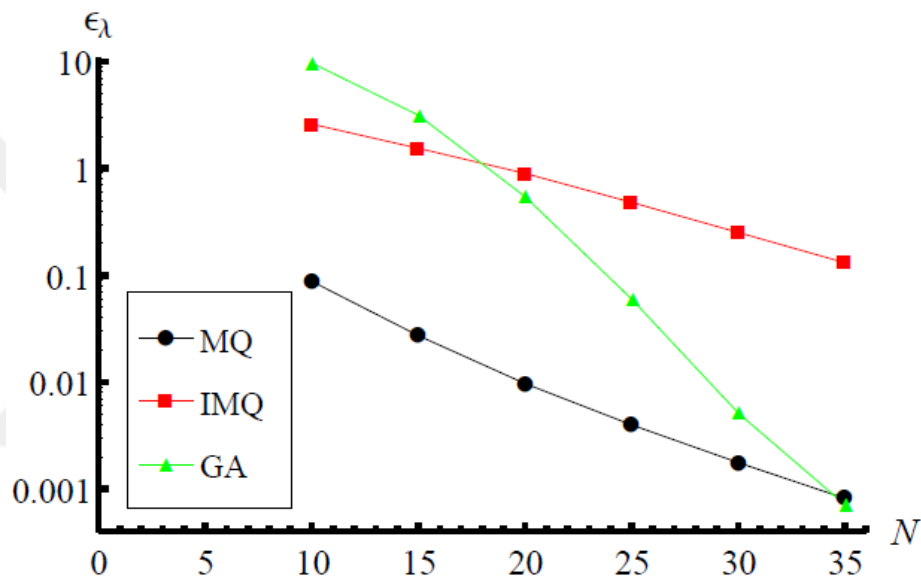


Figure 4.14a: Comparison of MQ, IMQ and GA for ϵ_λ .

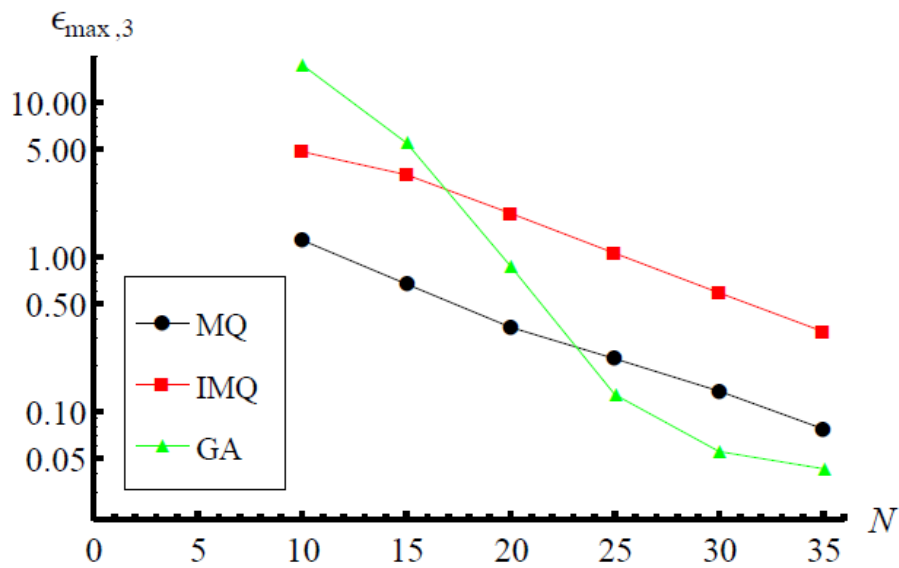


Figure 4.14b: Comparison of MQ, IMQ and GA for $\epsilon_{max,3}$.

In order to make a comparison, the convergence curves of MQ collocation, FEM and BEM for ϵ_λ and $\epsilon_{max,2}$ are presented in Figures 4.15a and 4.15b, respectively, where $\lambda = 0.87227$. The shape parameter for MQ is chosen as $c^2 = 0.04$. As observed from this figure, for the calculation of the multiplication factor, with its exponential convergence rate, MQ collocation has performed much better than both FEM and BEM, especially as N increases. MQ collocation has yielded $\epsilon_\lambda = 6.16 \times 10^{-3}$ at $N = 20$, which is more accurate than the results of FEM and BEM at $N = 45$. However, although MQ collocation converges faster, BEM has provided the best results when group fluxes are considered. Furthermore, if the stability is taken into account, similar to the external source problem, the collocation technique has the disadvantage of being less stable than FEM and BEM. The MQ collocation becomes unstable at $N = 50$, whereas FEM and BEM have kept to provide convergent solutions.

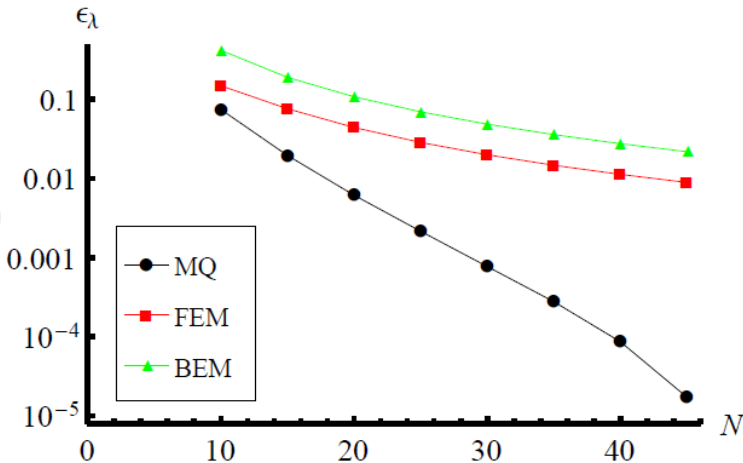


Figure 4.15a: Comparison of MQ collocation, FEM and BEM for ϵ_λ .

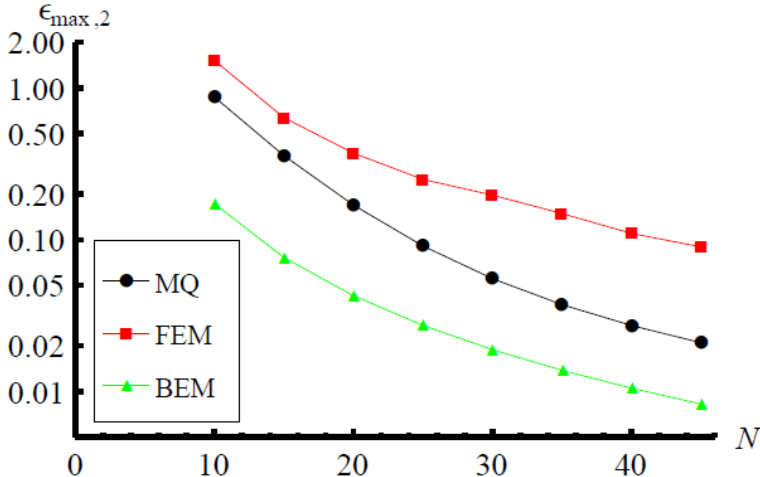


Figure 4.15b: Comparison of MQ collocation, FEM and BEM for $\epsilon_{max,2}$.

Finally, in Figure 4.16, the variation of CPU times of MQ collocation, FEM and BEM for the subcritical problem is illustrated. This figure shows that FEM is more efficient than both MQ collocation and BEM. With increasing N , FEM becomes superior, at $N = 50$ it is better than the other methods by an order of magnitude. MQ collocation is slightly better than the BEM. The number of iterations, determined by the convergence criterion, is an important factor in neutron diffusion calculations, and for the subcritical problem it was found that for all methods, the numerical solution is obtained after 14 iterations. Hence, the advantage of FEM in computation cost can be attributed to its sparse and symmetric stiffness matrix.

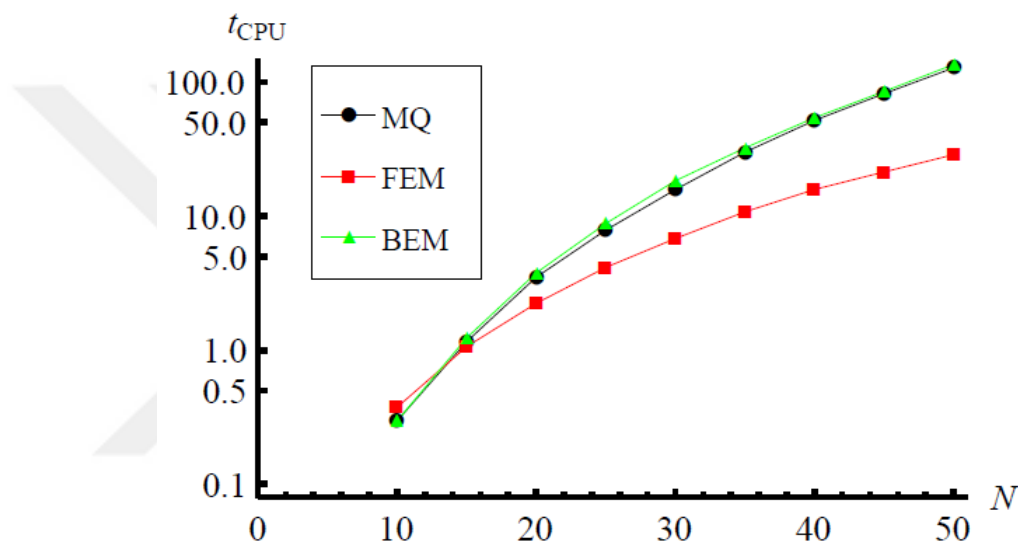


Figure 4.16: CPU times of the MQ collocation, FEM and BEM.

4.3 Improving the Performance of the RBF Collocation Method

The effectiveness of a numerical method, whether it is meshless or mesh-based, is evaluated by its accuracy, stability and CPU time usage. It is necessary to investigate how a numerical scheme can become more preferable to its opponents. Since the radial basis function collocation method approximates partial differential equations globally, the stability of the method becomes an important issue. The numerical tests, based on new approaches would play a valuable role before going into multiregion problems.

4.3.1 Increasing the precision

A brute force method to improve the stability of the method is to increase the precision. Generally, the matrix condition number is used to test whether a numerical

method is stable or not. For an algebraic system $\mathbf{Ku} = \mathbf{f}$, the relative round-off error can be estimated by [58]

$$\varepsilon_{\text{round}} \leq \kappa \varepsilon_{\text{mach}} \quad (4.39)$$

where κ is the condition number and $\varepsilon_{\text{mach}}$ is the machine precision. Using higher precision arithmetic decreases the machine precision and therefore it provides a more stable computation environment, since for a specified round-off error it is possible to achieve higher condition numbers.

In order to test the effect of precision on the stability of the method the external source problem with the constant source is considered. Figure 4.17 shows the comparison of results obtained by FORTRAN's double precision and MATHEMATICA's 100-precision arithmetic. In these calculations the shape parameter of the multiquadric radial basis function is chosen as $c^2 = 0.1$. It is clear from this figure that using a higher precision has improved the stability of the method. For the double precision, the RMS error has started to increase above $N = 30$ whereas it has continued to decrease when calculations are done with 100 precision.

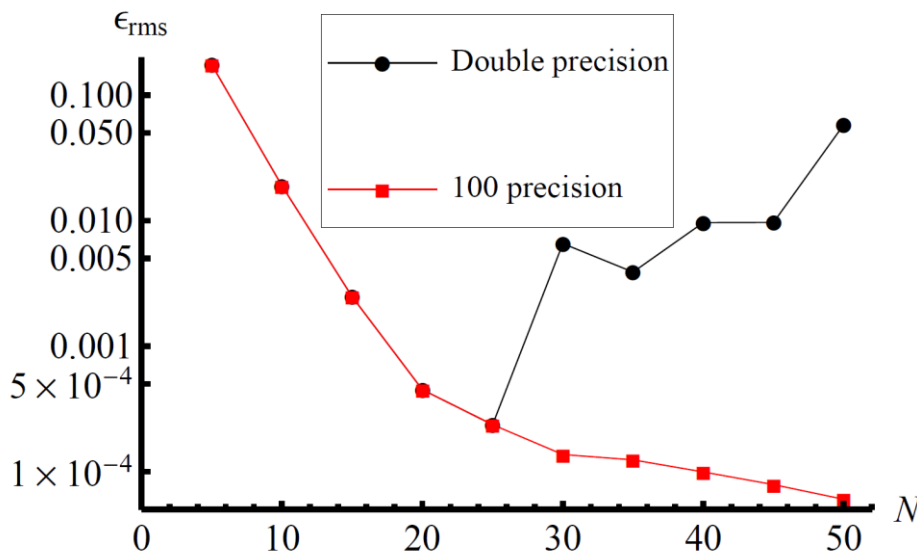


Figure 4.17: Comparison of double and 100 precision calculations in the RBF collocation method.

The price to pay when the precision is increased is the CPU time, as expected. To see the relation between precision and CPU time several numerical tests are performed with different precision values, and it is found that higher precision arithmetic

becomes worse in terms of CPU time as the number of nodes used in discretization gets higher. As an example, when $N = 50$, the CPU time is %20 more when 100 and 20 precision computations are compared.

4.3.2 Exponent of the generalized multiquadric

In the previous section the effect of the shape parameter on the performance of the RBF collocation method was illustrated. Also, in Chapter 3 the role of this parameter on the interpolant was illustrated (see Figure 3.4). As the value of c increases the RBF becomes flatter and it becomes less sensitive to the distance between the nodes. In computations, the condition number of the collocation matrix increases with increasing shape parameter and the method becomes less stable. It was found that by fine-tuning of this parameter one can obtain high level of accuracies for both external and fission source problems even when the number of nodes is low. The convergence rate is also affected by c , the errors diminish faster as the shape parameter becomes larger.

The exponent, q , of the generalized multiquadric has an effect on the RBF, similar to that of the shape parameter c as shown in Figure 4.18 where $c = 0.2$. So, it is expected that the performance of the method can be improved by optimizing this parameter.

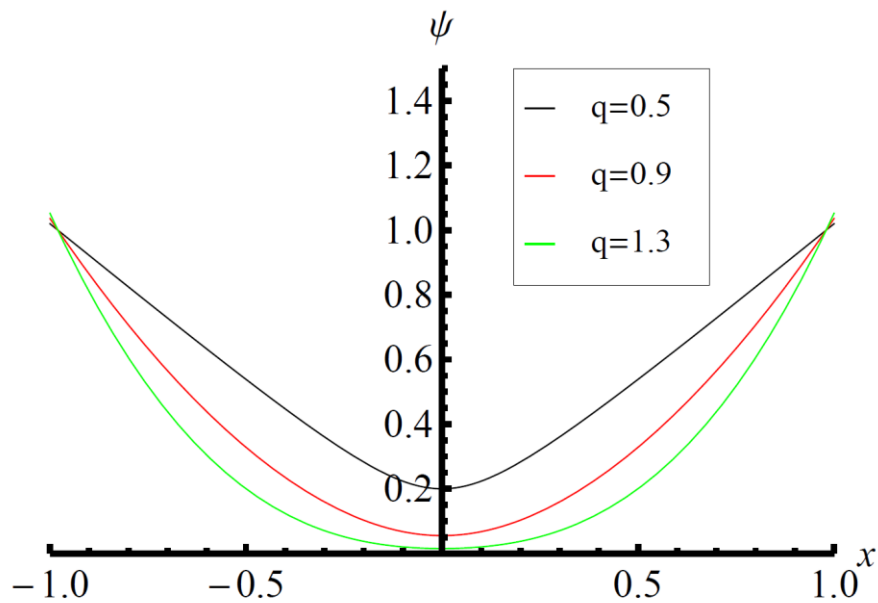


Figure 4.18: Effect of the exponent on generalized multiquadric centered at the origin.

To see the influence of q on the accuracy and stability of the algorithm, once again, the constant source problem is considered. Calculations are done with FORTRAN and the shape parameter is chosen as $c^2 = 0.02$. In Figure 4.19, the RMS error with respect to N is plotted for three values of the exponent, q . It is observed from this figure that the accuracy of the method increases with increasing q value, but on the other hand the algorithm becomes less stable. When $q = 0.5$ (the MQ case), the RMS error decreases with the fill distance continuously, while it started to increase above $N = 30$ for $q = 2.5$. It can also be deduced from this figure that increasing the exponent enhances the convergence rate of the collocation method. These results show that, it is possible to improve the characteristics of the RBF collocation method by varying the exponent of the generalized multiquadric radial basis function.

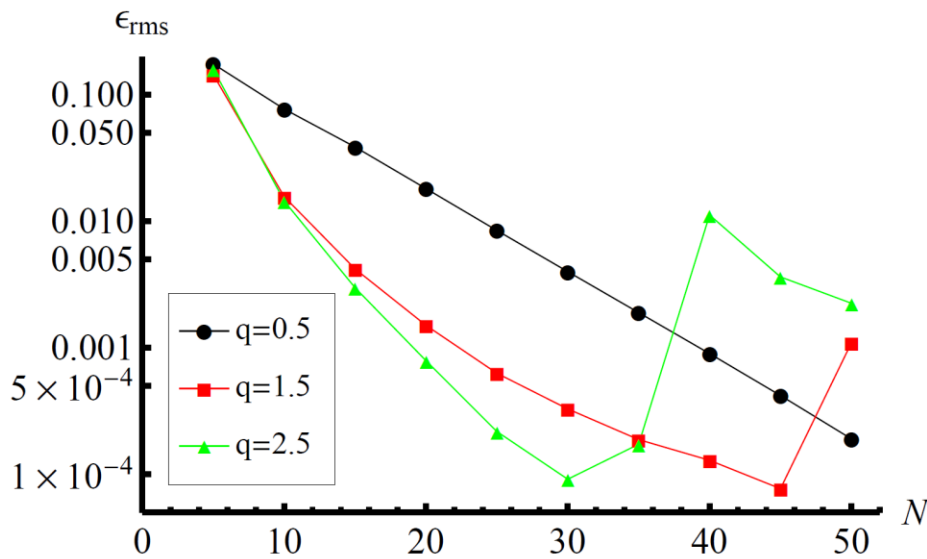


Figure 4.19: RMS error with respect to N for the constant source problem.

4.3.3 Node number dependent shape parameter strategy

Radial basis functions can be expressed in different forms. As an example, the MQ can be stated as follows

$$\psi_j = \left\{ \left[\frac{(x - x_j)^2 + (y - y_j)^2}{h^2} \right] \alpha^2 + 1 \right\}^q \quad (4.40)$$

where α is called the relative width parameter since it is the width relative to the fill distance h [76]. It is obvious that the traditional form, and Eq. (4.40) are related by $\alpha = 1/hc$.

In [76] six strategies were tested to treat the Runge phenomenon which is a source of accuracy degradation in numerical methods. One of these strategies is to use a variable α scheme instead of a constant shape parameter. It was found that by decreasing α as $a/N^{1/4}$, the Runge phenomenon can be defeated in interpolation of functions where N is the number of nodes and a is some constant.

This node number dependent shape parameter approach is tried for the solution of the constant source problem. The results are presented in Figure 4.20 together with those of constant α strategy. This figure shows that variable shape parameters can provide accurate results with few nodes, but on the other hand they do not improve the stability of the method, since oscillatory behavior is observed for $\alpha = 0.5/N^{1/4}$ and the method diverges when $\alpha = 0.3/N^{1/4}$. These instabilities can be dealt with by choosing lower values for a , but this results in degraded accuracy. Therefore node number dependent shape parameter strategy does not affect the performance of the RBF collocation technique significantly.

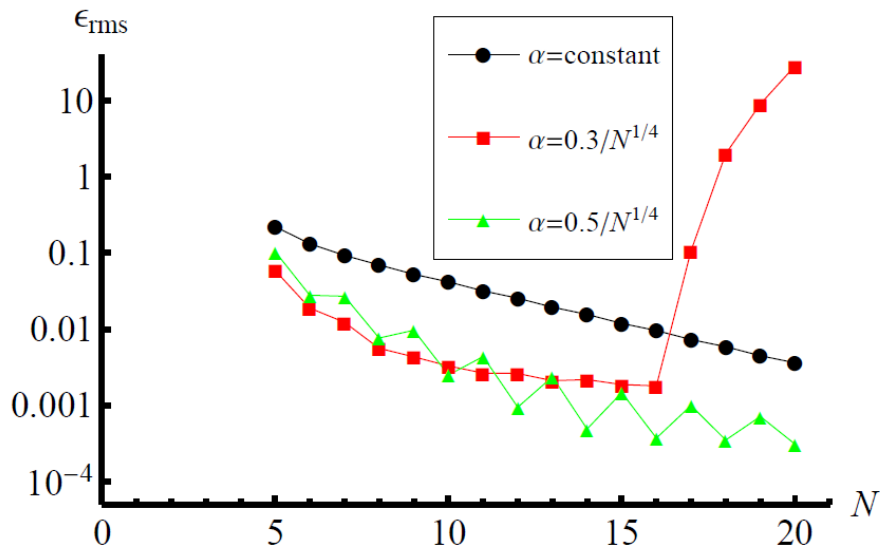


Figure 4.20: Results of node number dependent shape parameter strategy.

4.3.4 Singular value decomposition filtering

For an $m \times n$ matrix A the singular value decomposition (SVD) is defined as

$$A = U^T \Sigma V \quad (4.41)$$

where U and V are orthogonal matrices and Σ is a square diagonal matrix containing the singular values. These matrices satisfy [77]

$$\mathbf{U}^T \mathbf{A} \mathbf{V} = \mathbf{\Sigma} = \text{diag}(\sigma_1, \dots, \sigma_p) \in R^{m \times n}, \quad p = \min\{m, n\} \quad (4.42)$$

where $\sigma_1 \geq \sigma_2 \geq \dots \geq \sigma_p \geq 0$. In [78] it has been shown that SVD can be used as a tool for teaching linear algebra geometrically, and also it is applied in solving least squares problems and in data compression.

SVD is an effective tool for solving linear systems when the matrix in question is ill-conditioned. Since the RBF collocation method is a global approximation scheme it gives a full matrix at the end of discretization process. As it is shown in previous simulations, the solution can become unstable depending on the values of the fill distance, h and shape parameter, c . Hence, SVD may improve the performance of the algorithm by treating the ill-conditioning of the collocation matrix.

Now suppose that the linear system resulting from approximation of a PDE with its BCs is given by

$$\mathbf{K} \mathbf{a} = \mathbf{f} \quad (4.43)$$

If this system is decomposed into its singular values one has

$$\mathbf{U}^T \mathbf{\Sigma} \mathbf{V} \mathbf{a} = \mathbf{f} \quad (4.44)$$

and the vector whose elements are the coefficients of the RBFs can be found by

$$\mathbf{a} = \mathbf{V}^T \mathbf{\Sigma}^{-1} \mathbf{U} \mathbf{f} \quad (4.45)$$

When the condition number of \mathbf{K} is high it is useful to omit the smallest singular values by replacing $1/\sigma_j$ with zero in $\mathbf{\Sigma}^{-1}$. By this SVD filtering, the amplification of round-off errors corresponding to the smallest singular values is depressed [76].

Numerical experiments are performed in MATHEMATICA to see the effect of SVD filtering with 50-precision arithmetic, again, for the constant external source case. The fill distance is chosen to be $N = 15$ which means that there are 320 singular values. For these fill distance and precision values instability is observed when $c^2 \geq 0.8$ if all singular values are kept. The contour plot in Figure 4.21 demonstrates the RMS error with respect to the shape parameter, c and the number of singular values omitted in calculations, n_{sv} . This figure shows that SVD filtering can improve the accuracy of the RBF collocation method in both stable and unstable regions. It is

also observed from this figure that as the shape parameter increases (i.e., the collocation matrix becomes more ill-conditioned), n_{SV} has to be increased to get the best results.

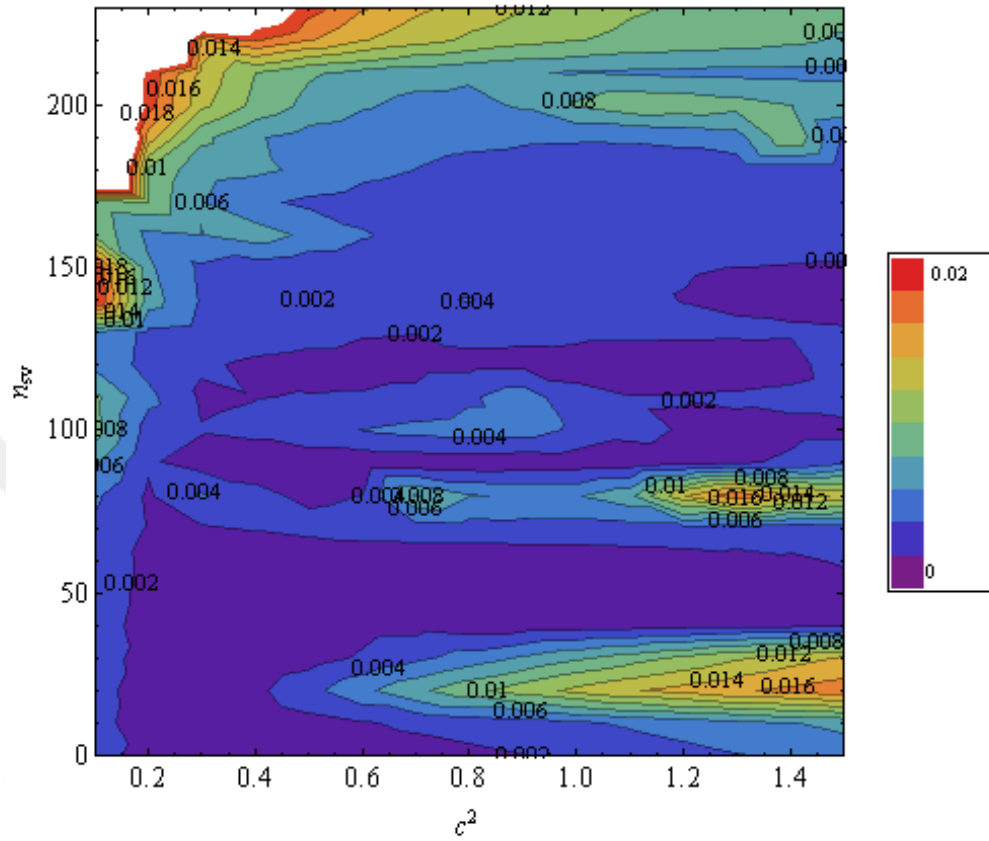


Figure 4.21: RMS error of constant source problem with respect to c and n_{SV} .



5. MODELLING OF MULTIREGION NEUTRON DIFFUSION

This chapter deals with the numerical modelling of multiregion neutron diffusion problems with the RBF collocation method. As stated in the third chapter, when this type of collocation scheme is chosen for the solution of problems involving heterogeneous media, the weighted version of the method is applied. Taking this situation into account, the weighted RBF collocation method is used for multiregion neutron diffusion problems together with the classical collocation scheme, and therefore, initially the numerical formulation of the weighted collocation method is presented. Next, the accuracy and stability of the classical and weighted approaches are tested by working on five problems. First two of these five cases are two-region configurations for which analytical solutions exist. Then a more complex two-region problem which contains a corner singularity is considered. To assess the robustness of the numerical scheme, this corner singularity problem is studied again, this time with a high level of heterogeneity, and finally a five-region IAEA (International Atomic Energy Agency) benchmark problem is solved with the RBF collocation method.

5.1 Numerical Formulation for the Weighted RBF Collocation Method

For ease of illustration a system consisting of two-regions is considered as shown in Figure 5.1. Here S_1 and S_2 are two domains with different properties, Γ_0 is the interface of these regions, and Γ_V and Γ_R are the vacuum and reflective boundaries, respectively. The one-group neutron diffusion equation can be expressed in the following operator form:

$$\begin{aligned} L_i \phi_i(\mathbf{r}) &= q_i(\mathbf{r}), \quad \mathbf{r} \in S_i, \quad i = 1,2 \\ \phi_i(\mathbf{r}) &= 0, \quad \mathbf{r} \in \Gamma_V, \quad i = 1,2 \\ \frac{\partial \phi_i(\mathbf{r})}{\partial n} &= 0, \quad \mathbf{r} \in \Gamma_R, \quad i = 1,2 \\ \phi_1(\mathbf{r}) &= \phi_2(\mathbf{r}), \quad \mathbf{r} \in \Gamma_0 \\ D_1 \frac{\partial \phi_1(\mathbf{r})}{\partial n} &= D_2 \frac{\partial \phi_2(\mathbf{r})}{\partial n}, \quad \mathbf{r} \in \Gamma_0 \end{aligned} \tag{5.1}$$

The source term, $q_i(\mathbf{r})$, represents an external or fission source. For the vacuum boundary term a Dirichlet type BC is chosen, however a Robin type vacuum condition can also be treated in the same way. In the one-energy group approximation L_i takes the following form

$$L_i \equiv -\nabla D_i(\mathbf{r})\nabla + \Sigma_{a,i} \quad (5.2)$$

where D_i and $\Sigma_{a,i}$ are the diffusion constant and absorption coefficient of the i th region, respectively.

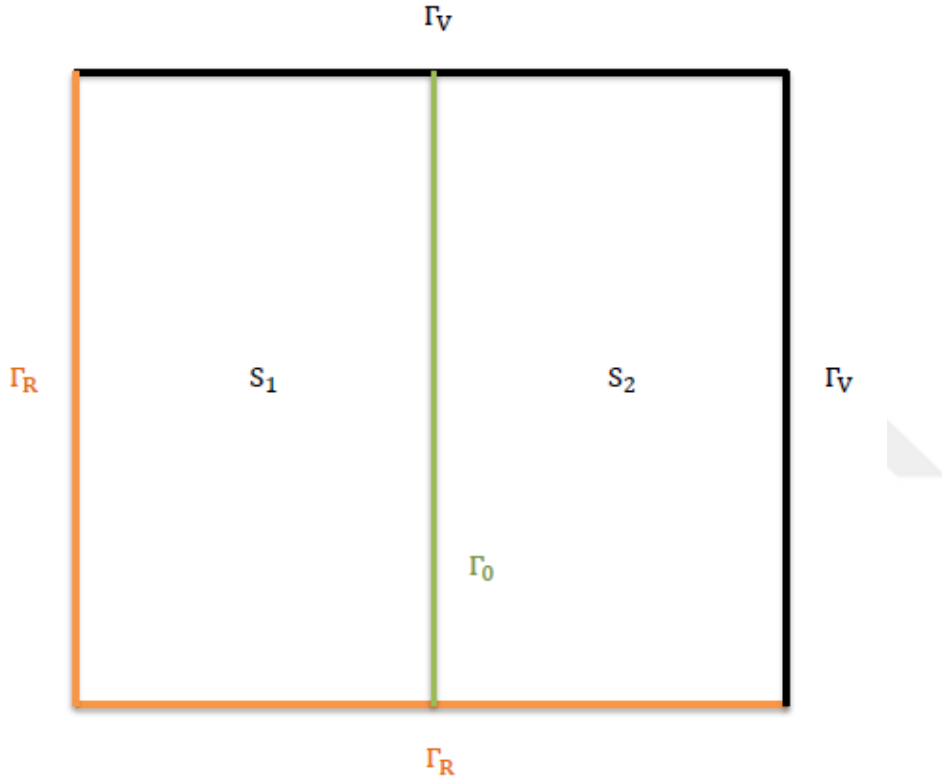


Figure 5.1: A typical two-region problem.

The numerical formulation starts by defining the following weighted least squares functional:

$$I[u_i] = \frac{1}{2} \left\{ \iint_{S_i} (L_i u_i - q_i)^2 dS + \bar{w}_V \int_{\Gamma_0} (u_1 - u_2)^2 d\Gamma \right. \\ \left. + \bar{w}_R \int_{\Gamma_0} \left(D_1 \frac{\partial u_1}{\partial n} - D_2 \frac{\partial u_2}{\partial n} \right)^2 d\Gamma + w_{V,i} \int_{\Gamma_V} u_i^2 d\Gamma + w_{R,i} \int_{\Gamma_R} \left(D_i \frac{\partial u_i}{\partial n} \right)^2 d\Gamma \right\} \quad (5.3)$$

where $i = 1, 2$. Here \bar{w}_V and \bar{w}_R refer to the vacuum and reflective type interface conditions, respectively (i.e., continuity of the neutron flux and current), whereas $w_{V,i}$ and $w_{R,i}$ are the weights related to vacuum and reflective boundaries. The aim of the least-squares approximation is to find a solution ϕ_i , such that the functional $I[u_i]$ is minimized:

$$I[\phi_i] = \min_{u_i \in U} I[u_i] \quad (5.4)$$

Since ϕ_i is the function minimizing $I[u_i]$ and the solution to Eq. (5.1) one can write

$$u_i = \phi_i + v_i \quad (5.5)$$

If Eq. (5.5) is substituted into Eq. (5.3), the first integral term on the right hand side of Eq. (5.3) becomes

$$\begin{aligned} \iint_{S_i} (L_i u_i - q_i)^2 dS &= \iint_{S_i} [(L_i u_i)^2 - 2q_i L_i u_i + q_i^2] dS \\ &= \iint_{S_i} \{[L_i(\phi_i + v_i)]^2 - 2q_i L_i(\phi_i + v_i) + q_i^2\} dS \\ &= \iint_{S_i} \{(L_i \phi_i)^2 + 2L_i \phi_i L_i v_i + (L_i v_i)^2 - 2q_i L_i \phi_i - 2q_i L_i v_i + q_i^2\} dS \\ &= \iint_{S_i} [(L_i \phi_i)^2 - 2q_i L_i \phi_i + q_i^2] dS + \iint_{S_i} (L_i v_i)^2 dS \\ &\quad + 2 \iint_{S_i} [L_i \phi_i L_i v_i - q_i L_i v_i] dS \\ &= \iint_{S_i} (L_i \phi_i - q_i)^2 dS + \iint_{S_i} (L_i v_i)^2 dS + 2 \iint_{S_i} [L_i \phi_i L_i v_i - q_i L_i v_i] dS \end{aligned} \quad (5.6)$$

The second term

$$\int_{\Gamma_0} (u_1 - u_2)^2 d\Gamma = \int_{\Gamma_0} (u_1^2 - 2u_1 u_2 + u_2^2) d\Gamma$$

$$\begin{aligned}
&= \int_{\Gamma_0} [(\phi_1^2 + 2\phi_1 v_1 + v_1^2) - 2(\phi_1 \phi_2 + \phi_1 v_2 + \phi_2 v_1 + v_1 v_2) \\
&+ (\phi_2^2 + 2\phi_2 v_2 + v_2^2)] d\Gamma \tag{5.7}
\end{aligned}$$

$$\begin{aligned}
&= \int_{\Gamma_0} [(\phi_1^2 - 2\phi_1 \phi_2 + \phi_2^2) + (2\phi_1 v_1 - 2\phi_1 v_2 - 2\phi_2 v_1 + 2\phi_2 v_2) \\
&+ (v_1^2 - 2v_1 v_2 + v_2^2)] d\Gamma \\
&= \int_{\Gamma_0} (\phi_1 - \phi_2)^2 d\Gamma + 2 \int_{\Gamma_0} (\phi_1 - \phi_2)(v_1 - v_2) d\Gamma + \int_{\Gamma_0} (v_1 - v_2)^2 d\Gamma
\end{aligned}$$

The third term can be manipulated in a similar manner

$$\begin{aligned}
&\int_{\Gamma_0} \left(D_1 \frac{\partial u_1}{\partial n} - D_2 \frac{\partial u_2}{\partial n} \right)^2 d\Gamma \\
&= \int_{\Gamma_0} \left(D_1 \frac{\partial \phi_1}{\partial n} - D_2 \frac{\partial \phi_2}{\partial n} \right)^2 d\Gamma + \int_{\Gamma_0} \left(D_1 \frac{\partial v_1}{\partial n} - D_2 \frac{\partial v_2}{\partial n} \right)^2 d\Gamma \tag{5.8} \\
&+ 2 \int_{\Gamma_0} \left(D_1 \frac{\partial \phi_1}{\partial n} - D_2 \frac{\partial \phi_2}{\partial n} \right) \left(D_1 \frac{\partial v_1}{\partial n} - D_2 \frac{\partial v_2}{\partial n} \right) d\Gamma
\end{aligned}$$

The last two terms have the following forms:

$$\int_{\Gamma_V} u_i^2 d\Gamma = \int_{\Gamma_V} \phi_i^2 d\Gamma + 2 \int_{\Gamma_V} \phi_i v_i d\Gamma + \int_{\Gamma_V} v_i^2 d\Gamma \tag{5.9}$$

$$\begin{aligned}
\int_{\Gamma_R} \left(D_i \frac{\partial u_i}{\partial n} \right)^2 d\Gamma &= D_i^2 \left[\int_{\Gamma_R} \left(\frac{\partial \phi_i}{\partial n} \right)^2 d\Gamma + 2 \int_{\Gamma_R} \frac{\partial \phi_i}{\partial n} \frac{\partial v_i}{\partial n} d\Gamma \right. \\
&\quad \left. + \int_{\Gamma_R} \left(\frac{\partial v_i}{\partial n} \right)^2 d\Gamma \right] \tag{5.10}
\end{aligned}$$

Substituting Eqs. (5.6-5.10) into Eq. (5.3)

$$\begin{aligned}
I[u_i] = & \frac{1}{2} \left\{ \iint_{S_i} (L_i \phi_i - q_i)^2 dS + \iint_{S_i} (L_i v_i)^2 dS \right. \\
& + 2 \iint_{S_i} [L_i \phi_i L_i v_i - q_i L_i v_i] dS + \bar{w}_V \left[\int_{\Gamma_0} (\phi_1 - \phi_2)^2 d\Gamma \right. \\
& \left. + 2 \int_{\Gamma_0} (\phi_1 - \phi_2)(v_1 - v_2) d\Gamma + \int_{\Gamma_0} (v_1 - v_2)^2 d\Gamma \right] \\
& + \bar{w}_R \left[\int_{\Gamma_0} \left(D_1 \frac{\partial \phi_1}{\partial n} - D_2 \frac{\partial \phi_2}{\partial n} \right)^2 d\Gamma + \int_{\Gamma_0} \left(D_1 \frac{\partial v_1}{\partial n} - D_2 \frac{\partial v_2}{\partial n} \right)^2 d\Gamma \right. \\
& \left. + 2 \int_{\Gamma_0} \left(D_1 \frac{\partial \phi_1}{\partial n} - D_2 \frac{\partial \phi_2}{\partial n} \right) \left(D_1 \frac{\partial v_1}{\partial n} - D_2 \frac{\partial v_2}{\partial n} \right) d\Gamma \right] \\
& + w_{V,i} \left[\int_{\Gamma_V} \phi_i^2 d\Gamma + 2 \int_{\Gamma_V} \phi_i v_i d\Gamma + \int_{\Gamma_V} v_i^2 d\Gamma \right] \\
& \left. + w_{R,i} D_i^2 \left[\int_{\Gamma_R} \left(\frac{\partial \phi_i}{\partial n} \right)^2 d\Gamma + 2 \int_{\Gamma_R} \frac{\partial \phi_i}{\partial n} \frac{\partial v_i}{\partial n} d\Gamma + \int_{\Gamma_R} \left(\frac{\partial v_i}{\partial n} \right)^2 d\Gamma \right] \right\} \quad (5.11)
\end{aligned}$$

Rearranging terms yields

$$\begin{aligned}
I[u_i] = & \frac{1}{2} \left\{ \iint_{S_i} (L_i \phi_i - q_i)^2 dS + \bar{w}_V \int_{\Gamma_0} (\phi_1 - \phi_2)^2 d\Gamma + w_{V,i} \int_{\Gamma_V} \phi_i^2 d\Gamma \right. \\
& \left. + \bar{w}_R \int_{\Gamma_0} \left(D_1 \frac{\partial \phi_1}{\partial n} - D_2 \frac{\partial \phi_2}{\partial n} \right)^2 d\Gamma + w_{R,i} D_i^2 \int_{\Gamma_R} \left(\frac{\partial \phi_i}{\partial n} \right)^2 d\Gamma \right\} \\
& + \left\{ \iint_{S_i} [L_i \phi_i L_i v_i - q_i L_i v_i] dS + \bar{w}_V \int_{\Gamma_0} (\phi_1 - \phi_2)(v_1 - v_2) d\Gamma \right. \\
& + \bar{w}_R \int_{\Gamma_0} \left(D_1 \frac{\partial \phi_1}{\partial n} - D_2 \frac{\partial \phi_2}{\partial n} \right) \left(D_1 \frac{\partial v_1}{\partial n} - D_2 \frac{\partial v_2}{\partial n} \right) d\Gamma + w_{V,i} \int_{\Gamma_V} \tilde{\phi}_i v_i d\Gamma \\
& \left. + w_{R,i} D_i^2 \int_{\Gamma_R} \frac{\partial \phi_i}{\partial n} \frac{\partial v_i}{\partial n} d\Gamma \right\} + \frac{1}{2} \left\{ \iint_{S_i} (L_i v_i)^2 dS + \bar{w}_V \int_{\Gamma_0} (v_1 - v_2)^2 d\Gamma \right. \\
& \left. + 2 \int_{\Gamma_0} (\phi_1 - \phi_2)(v_1 - v_2) d\Gamma + \int_{\Gamma_0} (v_1 - v_2)^2 d\Gamma \right\} \quad (5.12)
\end{aligned}$$

$$\left. +\bar{w}_R \int_{\Gamma_0} \left(D_1 \frac{\partial v_1}{\partial n} - D_2 \frac{\partial v_2}{\partial n} \right)^2 d\Gamma + w_{V,i} \int_{\Gamma_V} v_i^2 d\Gamma + w_{R,i} D_i^2 \int_{\Gamma_R} \left(\frac{\partial v_i}{\partial n} \right)^2 d\Gamma \right\}$$

Next, the following definitions are made

$$I[\phi_i] \equiv \frac{1}{2} \left\{ \iint_{S_i} (L_i \phi_i - q_i)^2 dS + +\bar{w}_R \int_{\Gamma_0} \left(D_1 \frac{\partial \phi_1}{\partial n} - D_2 \frac{\partial \phi_2}{\partial n} \right)^2 d\Gamma \right. \quad (5.13)$$

$$\left. +\bar{w}_V \int_{\Gamma_0} (\phi_1 - \phi_2)^2 d\Gamma + w_{V,i} \int_{\Gamma_V} \phi_i^2 d\Gamma + w_{R,i} D_i^2 \int_{\Gamma_R} \left(\frac{\partial \phi_i}{\partial n} \right)^2 d\Gamma \right.$$

$$\delta I[\phi_i, v_i] \equiv \iint_{S_i} [L_i \phi_i L_i v_i - q_i L_i v_i] dS + w_{R,i} D_i^2 \int_{\Gamma_R} \frac{\partial \phi_i}{\partial n} \frac{\partial v_i}{\partial n} d\Gamma$$

$$+ \bar{w}_V \int_{\Gamma_0} (\phi_1 - \phi_2)(v_1 - v_2) d\Gamma + w_{V,i} \int_{\Gamma_V} \phi_i v_i d\Gamma \quad (5.14)$$

$$+ \bar{w}_R \int_{\Gamma_0} \left(D_1 \frac{\partial \phi_1}{\partial n} - D_2 \frac{\partial \phi_2}{\partial n} \right) \left(D_1 \frac{\partial v_1}{\partial n} - D_2 \frac{\partial v_2}{\partial n} \right) d\Gamma$$

$$\delta^2 I[v_i] \equiv \frac{1}{2} \left\{ \iint_{S_i} (L_i v_i)^2 dS + \bar{w}_V \int_{\Gamma_0} (v_1 - v_2)^2 d\Gamma + w_{V,i} \int_{\Gamma_V} v_i^2 d\Gamma \right. \quad (5.15)$$

$$\left. + \bar{w}_R \int_{\Gamma_0} \left(D_1 \frac{\partial v_1}{\partial n} - D_2 \frac{\partial v_2}{\partial n} \right)^2 d\Gamma + w_{V,i} \int_{\Gamma_V} v_i^2 d\Gamma + w_{R,i} D_i^2 \int_{\Gamma_R} \left(\frac{\partial v_i}{\partial n} \right)^2 d\Gamma \right.$$

Since $\delta^2 I[v_i] > 0$, to minimize $I[u_i]$, one must have $\delta I[\phi_i, v_i] = 0$. This is the stationary condition and hence the bilinear form of Eq. (5.1) is obtained:

$$a(\phi, v) = f(v) \quad (5.16)$$

where

$$f(v) \equiv \iint_{S_i} q_i L_i v_i dS \quad (5.17)$$

$$\begin{aligned}
a(\phi, v) &\equiv \iint_{S_i} L_i \phi_i L_i v_i dS + \bar{w}_V \int_{\Gamma_0} (\phi_1 - \phi_2)(v_1 - v_2) d\Gamma \\
&+ \bar{w}_R \int_{\Gamma_0} \left(D_1 \frac{\partial \phi_1}{\partial n} - D_2 \frac{\partial \phi_2}{\partial n} \right) \left(D_1 \frac{\partial v_1}{\partial n} - D_2 \frac{\partial v_2}{\partial n} \right) d\Gamma \\
&+ w_{V,i} \int_{\Gamma_V} \phi_i v_i d\Gamma + w_{R,i} D_i^2 \int_{\Gamma_R} \frac{\partial \phi_i}{\partial n} \frac{\partial v_i}{\partial n} d\Gamma
\end{aligned} \tag{5.18}$$

The next step of the numerical formulation is to determine the weights. To accomplish this task, first, a weighted norm is defined as it was done in Eq. (3.90), and it is recalled that the error introduced by the weighted collocation method is bounded by

$$\|\phi - \phi_h\|_H \leq M \inf_{v \in V} \|\phi - v\|_H \tag{5.19}$$

provided that the bilinear form, $a(\phi, v)$, is continuous and coercive. For the problem considered Eq. (5.19) becomes

$$\begin{aligned}
\|\phi - \phi_h\|_H &\leq C_1 \alpha_1 \|\phi_1 - v_1\|_{2,S_1} + C_2 \alpha_2 \|\phi_2 - v_2\|_{2,S_2} \\
&+ C_3 w_{V,1} \|\phi_1 - v_1\|_{0,\Gamma_{V,1}} + C_4 w_{V,2} \|\phi_2 - v_2\|_{0,\partial\Gamma_{V,2}} \\
&+ C_5 w_{R,1} \left\| D_1 \frac{\partial}{\partial n} (\phi_1 - v_1) \right\|_{0,\Gamma_{R,1}} + C_6 w_{R,2} \left\| D_2 \frac{\partial}{\partial n} (\phi_2 - v_2) \right\|_{0,\Gamma_{R,2}} \\
&+ C_7 \bar{w}_V \|v_1 - v_2\|_{0,\Gamma_0} + C_8 \bar{w}_R \left\| D_1 \frac{\partial v_1}{\partial n} - D_2 \frac{\partial v_2}{\partial n} \right\|_{0,\Gamma_0}
\end{aligned} \tag{5.20}$$

where ϕ_h is the optimal numerical solution, $\alpha_i = \max[D_i, \Sigma_{a,i}]$, $i = 1, 2$ and $C_j, j = 1, \dots, 8$ are generic constants. Since the approximation error is larger on the boundaries of the domain as compared to the error resulting from the approximation of PDE, all norms on right hand side of Eq. (5.20) will be transformed to $\|\cdot\|_{1,S}$, and then these error terms will be balanced by selecting appropriate weights for the boundary and interface terms. The following inequalities, given in [61,62,65,67,70], will be utilized for this purpose

$$\begin{aligned}
\|a_i\|_{2,S_i} &\leq CN_{i,int}\|a\|_{1,S_i} \\
\|a_i\|_{0,\Gamma_{V,i}} &\leq C\|a\|_{1,S} \\
\left\|\frac{\partial a_i}{\partial n}\right\|_{0,\Gamma_{R,i}} &\leq C\bar{N}_{int}\sqrt{\bar{\alpha}}\|a\|_{1,S} \\
\|a_i\|_{0,\Gamma_0} &\leq C\|a\|_{1,S} \\
\left\|\frac{\partial a_i}{\partial n}\right\|_{0,\Gamma_0} &\leq CN_{i,int}\sqrt{\bar{\alpha}}\|a\|_{1,S}
\end{aligned} \tag{5.21}$$

where $\bar{N}_{int} = \max[N_{1,int}, N_{2,int}]$.

For the C_1 and C_2 terms

$$\begin{aligned}
C_1\alpha_1\|\phi_1 - v_1\|_{2,S_1} &\leq \bar{C}_1\alpha_1N_{1,int}\|\phi_1 - v_1\|_{1,S_1} \\
C_2\alpha_2\|\phi_2 - v_2\|_{2,S_2} &\leq \bar{C}_2\alpha_2N_{2,int}\|\phi_2 - v_2\|_{1,S_2}
\end{aligned} \tag{5.22}$$

note that $\bar{C}_i \equiv CC_i$. Since the same PDE governs both regions it is expected that $\|\phi_1 - v_1\|_{1,S_1} \approx \|\phi_2 - v_2\|_{1,S_2}$ and thus the error, due to the approximation of the flux by RBFs will be dominated by $\alpha_i N_{i,int}$, and therefore one can write

$$\begin{aligned}
&\bar{C}_1\alpha_1N_{1,int}\|\phi_1 - v_1\|_{1,S_1} + \bar{C}_2\alpha_2N_{2,int}\|\phi_2 - v_2\|_{1,S_2} \\
&= (\bar{C}_1\alpha_1N_{1,int} + \bar{C}_2\alpha_2N_{2,int})\|\phi - v\|_{1,S} \sim \bar{C}_{1-2}\bar{\alpha}\bar{N}_{int}\|\phi - v\|_{1,S}
\end{aligned} \tag{5.23}$$

where $\bar{\alpha} = \max[\alpha_1, \alpha_2]$. Next, the vacuum and reflective BC terms will be treated

$$C_3w_{V,1}\|\phi_1 - v_1\|_{0,\Gamma_{V,1}} \leq \bar{C}_3w_{V,1}\|\phi - v\|_{1,S} \tag{5.24}$$

$$C_4w_{V,2}\|\phi_2 - v_2\|_{0,\Gamma_{V,2}} \leq \bar{C}_4w_{V,2}\|\phi - v\|_{1,S} \tag{5.25}$$

$$\begin{aligned}
C_5w_{R,1}\left\|D_1\frac{\partial}{\partial n}(\phi_1 - v_1)\right\|_{0,\Gamma_{R,1}} &= C_5w_{R,1}D_1\left\|\frac{\partial}{\partial n}(\phi_1 - v_1)\right\|_{0,\Gamma_{R,1}} \\
&\leq C_5Cw_{R,1}\bar{N}_{int}\sqrt{\bar{\alpha}}D_1\|\phi - v\|_{1,S} \\
&= \bar{C}_5w_{R,1}\bar{N}_{int}\sqrt{\bar{\alpha}}D_1\|\phi - v\|_{1,S}
\end{aligned} \tag{5.26}$$

$$\begin{aligned}
C_6w_{R,2}\left\|D_2\frac{\partial}{\partial n}(\phi_2 - v_2)\right\|_{0,\Gamma_{R,2}} &= C_6w_{R,2}D_2\left\|\frac{\partial}{\partial n}(\phi_2 - v_2)\right\|_{0,\Gamma_{R,2}} \\
&\leq C_6Cw_{R,2}\bar{N}_{int}\sqrt{\bar{\alpha}}D_2\|\phi - v\|_{1,S} \\
&= \bar{C}_6w_{R,2}\bar{N}_{int}\sqrt{\bar{\alpha}}D_2\|\phi - v\|_{1,S}
\end{aligned} \tag{5.27}$$

When the continuity of the neutron flux condition is considered it is first noted that $\phi_1 - \phi_2 = 0$ on Γ_0 . Then

$$\begin{aligned} C_7 \bar{w}_V \|v_1 - v_2\|_{0,\Gamma_0} &= C_7 \bar{w}_V \|v_1 - v_2 - (\phi_1 - \phi_2)\|_{0,\Gamma_0} \\ &= C_7 \bar{w}_V \|v_1 - \phi_1 + \phi_2 - v_2\|_{0,\Gamma_0} \\ &\leq C_7 \bar{w}_V [\|\phi_1 - v_1\|_{0,\Gamma_0} + \|\phi_2 - v_2\|_{0,\Gamma_0}] \end{aligned} \quad (5.28)$$

Assuming that $\|\phi_1 - v_1\|_{0,\Gamma_0} \approx \|\phi_2 - v_2\|_{0,\Gamma_0}$ one can write

$$C_7 \bar{w}_V [\|\phi_1 - v_1\|_{0,\Gamma_0} + \|\phi_2 - v_2\|_{0,\Gamma_0}] \sim C_7 \bar{w}_V \|\phi - v\|_{0,\Gamma_0} \quad (5.29)$$

and therefore

$$C_7 \bar{w}_V \|\phi - v\|_{0,\Gamma_0} \leq C_7 C \bar{w}_V \|\phi - v\|_{1,S} = \bar{C}_7 \bar{w}_V \|\phi - v\|_{1,S} \quad (5.30)$$

The treatment of the continuity of neutron current condition is similar to that of the neutron flux. Noting that $D_1 \frac{\partial \phi_1}{\partial n} - D_2 \frac{\partial \phi_2}{\partial n} = 0$ on Γ_0

$$\begin{aligned} C_8 \bar{w}_R \left\| D_1 \frac{\partial v_1}{\partial n} - D_2 \frac{\partial v_2}{\partial n} - \left(D_1 \frac{\partial \phi_1}{\partial n} - D_2 \frac{\partial \phi_2}{\partial n} \right) \right\|_{0,\Gamma_0} \\ = C_8 \bar{w}_R \left\| D_1 \frac{\partial}{\partial n} (v_1 - \phi_1) + D_2 \frac{\partial}{\partial n} (\phi_2 - v_2) \right\|_{0,\Gamma_0} \\ \leq C_8 \bar{w}_R \left[D_1 \left\| \frac{\partial}{\partial n} (\phi_1 - v_1) \right\|_{0,\Gamma_0} + D_2 \left\| \frac{\partial}{\partial n} (\phi_2 - v_2) \right\|_{0,\Gamma_0} \right] \end{aligned} \quad (5.31)$$

Substituting the last inequality of Eq. (5.21) into Eq. (5.31)

$$\begin{aligned} C_8 \bar{w}_R \left[D_1 \left\| \frac{\partial}{\partial n} (\phi_1 - v_1) \right\|_{0,\Gamma_0} + D_2 \left\| \frac{\partial}{\partial n} (\phi_2 - v_2) \right\|_{0,\Gamma_0} \right] \\ \leq C_8 \bar{w}_R [D_1 C N_{1,int} \sqrt{\bar{\alpha}} \|\phi - v\|_{1,S} + D_2 C N_{2,int} \sqrt{\bar{\alpha}} \|\phi - v\|_{1,S}] \\ = \bar{C}_8 \bar{w}_R [D_1 N_{1,int} \sqrt{\bar{\alpha}} \|\phi - v\|_{1,S} + D_2 N_{2,int} \sqrt{\bar{\alpha}} \|\phi - v\|_{1,S}] \\ \sim \bar{C}_8 \bar{D} \bar{N}_{int} \sqrt{\bar{\alpha}} \bar{w}_R \|\phi - v\|_{1,S} \end{aligned} \quad (5.32)$$

where, $\bar{D} = \max[D_1, D_2]$, and it is considered that $D_i N_{i,int} \sqrt{\bar{\alpha}}$ term has determined the order of error.

To obtain the weights related to the boundary and interface conditions Eqs. (5.23)-(5.27), (5.30) and (5.32) have to be substituted into Eq. (5.20). This gives

$$\begin{aligned}
\|\phi - \phi_h\|_H \leq & \bar{C}_{1-2} \bar{\alpha} \bar{N}_{int} \|\phi - v\|_{1,S} + \bar{C}_3 w_{V,1} \|\phi - v\|_{1,S} \\
& + \bar{C}_4 w_{V,2} \|\phi - v\|_{1,S} + \bar{C}_5 w_{R,1} \bar{N}_{int} \sqrt{\bar{\alpha}} D_1 \|\phi - v\|_{1,S} \\
& + \bar{C}_6 w_{R,2} \sqrt{\bar{\alpha}} \bar{N}_{int} D_2 \|\phi - v\|_{1,S} + \bar{C}_7 \bar{w}_V \|\phi - v\|_{1,S} \\
& + \bar{C}_8 \bar{D} \bar{N}_{int} \sqrt{\bar{\alpha}} \bar{w}_R \|\phi - v\|_{1,S}
\end{aligned} \tag{5.33}$$

To get a balance in errors the following weights must be chosen:

$$w_{V,1} = w_{V,2} = \bar{w}_V = \bar{\alpha} \bar{N}_{int}, \quad w_{R,1} = \frac{\sqrt{\bar{\alpha}}}{D_1}, \quad w_{R,2} = \frac{\sqrt{\bar{\alpha}}}{D_2}, \quad \bar{w}_R = \frac{\sqrt{\bar{\alpha}}}{\bar{D}} \tag{5.34}$$

Now that the weights are determined, the rest of the numerical solution procedure is similar to that presented for homogeneous cases. The domain of the problem is discretized by introducing sets of interpolation nodes for the two subdomains ($\mathbf{D}^1, \mathbf{D}^2$), interface (\mathbf{I}), vacuum type boundaries ($\mathbf{B}_V^1, \mathbf{B}_V^2$) and reflective type boundaries ($\mathbf{B}_R^1, \mathbf{B}_R^2$). Also a set of external nodes (\mathbf{E}) are created to enhance the accuracy of the method:

$$\begin{aligned}
\mathbf{D}^1 &= \{d_1^1, d_2^1, \dots, d_{N_{D^1}}^1\}, \quad \mathbf{D}^2 = \{d_1^2, d_2^2, \dots, d_{N_{D^2}}^2\} \\
\mathbf{I} &= \{i_1, i_2, \dots, i_{N_I}\} \\
\mathbf{B}_V^1 &= \{b_{V,1}^1, b_{V,2}^1, \dots, b_{N_{B_V^1}}^1\}, \quad \mathbf{B}_V^2 = \{b_{V,1}^2, b_{V,2}^2, \dots, b_{N_{B_V^2}}^2\} \\
\mathbf{B}_R^1 &= \{b_{R,1}^1, b_{R,2}^1, \dots, b_{N_{B_R^1}}^1\}, \quad \mathbf{B}_R^2 = \{b_{R,1}^2, b_{R,2}^2, \dots, b_{N_{B_R^2}}^2\} \\
\mathbf{E}^1 &= \{e_1^1, e_2^1, \dots, e_{N_{E^1}}^1\}, \quad \mathbf{E}^2 = \{e_1^2, e_2^2, \dots, e_{N_{E^2}}^2\}
\end{aligned} \tag{5.35}$$

Here N_x denotes the number of nodes contained in the region x . A typical uniform distribution with 49 domain nodes and 24 exterior nodes is presented in Figure 5.2a. It should be noted that the domain nodes will also be used in the collocation step of the numerical procedure.

As stated in Chapter 3, the accuracy of the weighted RBF collocation method can be improved by utilizing more collocation nodes than the interpolation nodes, and a distribution with $h_{int} = 2h_{col}$, where h is the distance between adjacent nodes is presented in Figure 5.2b.

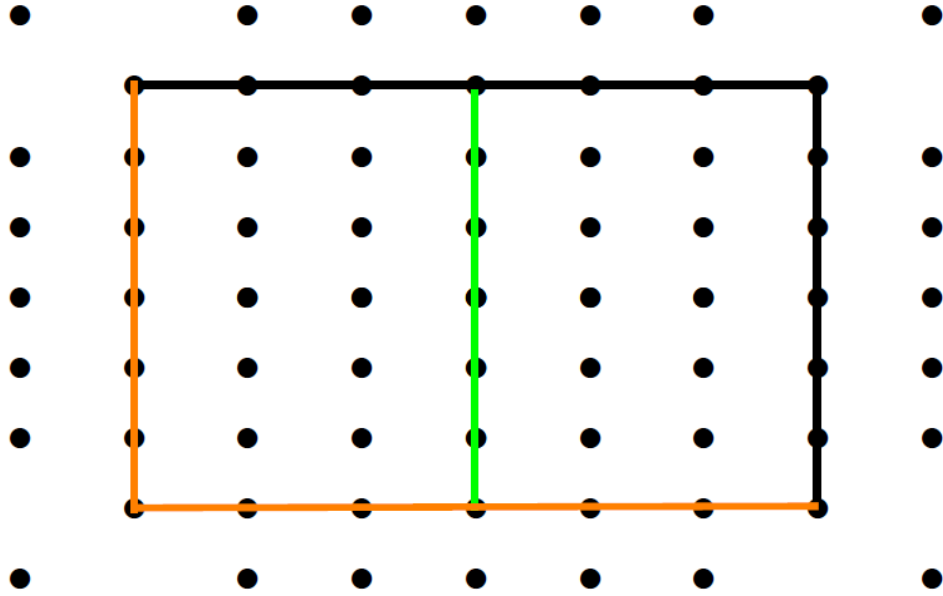


Figure 5.2a: A typical uniform node distribution for the 2-region problem with 49 domain nodes and 24 exterior nodes.

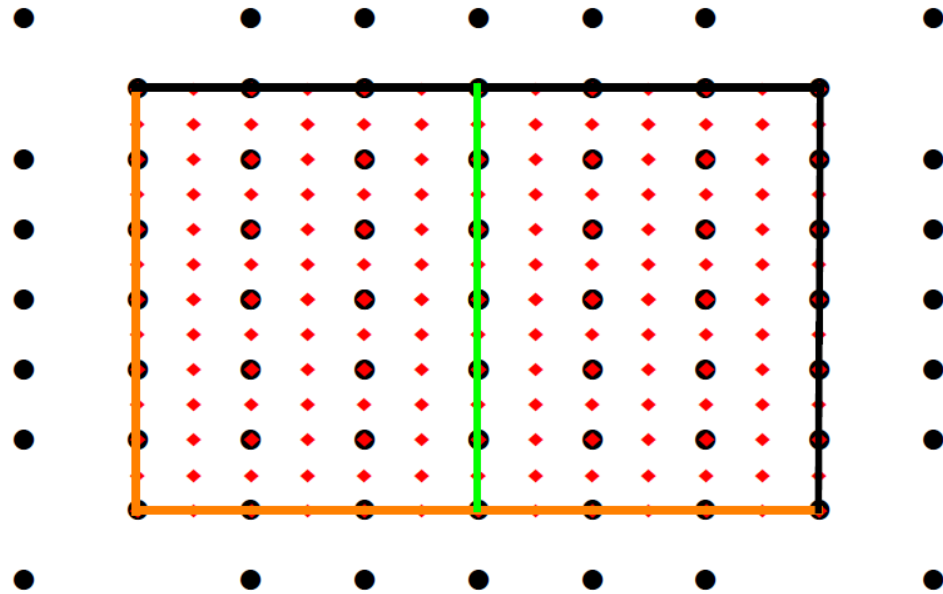


Figure 5.2b: Uniformly distributed interpolation and collocation nodes where $h_{int} = 2h_{col}$.

After the discretization of the domain, the neutron fluxes are approximated by the radial basis functions at the interpolation nodes

$$\phi^1(\mathbf{r}^1) = \sum_{j=1}^{N^1} a_j^1 \psi_j^1(\mathbf{r}), \quad \phi^2(\mathbf{r}^2) = \sum_{j=1}^{N^2} a_j^2 \psi_j^2(\mathbf{r}) \quad (5.36)$$

where \mathbf{r}^1 and \mathbf{r}^2 are the interpolation nodes contained in regions 1 and 2, respectively, and

$$N^i = N_{D^i} + N_I + N_{B_V^i} + N_{B_R^i} + N_{E^i}, \quad i = 1, 2 \quad (5.37)$$

Substituting the series in Eq. (5.36) into the governing equations, Eq. (5.1), collocating at the collocation nodes, and taking into account of the fact that the least-squares residual method is an approximation of the direct strong form collocation method, the collocation matrix of this method is

$$\begin{bmatrix} \mathbf{K}_1 & \mathbf{0} \\ w_{V,1} \mathbf{K}_{v,1} & \mathbf{0} \\ w_{R,1} \mathbf{K}_{r,1} & \mathbf{0} \\ \bar{w}_V \mathbf{I}_{v,1} & -\bar{w}_V \mathbf{I}_{v,2} \\ \bar{w}_R \mathbf{I}_{r,1} & -\bar{w}_R \mathbf{I}_{r,2} \\ \mathbf{0} & \mathbf{K}_2 \\ \mathbf{0} & w_{V,2} \mathbf{K}_{v,2} \\ \mathbf{0} & w_{R,2} \mathbf{K}_{r,2} \end{bmatrix} \mathbf{a} = \begin{bmatrix} \mathbf{Q}_1 \\ \mathbf{0} \\ \mathbf{0} \\ \mathbf{0} \\ \mathbf{0} \\ \mathbf{Q}_2 \\ \mathbf{0} \\ \mathbf{0} \end{bmatrix} \quad (5.38)$$

The block matrices $\mathbf{K}_i, \mathbf{K}_{v,i}, \mathbf{K}_{r,i}, \mathbf{I}_{v,i}$ and $\mathbf{I}_{r,i}$ and vectors $\mathbf{Q}_i, i = 1, 2$ of Eq. (5.38) are calculated by

$$\begin{aligned} \mathbf{K}_i &= -\nabla D_i(\mathbf{r}_k) \nabla \psi_i(\mathbf{r}_k, \mathbf{r}_j) + \Sigma_{a,i} \psi_i(\mathbf{r}_k, \mathbf{r}_j), \quad \mathbf{r}_k \in \mathbf{D}^{i,col}, \quad \mathbf{r}_j \in \mathbf{S}^i \\ \mathbf{K}_{v,i} &= \psi_i(\mathbf{r}_k, \mathbf{r}_j), \quad \mathbf{r}_k \in \mathbf{B}_V^{i,col}, \quad \mathbf{r}_j \in \mathbf{S}^i \\ \mathbf{K}_{r,i} &= D_i \frac{\partial \psi_i(\mathbf{r}_k, \mathbf{r}_j)}{\partial n}, \quad \mathbf{r}_k \in \mathbf{B}_R^{i,col}, \quad \mathbf{r}_j \in \mathbf{S}^i \\ \mathbf{I}_{v,i} &= \psi_i(\mathbf{r}_k, \mathbf{r}_j), \quad \mathbf{r}_k \in \mathbf{I}^{col}, \quad \mathbf{r}_j \in \mathbf{S}^i \\ \mathbf{I}_{r,i} &= D_i(\mathbf{r}_k) \frac{\partial \psi_i(\mathbf{r}_k, \mathbf{r}_j)}{\partial n}, \quad \mathbf{r}_k \in \mathbf{I}^{col}, \quad \mathbf{r}_j \in \mathbf{S}^i \\ \mathbf{Q}_i &= q_i(\mathbf{r}_k), \quad \mathbf{r}_k \in \mathbf{D}^{i,col} \end{aligned} \quad (5.39)$$

The solution of Eq. (5.38) reveals the coefficient vector

$$\mathbf{a} = \{a_1^1, a_2^1, \dots, a_j^{N^1}, a_1^2, a_2^2, \dots, a_j^{N^2}\} \quad (5.40)$$

and hence the numerical solution. Note that when the number of collocation and interpolation nodes is the same Gauss elimination can be used to deal with Eq. (5.38), whereas a least squares solver is required when the number of collocation nodes is higher.

5.2 Numerical Results

5.2.1 One-dimensional external source problem

The first problem considered is a 1-D two region external source case with the following mathematical description.

$$\begin{aligned}
 -D_1 \frac{d^2 \phi_1(x)}{dx^2} + \Sigma_{a,1} \phi_1(x) &= 0, & 0 \leq x \leq a \\
 -D_2 \frac{d^2 \phi_2(x)}{dx^2} + \Sigma_{a,2} \phi_2(x) &= s_2, & a \leq x \leq b \\
 \frac{d\phi_1(0)}{dx} &= 0, \quad \phi_2(b) = 0 \\
 \phi_1(a) &= \phi_2(a), \quad D_1 \frac{d\phi_1(a)}{dx} = D_2 \frac{d\phi_2(a)}{dx}
 \end{aligned} \tag{5.41}$$

This problem is studied in [5] to explain the spatial self-shielding phenomenon and the analytical solution is

$$\begin{aligned}
 \phi_1(x) &= \frac{s_2 \cosh\left(\frac{x}{L_1}\right)}{\left[\frac{L_1}{D_1} \coth\left(\frac{a}{L_1}\right) + \frac{L_2}{D_2} \coth\left(\frac{b-a}{L_2}\right)\right] \frac{D_1}{L_1} \Sigma_{a,2} \sinh\left(\frac{a}{L_1}\right)} \\
 \phi_2(x) &= \frac{s_2}{\Sigma_{a,2}} \left[1 - \frac{\cosh\left(\frac{b-x}{L_2}\right)}{\left[\frac{L_1}{D_1} \coth\left(\frac{a}{L_1}\right) + \frac{L_2}{D_2} \coth\left(\frac{b-a}{L_2}\right)\right] \frac{D_2}{L_2} \sinh\left(\frac{b-a}{L_2}\right)} \right]
 \end{aligned} \tag{5.42}$$

where a is the junction point, b is the size of the domain and $L_i = \sqrt{D_i/\Sigma_{a,i}}$ is the diffusion length of the i th region. A typical node distribution, where both regions are interpolated by 4 domain nodes and an external node is given in Figure 5.3.

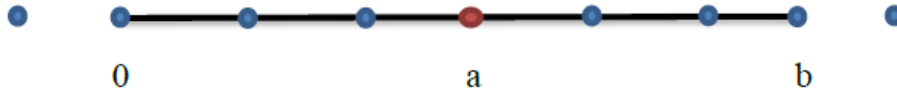


Figure 5.3: A typical distribution of interpolation nodes for the 1-D problem.

This problem is solved with the RBF collocation method with no weights. The multiquadric is used as the RBF. In the numerical experiments two sets of collocation points, $h_{int} = h_{col}$ and $h_{int} = 4h_{col}$, are utilized. Physical parameters are taken as $a = 50 \text{ cm}$, $b = 100 \text{ cm}$, $s_2 = 1 \text{ n/cm}^3\text{s}$, $D_1 = 1.77764 \text{ cm}$, $D_2 =$

1.558 cm, $\Sigma_{a,1} = 0.0143676 \text{ cm}^{-1}$ and $\Sigma_{a,2} = 0.01112 \text{ cm}^{-1}$. The analytical flux distribution obtained with these values is illustrated in Figure 5.4.

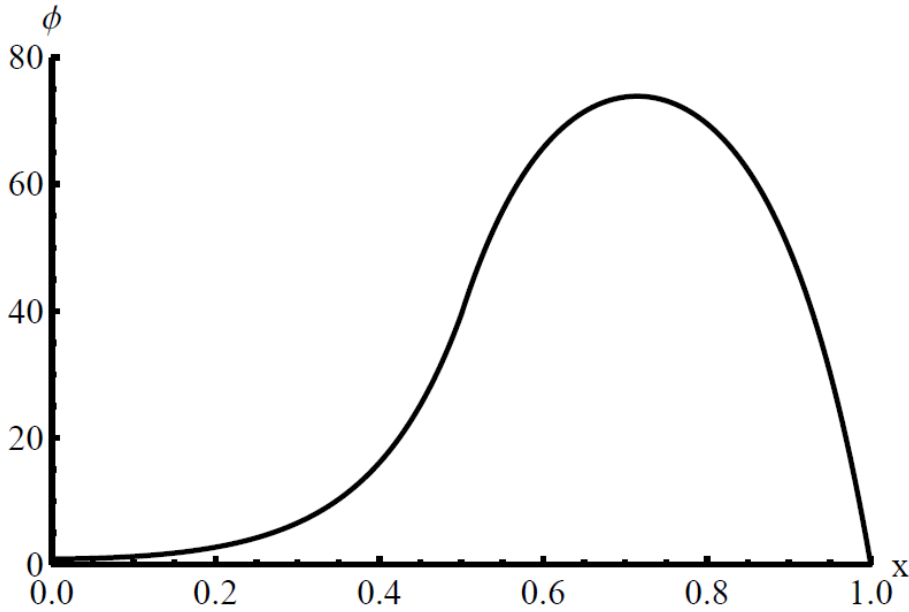


Figure 5.4: Analytical flux distribution for the one-dimensional problem.

Since the problem is 1-D, the arbitrary precision computation property of MATHEMATICA has been appealed in calculations. The number of interpolation and collocation nodes is the same and the shape parameter is chosen to be $c^2 = 0.05$. The results for maximum error and RMS error in flux are presented in Figure 5.5 in semi-log scale for both machine precision and a 100-precision solution. This figure clearly shows the power of utilizing high precision computation for the RBF collocation technique. When machine precision is used the numerical method becomes unstable above $1/h_{int} = 40$, whereas the 100-precision case yields a smooth decrease in both maximum and RMS errors. In addition to its superiority in stability, the high precision arithmetic gives highly accurate results. The RMS error of 100-precision calculation is 7.52×10^{-15} when $1/h_{int} = 100$.

The results observed can be improved further by increasing the number of collocation points and the value of the shape parameter. Figure 5.6 shows the variation of RMS error with $1/h_{int}$ for $h_{int} = h_{col}$ and $h_{int} = 4h_{col}$, when $c^2 = 0.1$. It is seen from this figure that extraordinary accuracy is achievable when the RBF collocation method is used with oversampling. When $1/h_{int} = 100$ the RMS error is 2.43×10^{-28} for $h_{int} = 4h_{col}$.

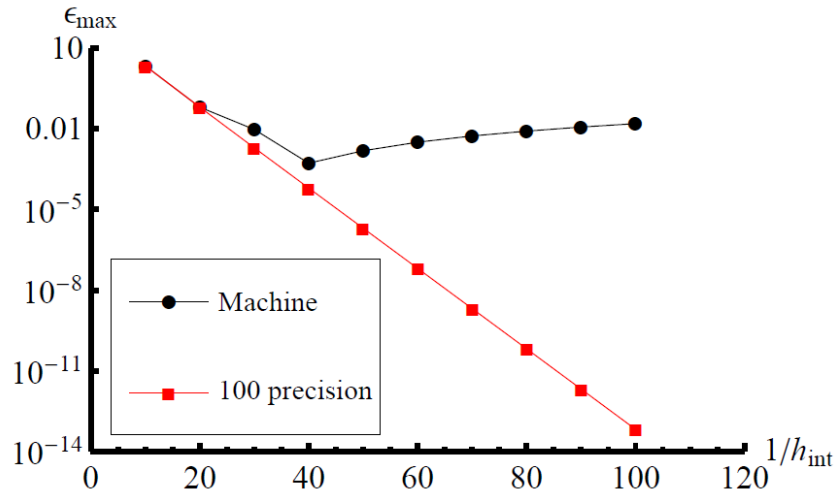


Figure 5.5a: ϵ_{max} for machine precision and 100-precision calculations.

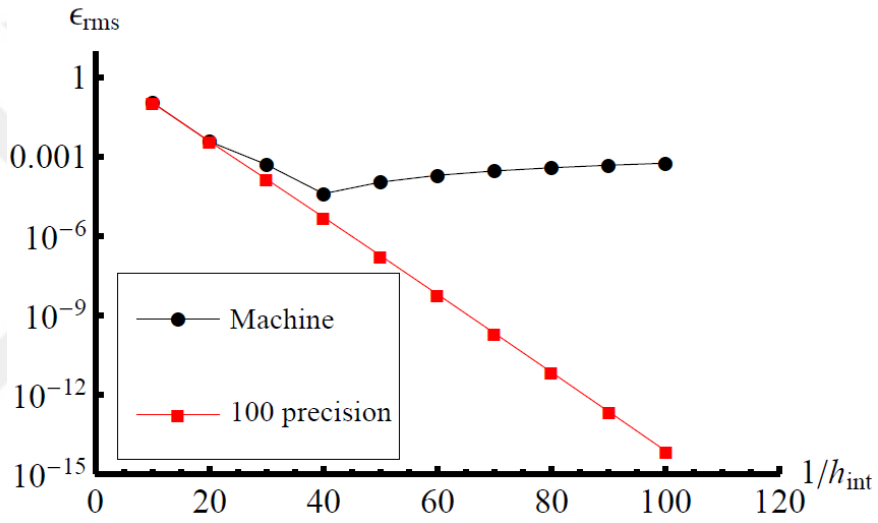


Figure 5.5b: ϵ_{rms} for machine precision and 100-precision calculations.

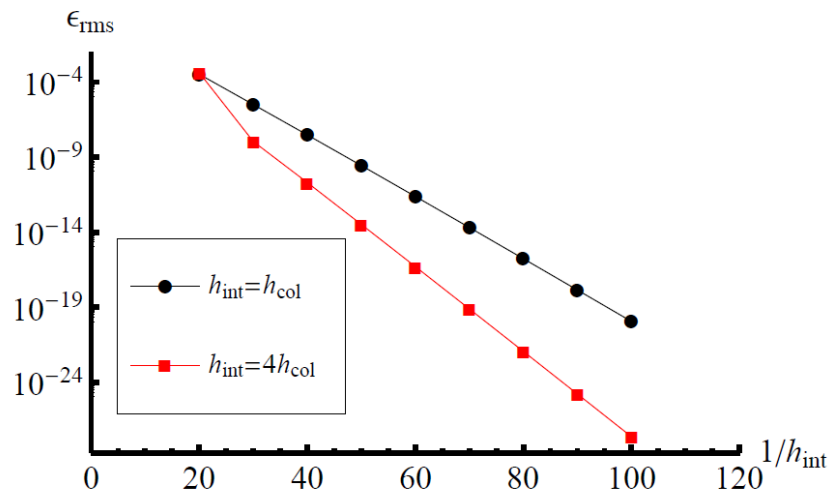


Figure 5.6: ϵ_{rms} for the 1-D problem when $h_{int} = h_{col}$ and $h_{int} = 4h_{col}$.

5.2.2 Two-dimensional problem without corner singularity

The next problem considered is a two-dimensional two-group fission source case for which an analytical solution exists. The geometry and boundary conditions of this configuration are illustrated in Figure 5.7, and the two-group parameters are presented in Table 5.1.

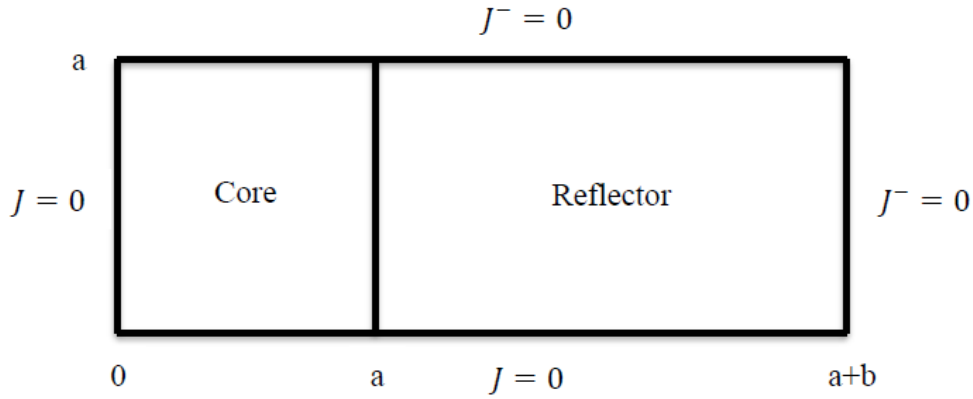


Figure 5.7: The geometry and boundary conditions of the 2-D problem without corner singularity.

Table 5.1: Two-group parameters for the 2-D problem without corner singularity.

	Core	Reflector
D_1	0.6165356	0.6165356
D_2	0.6165356	0.6165356
$\Sigma_{r,1}$	0.080117	0.01021
$\Sigma_{r,2}$	0.11484	0.00267
$\Sigma_{f,1}$	0.03252	0
$\Sigma_{f,2}$	0.071372	0
$\Sigma_{s,1 \rightarrow 2}$	0.063567	0.01005
$\nu \Sigma_{f,1}$	0.0813	0
$\nu \Sigma_{f,2}$	0.17843	0
χ_1	1	0
χ_2	1	0

The analytical solution of this problem is given in [79], and with the parameters given in Table 5.1, a critical system is achieved when $a = 4.86 \text{ cm}$ and $b = 20 \text{ cm}$. This problem is solved with both RBF collocation and weighted RBF collocation methods, and inverse multiquadric is chosen as the RBF. Overcollocation is utilized with $h_{int} = 2h_{col}$. The convergence criterion for the fission source iteration is chosen to be $\varepsilon = 10^{-6}$.

The percent error in the multiplication factor, λ , due to approximation with weighted RBF collocation and RBF collocation is given in Tables 5.2 and 5.3, respectively, for several values of the shape parameter, $c = a \times \sqrt{m}$. The linear boundary element solutions are also given in these tables. Here N is the number of equidistant intervals on each side of the core and on the side of the reflector parallel to the y-axis and M is the number of equidistant intervals on the sides of the reflector parallel to and on the x-axis.

The error values presented in Tables 5.2 and 5.3 show that RBF collocation and weighted RBF collocation methods can produce highly accurate solutions for the 2-region problem considered. Although the boundary element method gives a better accuracy than collocation methods when $N = 4$ and $M = 5$, with their faster convergence rates radial basis functions yields better results for higher values of N and M . When $N = 32$ and $M = 40$ the percent error is 0.000137, which is better than the boundary element solution by approximately three orders of magnitude. On the other hand the results obtained with $m = 0.2, 0.3$ reveals that the weighted collocation method has a broader range of stable computation in terms of the shape parameter.

Table 5.2: The percent error in λ for weighted RBF collocation calculations.

N	M	LBE	$m = 0.08$	$m = 0.09$	$m = 0.1$	$m = 0.2$	$m = 0.3$
4	5	2.17	8.170	7.716	7.309	5.052	3.584
8	10	0.71	0.199	0.152	0.672	0.269	0.165
16	20	0.22	0.0610	0.0467	0.0371	0.00565	0.00352
24	30	0.11	0.00525	0.00400	0.003215	0.00201	0.00208
32	40	0.09	0.00162	0.00166	0.00149	0.00132	0.00126

Table 5.3: The percent error in λ for RBF collocation calculations.

N	M	LBE	$m = 0.08$	$m = 0.09$	$m = 0.1$	$m = 0.2$	$m = 0.3$
4	5	2.17	11.484	9.727	8.209	1.831	0.551
8	10	0.71	0.407	0.338	0.329	0.192	0.142
16	20	0.22	0.0686	0.0550	0.0606	0.0118	0.00654
24	30	0.11	0.0104	0.00733	0.00449	0.00364	0.00424
32	40	0.09	0.000137	0.000724	0.000899	0.00382	0.00547

5.2.3 Two-dimensional problem with corner singularity

It is a well-known fact that when a singularity is present in the geometry, material properties or boundary conditions of the problem, the performance of the numerical

method, whether it is meshless or mesh-based, may be deteriorated [80-82]. In this regard, the third example is a 2-group, 2-region problem containing a corner singularity. The configuration of the problem is shown in Figure 5.8, and the nuclear parameters are given in Table 5.4.

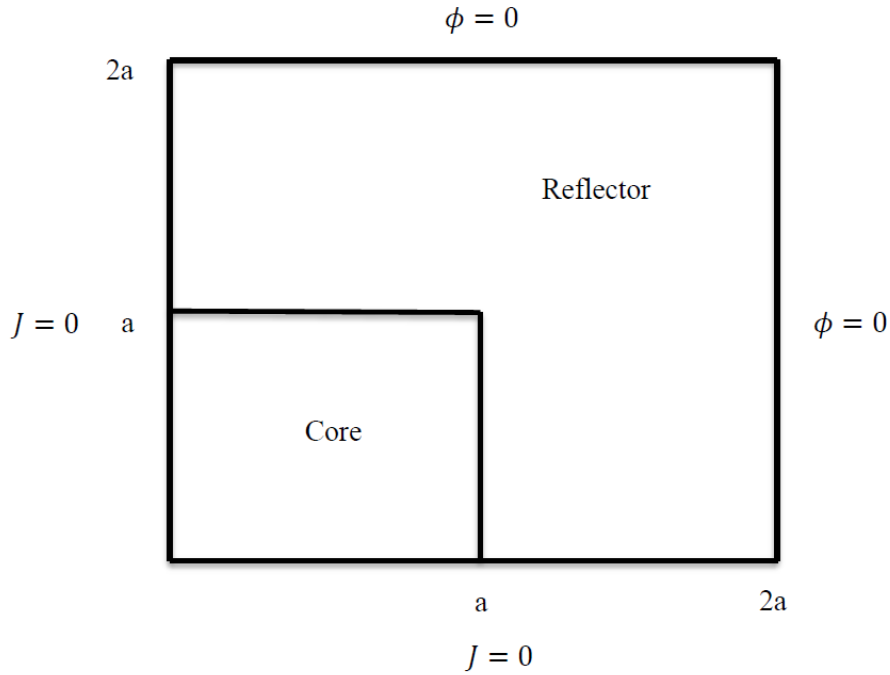


Figure 5.8: The geometry and boundary conditions of the 2-D problem with corner singularity.

Table 5.4: Two-group parameters for the 2-D problem with corner singularity.

	Core	Reflector
D_1	1.2	1.15
D_2	0.3	0.15
$\Sigma_{r,1}$	0.003	0.001
$\Sigma_{r,2}$	0.1016	0.02
$\Sigma_{f,1}$	0.0004166	0
$\Sigma_{f,2}$	0.05166	0
$\Sigma_{s,1 \rightarrow 2}$	0.025	0.06
$\nu \Sigma_{f,1}$	0.001	0
$\nu \Sigma_{f,2}$	0.124	0
χ_1	1	0
χ_2	0	0

In order to test the performance of the RBF collocation techniques, this problem is solved with FEM [71], and when $a = 7.5 \text{ cm}$ a reference solution of $\lambda =$

1.125893191 is found with 180000 linear finite elements. The RBF collocation and its weighted version are employed by dividing the problem domain into four square subdomains to better capture the corner singularity. Inverse multiquadric is used as the RBF, and calculations are performed with both $h_{int} = h_{col}$ and $h_{int} = 2h_{col}$. The convergence criterion for the fission source iteration is 10^{-6} .

Figures 5.9a and 5.9b show the relative percent error in the multiplication factor with respect to the number of equidistant intervals along one side of the square domain for weighted RBF collocation and RBF collocation, respectively. The shape parameter is chosen to be $c = b \times \sqrt{0.05}$, where $b = 2a$. The most significant observation of these figures is that, when the collocation techniques are utilized with overcollocation (i.e., $h_{int} = 2h_{col}$), the algorithm underestimates the reference λ value, contrary to the overestimated solutions of the $h_{int} = h_{col}$ route. As seen from Figure 5.9b, when overcollocation is employed without weights the collocation method produces unstable results with poor accuracy at low values of N . Finally, a comparison of the results plotted on Figure 5.9 shows that the collocation method with no weights and $h_{int} = h_{col}$ has produced the best results in terms of both accuracy and stability. This alternative has kept its stability and it gives an error value of $\epsilon_\lambda = -7.78 \times 10^{-5}$ at $N = 60$. On the other hand the weighted collocation method loses its stability at $N = 42$ and $N = 30$ for $h_{int} = h_{col}$ and $h_{int} = 2h_{col}$, respectively.

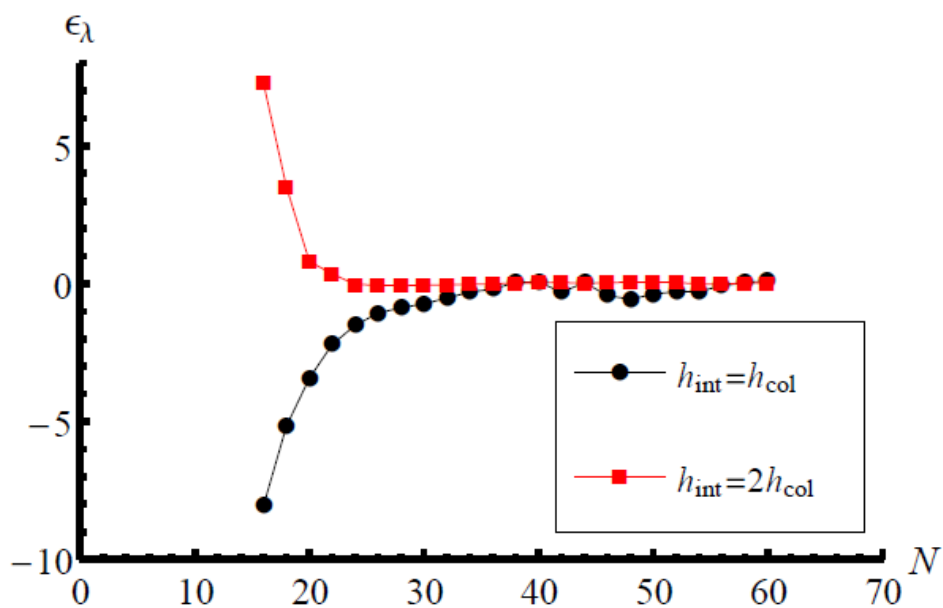


Figure 5.9a: Variation of ϵ_λ with respect to N for the weighted RBF collocation.

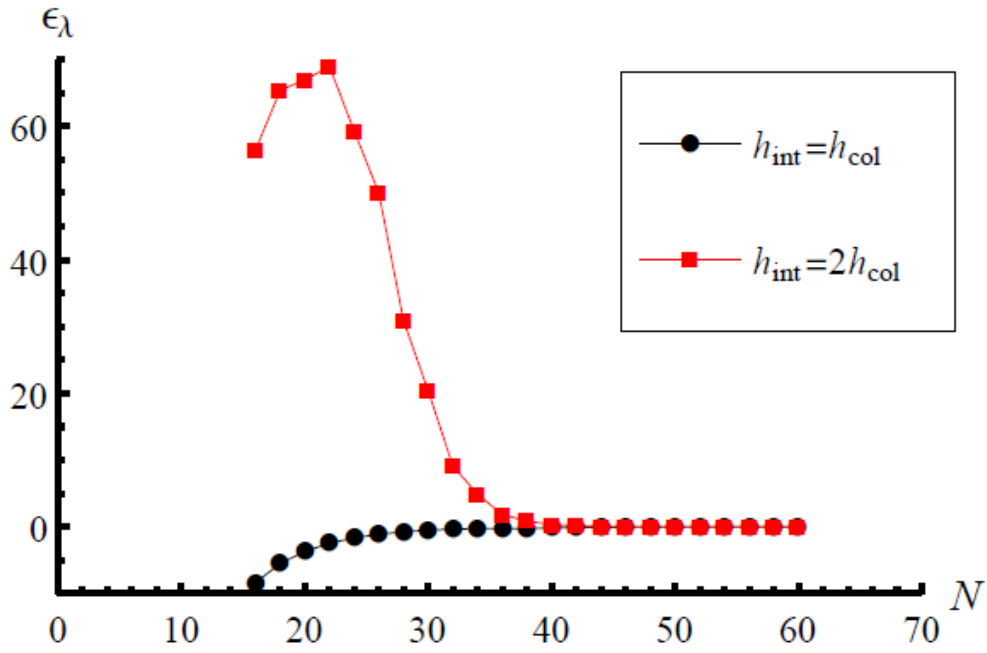


Figure 5.9b: Variation of ϵ_λ with respect to N for the RBF collocation.

The effect of the shape parameter, $c = b \times \sqrt{m}$ on the accuracy and convergence rate of the RBF collocation method is illustrated in Figure 5.10 on a semi-log scale. The relative percent errors presented on this graph are the absolute error values. Similar to the homogeneous problems, increasing the value of the shape parameter improves both the accuracy and the convergence rate of the scheme. The error at $N = 48$ decreases by an order of magnitude when the value of m is shifted from 0.06 to 0.08.

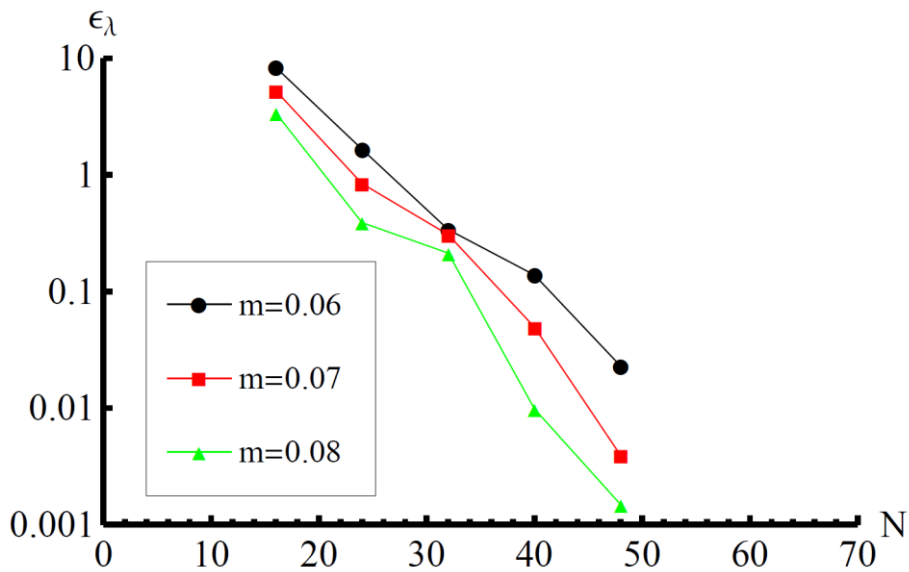


Figure 5.10: The effect of the shape parameter on the performance of the RBF collocation method.

5.2.4 Two-dimensional problem with corner singularity and high material heterogeneity

The fourth problem has the same geometric configuration with the third one, but this time the diffusion constants, removal and scattering cross sections of the core are chosen to be 10 times higher than those of the reflector region (i.e., $D_1^2 = 0.12$, $D_2^2 = 0.03$, $\Sigma_{r,1}^2 = 0.0003$, $\Sigma_{r,2}^2 = 0.01016$, $\Sigma_{s,1 \rightarrow 2}^2 = 0.0025$). This configuration results with $\lambda = 3.726583216$ when a FEM solution is obtained with 180000 linear finite elements. It should be noted that these types of differences in nuclear properties are not observed in practical applications, but this case of high material heterogeneity is studied to test the robustness of the weighted RBF collocation method.

The variation of the relative percent error in λ with respect to N is shown in Figure 5.11 for weighted and standard RBF collocation methods where $c = b \times \sqrt{0.2}$ and $h_{int} = 2h_{col}$. This figure clearly shows that the RBF collocation method has produced a much better performance than its weighted alternative. Although small oscillations are observed at low N the RBF collocation method has yielded accurate results, while the weighted collocation method gave up a divergent solution with poor accuracy. This high material heterogeneity problem shows that when the robustness of the method is taken into account the RBF collocation method is advantageous.

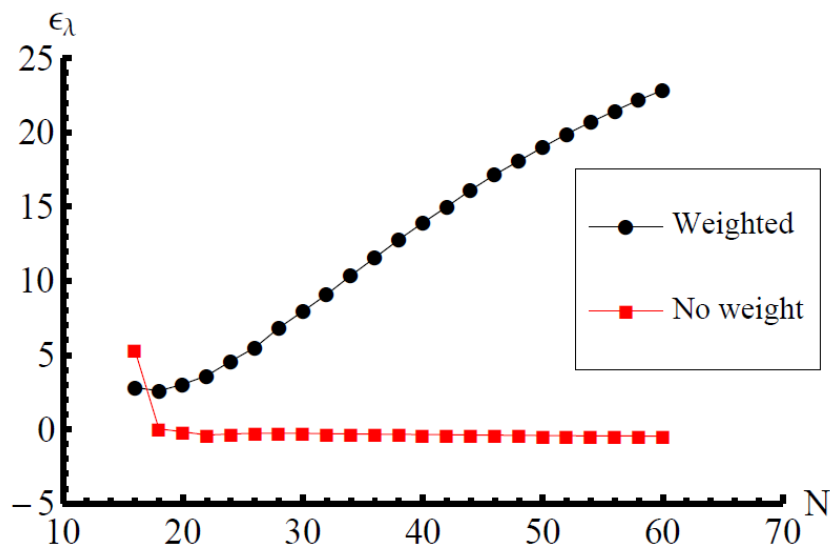


Figure 5.11: Variation of ϵ_λ with respect to N for weighted and standard collocation methods.

5.2.5 The IAEA two-dimensional benchmark problem

The last example considered in this chapter is a two-dimensional one-group IAEA benchmark problem consisting of five regions. The geometry of the problem is presented in Figure 5.12 where the dimensions are in cm , and the one-group parameters are given in Table 5.5 ($\nu = 2.43$ for regions 1 and 3). This benchmark is defined to be very difficult to solve because of the large differences in quadrant-averaged fluxes [83].

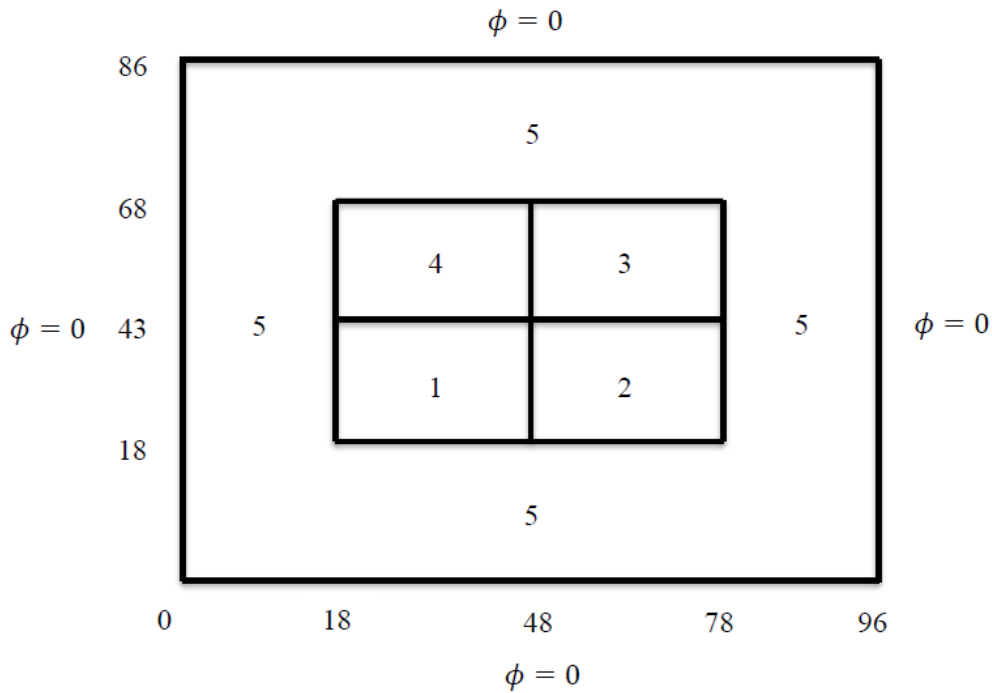


Figure 5.12: The geometry of the IAEA two-dimensional benchmark problem.

Table 5.5: The one-group parameters for the IAEA two-dimensional benchmark problem.

Region	$D(cm)$	$\Sigma_a(cm^{-1})$	$\nu\Sigma_f(cm^{-1})$
1	0.6536	0.07	0.079
2	0.7042	0.28	0
3	0.55556	0.04	0.043
4	0.55556	0.15	0
5	0.43478	0.01	0

This benchmark problem is solved with the RBF collocation method. The domain is divided into 16 subdomains to improve the performance of the numerical algorithm. Twelve subdomains are used to model the fifth region, and the remaining four subdomains represent regions 1-4. The calculations are performed with $h_{int} = h_{col}$.

In [83], the reference solution for the multiplication factor is reported to be $\lambda = 0.99222$.

The numerical multiplication factor values obtained with the RBF collocation technique are tabulated in Table 5.6 for three values of the shape parameter, $c = 0.96 \times \sqrt{m}$. All subdomains are interpolated with uniformly distributed nodes and N is the number of equidistant intervals in both directions. The results of this table show that the RBF collocation method has produced accurate results with a smooth convergence, and therefore it is successful in modelling multiregion neutron diffusion problems.

Table 5.6: Numerical λ values for the IAEA benchmark problem obtained with RBF collocation method for three values of the shape parameter.

N	$m = 0.08$	$m = 0.1$	$m = 0.2$
3	1.01613	1.01583	1.01632
4	1.01002	1.00973	1.00843
5	1.00389	1.00375	1.00214
6	1.00057	0.998703	0.998263
7	0.997276	0.9962	0.996151
8	0.994168	0.995012	0.994679
9	0.993303	0.994187	0.993785
10	0.993686	0.993749	0.993377
11	0.99339	0.993316	0.993156
12	0.992993	0.992985	0.992889
13	0.992833	0.992858	0.992613
14	0.992749	0.992702	0.992195
15	0.992605	0.992602	0.991776



6. NUMERICAL SOLUTION OF NEUTRON TRANSPORT PROBLEMS

6.1 The One-dimensional Neutron Transport Equation and Angular Approximations

Until now the distribution of neutrons in a multiplying or nonmultiplying system has been studied with the diffusion approximation, which ignored the angular behavior and required the numerical solution of a PDE and a set of PDEs for homogeneous and heterogeneous systems, respectively. Since the computational capabilities have increased substantially in the last decades, attention has been focused on the numerical solution of the more detailed neutron transport equation. Taking into account this fact, in this chapter, the meshless RBF collocation method has been introduced into the field of neutron transport as a spatial approximation tool.

For a one-dimensional configuration the within group neutron transport equation can be expressed as follows [1]:

$$\mu \frac{\partial \varphi}{\partial x}(x, \mu) + \Sigma_t(x)\varphi(x, \mu) = \sum_{l=0}^L (2l + 1)P_l(\mu)\Sigma_{sl}(x)\phi_l(x) + s(x, \mu) \quad (6.1)$$

Here μ is the directional cosine, φ is the angular flux, Σ_t is the total cross section and $s(x, \mu)$ is either an external source and/or fission source. As is seen from Eq. (6.1), the scattering term on the right hand side is expanded in Legendre polynomials, where $P_l(\mu)$ is the Legendre polynomial and the Legendre moments are given by

$$\phi_l(x) = \frac{1}{2} \int_{-1}^1 P_l(\mu)\varphi(x, \mu)d\mu \quad (6.2)$$

$$\Sigma_{sl}(x) = \frac{1}{2} \int_{-1}^1 P_l(\mu)\Sigma_s(x, \mu)d\mu \quad (6.3)$$

The Legendre polynomials $P_l(\mu)$ are defined by [84]

$$P_0(\mu) = 1 \quad (6.4)$$

$$P_l(\mu) = \frac{1}{2^l} \frac{d^l}{d\mu^l} (\mu^2 - 1)^l, \quad l = 1, 2, \dots \quad (6.5)$$

These polynomials satisfy the following orthogonality relation on the interval $-1 \leq \mu \leq 1$:

$$\frac{1}{2} \int_{-1}^1 d\mu P_l(\mu) P_{l'}(\mu) = \frac{\delta_{ll'}}{2l+1} \quad (6.6)$$

where $\delta_{ll'}$ is the Kronecker delta. $P_l(\mu)$ also satisfy the recurrence relation

$$\mu P_l(\mu) = \frac{1}{2l+1} [(l+1)P_{l+1}(\mu) + lP_{l-1}(\mu)] \quad (6.7)$$

For the treatment of the angular variable of the flux there exists two widely utilized techniques: the spherical harmonics method (P_N method) and the discrete ordinates method (S_N method). The spherical harmonics method is an old approach and it was first used by astrophysicists [85]. Approximately half a century later it was introduced into the field of neutron transport [86]. On the other hand the history of the S_N method goes back to the study of radiation transport in stellar atmospheres [87], and its first application in reactor physics is seen in [88].

In the P_N method, which is adopted for the angular treatment of the neutron transport equation in this study, the angular flux and the source term are expanded in a finite series of Legendre polynomials similar to the expansion of the scattering cross section on the right hand side of Eq. (6.1):

$$\varphi(x, \mu) \approx \sum_{l=0}^N (2l+1) \phi_l(x) P_l(\mu) \quad (6.8)$$

$$s(x, \mu) \approx \sum_{l=0}^N (2l+1) s_l(x) P_l(\mu) \quad (6.9)$$

These approximations are substituted into Eq. (6.1), then it is multiplied by $\frac{1}{2} P_{l'}(\mu)$, integrated from -1 to $+1$. With the help of orthogonality and recurrence relations the P_N equations can be found by setting $\phi_{N+1} = 0$ [1]

$$\frac{l}{2l+1} \frac{d\phi_{l-1}}{dx} + \frac{l+1}{2l+1} \frac{d\phi_{l+1}}{dx} + (\Sigma_t - \Sigma_{sl})\phi_l = s_l, \quad l = 0, 1, \dots, N-1 \quad (6.10)$$

$$\frac{N}{2N+1} \frac{d\phi_{N-1}}{dx} + (\Sigma_t - \Sigma_{sN})\phi_N = s_N \quad (6.11)$$

Eqs. (6.10) and (6.11) show that with the P_N method, the integrodifferential neutron transport equation is transformed into a set of N ordinary differential equations.

An important point in the solution of the neutron transport equation by Legendre polynomials is the vacuum type boundary conditions. A sum of these polynomials cannot satisfy this condition [3], and hence a modified boundary condition is needed for these kinds of boundaries. A well-known solution to this problem is to use the Marshak boundary conditions. Suppose that for a 1-D geometry with $0 \leq x \leq a$, the angular flux vanishes at $x = a$. Then the Marshak boundary conditions can be expressed as

$$\int_{-1}^0 P_l(\mu)\psi(a, \mu)d\mu = 0, \quad l = 0, 1, \dots, N \quad (6.12)$$

Another method in dealing with the vacuum boundary conditions is to use the double P_N or DP_N approximation which is also advantageous when a heterogeneous system is considered. This approach is also known as Yvon's method in the literature [89].

In the DP_N method separate expansions are used for $-1 \leq \mu \leq 0$ and $0 \leq \mu \leq 1$:

$$\varphi(x, \mu) \approx \begin{cases} \sum_{l=0}^N (2l+1)\phi_l^+(x)P_l(2\mu-1), & \mu > 0 \\ \sum_{l=0}^N (2l+1)\phi_l^-(x)P_l(2\mu+1), & \mu < 0 \end{cases} \quad (6.13)$$

It has been shown in [1] that for problems dominated by the diffusion of neutrons through optically thick regions, the P_N method yields better results than the DP_N approach. But when vacuum boundaries are present the DP_N method is found to be the better choice [90].

Another alternative for the angular approximation of the transport equation is the S_N method. In this approach the angular flux is evaluated in a number of discrete directions. The formulation of the method starts by satisfying Eq. (6.1) for distinct μ_n

$$\mu_n \frac{d}{dx} \varphi_n(x) + \Sigma(x) \varphi_n(x) = \sum_{l=0}^L (2l+1) P_l(\mu_n) \Sigma_l(x) \phi_l(x) + s(x, \mu_n) \quad (6.14)$$

where $\varphi_n(x) \equiv \varphi(x, \mu_n)$. The angles are chosen so that an accurate result is obtained for the flux moments by a quadrature formula [1].

In the S_N approach the scalar flux and the Legendre moments are approximated by

$$\phi(x) = \frac{1}{2} \sum_{n=1}^N w_n \varphi_n(x) \quad (6.15)$$

$$\phi_l(x) = \frac{1}{2} \sum_{n=1}^N w_n P_l(\mu_n) \psi_n(x) \quad (6.16)$$

respectively [1]. Here w_n are the weights of the quadrature and satisfy

$$\sum_n w_n = 2 \quad (6.17)$$

The quadrature formulas are generally constructed by choosing an even value for N taking into account the fact that right and left particles have equal importance. Hence the ordinates and the weights satisfy the following relations [1]

$$\begin{aligned} \mu_n &> 0 \\ \mu_{N+1-n} &= -\mu_n \\ w_{N+1-n} &= w_n \end{aligned} \quad n = 1, 2, \dots, \frac{N}{2} \quad (6.18)$$

The spherical harmonics approach and the discrete ordinates method are equivalent in 1-D Cartesian geometry when certain conditions are met [91].

6.2 Even Parity Form of the Neutron Transport Equation

In the last decades, a different methodology namely the even parity form or second order form has emerged for tackling neutron transport problems. With this approach the first order spatial derivatives of the integrodifferential neutron transport equation are transformed into second order derivatives. By doing this the necessity of solution over the full angular domain in the integrodifferential form has been reduced to the half angle range. The attention has been increased on this method due to its

advantages in variational formulations [1]. The even parity form of the transport equation is self-adjoint which gives rise to sparse symmetric coefficient matrices and therefore to effective numerical algorithms.

In what follows the derivation of the even-parity P_3 neutron transport equation will be presented for isotropic scattering and sources. Although anisotropy can be dealt with the even-parity form [92], it is known that the derivation of such equations is tiresome when it is compared to the treatment of the integrodifferential form of the neutron transport equation [1].

For a 1-group and 1-D case with a fission source the neutron transport equation takes the following form

$$\mu \frac{\partial}{\partial x} \varphi(x, \mu) + \Sigma_t \varphi(x, \mu) = \Sigma_s \phi(x) + \frac{1}{\lambda} \nu \Sigma_f \phi(x), \quad 0 \leq x \leq a \quad (6.19)$$

If a Marshak and a reflective boundary condition exist on the right and left sides of the domain, respectively then:

$$\int_{-1}^0 P_l(\mu) \varphi(a, \mu) d\mu = 0, \quad l = 1, 3 \quad (6.20)$$

$$J(0, \mu) = \frac{1}{2} \int_{-1}^1 \mu \varphi(0, \mu) d\mu = 0 \quad (6.21)$$

Formulation of the method starts by defining the even and odd pairs of the angular flux:

$$\varphi^+(x, \mu) = \frac{1}{2} [\varphi(x, \mu) + \varphi(x, -\mu)] \quad (6.22)$$

$$\varphi^-(x, \mu) = \frac{1}{2} [\varphi(x, \mu) - \varphi(x, -\mu)] \quad (6.23)$$

It is obvious that

$$\varphi(x, \mu) = \varphi^+(x, \mu) + \varphi^-(x, \mu) \quad (6.24)$$

Writing Eq. (6.19) for $-\mu$ gives

$$-\mu \frac{\partial}{\partial x} \varphi(x, -\mu) + \Sigma_t \varphi(x, -\mu) = \left[\Sigma_s + \frac{1}{\lambda} v \Sigma_f \right] \phi(x) \quad (6.25)$$

Then adding Eq. (6.19) and (6.25)

$$\begin{aligned} \mu \left[\frac{\partial}{\partial x} \varphi(x, \mu) - \frac{\partial}{\partial x} \varphi(x, -\mu) \right] + \Sigma_t [\varphi(x, \mu) + \varphi(x, -\mu)] &= 2 \left[\Sigma_s + \frac{1}{\lambda} v \Sigma_f \right] \phi(x) \\ \mu \frac{\partial}{\partial x} \underbrace{[\varphi(x, \mu) - \varphi(x, -\mu)]}_{2\varphi^-(x, \mu)} + \Sigma_t \underbrace{[\varphi(x, \mu) + \varphi(x, -\mu)]}_{2\varphi^+(x, \mu)} &= 2 \left[\Sigma_s + \frac{1}{\lambda} v \Sigma_f \right] \phi(x) \\ \mu \frac{\partial}{\partial x} \varphi^-(x, \mu) + \Sigma_t \varphi^+(x, \mu) &= \left[\Sigma_s + \frac{1}{\lambda} v \Sigma_f \right] \phi(x) \end{aligned} \quad (6.26)$$

Subtracting Eq. (6.19) from (6.25)

$$\begin{aligned} -\mu \frac{\partial}{\partial x} \varphi(x, -\mu) - \mu \frac{\partial}{\partial x} \varphi(x, \mu) + \Sigma_t \varphi(x, -\mu) - \Sigma_t \varphi(x, \mu) &= 0 \\ -\mu \frac{\partial}{\partial x} \underbrace{[\varphi(x, \mu) + \varphi(x, -\mu)]}_{2\varphi^+(x, \mu)} - \Sigma_t \underbrace{[\varphi(x, \mu) - \varphi(x, -\mu)]}_{2\varphi^-(x, \mu)} &= 0 \\ -\mu \frac{\partial}{\partial x} \varphi^+(x, \mu) - \Sigma_t \varphi^-(x, \mu) &= 0 \end{aligned} \quad (6.27)$$

Eq. (6.27) gives

$$\varphi^-(x, \mu) = -\frac{\mu}{\Sigma_t} \frac{\partial}{\partial x} \varphi^+(x, \mu) \quad (6.28)$$

Inserting Eq. (6.28) into (6.26):

$$-\frac{\mu^2}{\Sigma_t} \frac{\partial^2}{\partial x^2} \varphi^+(x, \mu) + \Sigma_t \varphi^+(x, \mu) = \left[\Sigma_s + \frac{1}{\lambda} v \Sigma_f \right] \phi(x) \quad (6.29)$$

Legendre expansion for the even flux

$$\varphi^+(x, \mu) = \sum_{\substack{l=0 \\ l \text{ even}}}^L (2l+1) P_l(\mu) \phi_l(x) \quad (6.30)$$

Substituting this expansion into Eq. (6.30) yields

$$\begin{aligned}
& -\frac{\mu^2}{\Sigma_t} \sum_{\substack{l=0 \\ l \text{ even}}}^L (2l+1)P_l(\mu) \frac{d^2\phi_l(x)}{dx^2} + \Sigma_t \sum_{\substack{l=0 \\ l \text{ even}}}^L (2l+1)P_l(\mu)\phi_l(x) \\
& = \left[\Sigma_s + \frac{1}{\lambda} \nu \Sigma_f \right] \phi(x)
\end{aligned} \tag{6.31}$$

Multiplying Eq. (6.31) by $\frac{1}{2}P_n(\mu)$ and integrating over μ

$$\begin{aligned}
& \frac{1}{\Sigma_t} \sum_{\substack{l=0 \\ l \text{ even}}}^L (2l+1) \left(\frac{1}{2} \int_{-1}^1 \mu^2 P_l(\mu) P_n(\mu) d\mu \right) \frac{d^2\phi_l(x)}{dx^2} \\
& + \Sigma_t \sum_{\substack{l=0 \\ l \text{ even}}}^L (2l+1) \left(\frac{1}{2} \int_{-1}^1 P_l(\mu) P_n(\mu) d\mu \right) \phi_l(x) \\
& = \left[\Sigma_s + \frac{1}{\lambda} \nu \Sigma_f \right] \left(\frac{1}{2} \int_{-1}^1 P_n(\mu) d\mu \right) \phi(x)
\end{aligned} \tag{6.32}$$

With P_3 approximation:

$$\begin{aligned}
& -\frac{1}{\Sigma_t} \left[\left(\frac{1}{2} \int_{-1}^1 \mu^2 P_0(\mu) P_n(\mu) d\mu \right) \frac{d^2\phi_0}{dx^2} + 5 \left(\frac{1}{2} \int_{-1}^1 \mu^2 P_2(\mu) P_n(\mu) d\mu \right) \frac{d^2\phi_2}{dx^2} \right] \\
& + \Sigma_t \left[\left(\frac{1}{2} \int_{-1}^1 P_0(\mu) P_n(\mu) d\mu \right) \phi_0 + 5 \left(\frac{1}{2} \int_{-1}^1 P_2(\mu) P_n(\mu) d\mu \right) \phi_2 \right] \\
& = \left[\Sigma_s + \frac{1}{\lambda} \nu \Sigma_f \right] \left(\frac{1}{2} \int_{-1}^1 P_n(\mu) d\mu \right) \phi_0
\end{aligned} \tag{6.33}$$

since $\phi_0(x) \cong \phi(x)$ [1]. For $n = 0$:

$$\begin{aligned}
& -\frac{1}{\Sigma_t} \left[\left(\frac{1}{2} \int_{-1}^1 \mu^2 P_0^2(\mu) d\mu \right) \frac{d^2\phi_0}{dx^2} + 5 \left(\frac{1}{2} \int_{-1}^1 \mu^2 P_2(\mu) P_0(\mu) d\mu \right) \frac{d^2\phi_2}{dx^2} \right] \\
& + \Sigma_t \left[\left(\frac{1}{2} \int_{-1}^1 P_0^2(\mu) d\mu \right) \phi_0 + 5 \left(\frac{1}{2} \int_{-1}^1 P_2(\mu) P_0(\mu) d\mu \right) \phi_2 \right]
\end{aligned}$$

$$= \left[\Sigma_s + \frac{1}{\lambda} v \Sigma_f \right] \left(\frac{1}{2} \int_{-1}^1 P_0(\mu) d\mu \right) \phi_0$$

With $P_0(\mu) = 1$ and $P_2(\mu) = (3\mu^2 - 1)/2$ it is easy to show that

$$-\frac{1}{3\Sigma_t} \frac{d^2 \phi_0(x)}{dx^2} - \frac{2}{3\Sigma_t} \frac{d^2 \phi_2(x)}{dx^2} + \Sigma_t \phi_0(x) = \Sigma_s \phi_0(x) + \frac{1}{\lambda} v \Sigma_f \phi_0(x) \quad (6.34)$$

For $n = 2$:

$$\begin{aligned} & -\frac{1}{\Sigma_t} \left[\left(\frac{1}{2} \int_{-1}^1 \mu^2 P_0(\mu) P_2(\mu) d\mu \right) \frac{d^2 \phi_0}{dx^2} + 5 \left(\frac{1}{2} \int_{-1}^1 \mu^2 P_2^2(\mu) d\mu \right) \frac{d^2 \phi_2}{dx^2} \right] \\ & + \Sigma_t \left[\left(\frac{1}{2} \int_{-1}^1 P_0(\mu) P_2(\mu) d\mu \right) \phi_0 + 5 \left(\frac{1}{2} \int_{-1}^1 P_2^2(\mu) d\mu \right) \phi_2 \right] \quad (6.35) \\ & = \left[\Sigma_s + \frac{1}{\lambda} v \Sigma_f \right] \left(\frac{1}{2} \int_{-1}^1 P_2(\mu) d\mu \right) \phi_0 \end{aligned}$$

Evaluating the integrals results with

$$-\frac{2}{15\Sigma_t} \frac{d^2 \phi_0(x)}{dx^2} - \frac{11}{21\Sigma_t} \frac{d^2 \phi_2(x)}{dx^2} + \Sigma_t \phi_2(x) = 0 \quad (6.36)$$

Therefore the equations of the even parity P_3 approximation, Eqs. (6.34) and (6.36), are obtained. These two ordinary differential equations can be cast into a fourth order equation so that an analytical solution can be found. To achieve this goal, first Eq. (6.34) is multiplied by $-3\sigma_t$

$$\frac{d^2 \phi_0(x)}{dx^2} + 2 \frac{d^2 \phi_2(x)}{dx^2} = 3\Sigma_t \left(\Sigma_a - \frac{1}{\lambda} v \Sigma_f \right) \phi_0(x) \quad (6.37)$$

where $\Sigma_a = \Sigma_t - \Sigma_s$. By utilizing Eqs. (6.34) and (6.36), the second flux moment can be written in terms of the zeroth moment as

$$\phi_2(x) = \frac{11}{14\Sigma_t} \left(\Sigma_a - \frac{1}{\lambda} v \Sigma_f \right) \phi_0(x) - \frac{9}{70\Sigma_t^2} \frac{d^2 \phi_0(x)}{dx^2} \quad (6.38)$$

Differentiating both sides of Eq. (6.38) with respect to x gives

$$\frac{d^2\phi_2(x)}{dx^2} = \frac{11}{14\Sigma_t} \left(\Sigma_a - \frac{1}{\lambda} v\Sigma_f \right) \frac{d^2\phi_0(x)}{dx^2} - \frac{9}{70\Sigma_t^2} \frac{d^4\phi_0(x)}{dx^4} \quad (6.39)$$

Inserting Eq. (6.39) into Eq. (6.37) and rearranging terms yields the fourth order equation:

$$\begin{aligned} \frac{d^4\phi_0(x)}{dx^4} - \frac{5}{9}\Sigma_t(11\Sigma_a + 7\Sigma_t) \frac{d^2\phi_0(x)}{dx^2} + \frac{35}{3}\Sigma_t^3\sigma_a\phi_0(x) \\ = \frac{35}{3}\Sigma_t^3 \frac{1}{\lambda} v\Sigma_f\phi_0(x) - \frac{55}{9}\Sigma_t \frac{1}{\lambda} v\Sigma_f \frac{d^2\phi_0(x)}{dx^2} \end{aligned} \quad (6.40)$$

Next, the boundary conditions will be derived. By using Eqs. (6.24) and (6.27) it can be shown that

$$\varphi(x, \mu) = \varphi^+(x, \mu) - \frac{\mu}{\Sigma_t} \frac{\partial}{\partial x} \varphi^+(x, \mu) \quad (6.41)$$

Substituting this into Eq. (6.20)

$$\frac{1}{2} \int_{-1}^0 P_l(\mu) \left[\varphi^+ - \frac{\mu}{\Sigma_t} \frac{\partial}{\partial x} \varphi^+ \right] d\mu = 0 \quad (6.42)$$

Then using the P_3 expansion

$$\varphi^+(x, \mu) = P_0(\mu)\phi_0(x) + 5P_2(\mu)\phi_2(x) \quad (6.43)$$

in Eq. (6.42) results with

$$\begin{aligned} \int_{-1}^0 P_l(\mu) [\phi_0(a) + 5P_2(\mu)\phi_2(a)] d\mu \\ - \frac{1}{\Sigma_t} \frac{\partial}{\partial x} \int_{-1}^0 \mu P_l(\mu) [\phi_0(x) + 5P_2(\mu)\phi_2(x)] d\mu \Big|_{x=a} = 0 \end{aligned} \quad (6.44)$$

For $l=1$ $P_1(\mu) = \mu$. Then evaluating the integrals gives

$$\frac{1}{2}\phi_0(a) + \frac{1}{3\Sigma_t} \frac{d\phi_0}{dx} \Big|_{x=a} + \frac{5}{8}\phi_2(a) + \frac{2}{3\Sigma_t} \frac{d\phi_2}{dx} \Big|_{x=a} = 0 \quad (6.45)$$

For $l = 3$ $P_3(\mu) = (5\mu^3 - 3\mu)/2$ and Eq. (6.44) yields

$$\frac{1}{8}\phi_0(a) - \frac{5}{8}\phi_2(a) - \frac{3}{7\Sigma_t} \left. \frac{d\phi_2}{dx} \right|_{x=a} = 0 \quad (6.46)$$

Boundary conditions can also be transformed so that a compatible form with the fourth order equation can be obtained. Using Eq. (6.46)

$$\left. \frac{d\phi_2}{dx} \right|_{x=a} = \frac{7\Sigma_t}{24}\phi_0(a) - \frac{35\Sigma_t}{24}\phi_2(a) \quad (6.47)$$

Inserting this result into Eq. (6.45)

$$\phi_2(a) = 2\phi_0(a) + \frac{24}{25\Sigma_t} \left. \frac{d\phi_0}{dx} \right|_{x=a} \quad (6.48)$$

Then using this in Eq. (6.47)

$$\left. \frac{d\phi_2}{dx} \right|_{x=a} = -\frac{21\Sigma_t}{8}\phi_0(a) - \frac{7}{5} \left. \frac{d\phi_0}{dx} \right|_{x=a} \quad (6.49)$$

Substituting Eq. (6.38) into Eq. (6.48) gives

$$\begin{aligned} & \frac{9}{70\Sigma_t^2} \left. \frac{d^2\phi_0}{dx^2} \right|_{x=a} + \frac{24}{25\Sigma_t} \left. \frac{d\phi_0}{dx} \right|_{x=a} + \left[2 - \frac{11\Sigma_a}{14\Sigma_t} \right] \phi_0(a) \\ & = -\frac{11}{14} \frac{1}{\lambda} \nu \Sigma_f \frac{1}{\Sigma_t} \phi_0(a) \end{aligned} \quad (6.50)$$

Differentiating Eq. (6.38) results with

$$\frac{d\phi_2}{dx} = -\frac{9}{70\Sigma_t^2} \frac{d^3\phi_0}{dx^3} + \frac{11}{14\Sigma_t} \left(\Sigma_a - \frac{1}{\lambda} \nu \Sigma_f \right) \frac{d\phi_0}{dx} \quad (6.51)$$

Substituting Eq. (6.49) into Eq. (6.51)

$$\begin{aligned} & -\frac{9}{70\Sigma_t^2} \left. \frac{d^3\phi_0}{dx^3} \right|_{x=a} + \left(\frac{7}{5} + \frac{11\Sigma_a}{14\Sigma_t} \right) \left. \frac{d\phi_0}{dx} \right|_{x=a} + \frac{21}{8} \Sigma_t \phi_0(a) \\ & = \frac{11}{14} \frac{\nu \Sigma_f}{\Sigma_t} \frac{1}{\lambda} \left. \frac{d\phi_0}{dx} \right|_{x=a} \end{aligned} \quad (6.52)$$

Therefore the derivation of Marshak boundary conditions compatible with the fourth order equation, Eqs. (6.50) and (6.52), is completed.

Final task is to derive the reflective boundary conditions. Substituting Eq. (6.41) into Eq. (6.21)

$$\int_{-1}^1 P_n(\mu) \varphi^+(0, \mu) d\mu - \frac{1}{\Sigma_t} \int_{-1}^1 \mu P_n(\mu) \left. \frac{\partial \varphi^+}{\partial x} \right|_{x=0} d\mu = 0 \quad (6.53)$$

Since the integrand is odd

$$\int_{-1}^1 P_n(\mu) \varphi^+(0, \mu) d\mu = 0 \quad (6.54)$$

and hence

$$\int_{-1}^1 \mu P_n(\mu) \left. \frac{\partial \varphi^+}{\partial x} \right|_{x=0} d\mu = 0 \quad (6.55)$$

Following a similar path to the derivation of Marshak boundary conditions the following reflective boundary conditions can be obtained:

$$\frac{1}{3} \left. \frac{d\phi_0(x)}{dx} \right|_{x=0} + \frac{2}{3} \left. \frac{d\phi_2(x)}{dx} \right|_{x=0} = 0 \quad (6.56)$$

$$\left. \frac{d\phi_2(x)}{dx} \right|_{x=0} = 0 \quad (6.57)$$

Finally, reflective boundary conditions compatible with the fourth order equation can be obtained by substituting Eq. (6.57) into Eq. (6.56) and from Eq. (6.51),

$$\left. \frac{d\phi_0(x)}{dx} \right|_{x=0} = 0 \quad (6.58)$$

$$\left. \frac{d^3 \phi_0(x)}{dx^3} \right|_{x=0} = 0 \quad (6.59)$$

respectively.

The analytical solution of Eq. (6.40) can be obtained as follows. By defining

$$\alpha = \frac{3}{35\Sigma_t}, \quad \beta = \frac{\Sigma_t}{3} + \frac{11}{21}(\Sigma_a - \nu\Sigma_f), \quad \gamma = \Sigma_t^2(\Sigma_a - \nu\Sigma_f) \quad (6.60)$$

one can write

$$\alpha \frac{d^4\phi}{dx^4} - \beta \frac{d^2\phi}{dx^2} + \gamma\phi = 0 \quad (6.61)$$

This equation can be rewritten as

$$\left(\frac{d^2}{dx^2} - \mu^2\right)\left(\frac{d^2}{dx^2} + \lambda^2\right)\phi = 0 \quad (6.62)$$

Then

$$\frac{d^4\phi}{dx^4} + (\lambda^2 - \mu^2)\frac{d^2\phi}{dx^2} - \mu^2\lambda^2\phi = 0 \quad (6.63)$$

Comparing Eq. (6.63) with Eq. (6.61)

$$\lambda^4 + \frac{\beta}{\alpha}\lambda^2 + \frac{\gamma}{\alpha} = 0 \quad (6.64)$$

Therefore

$$\lambda_1^2 = -\frac{\beta}{2\alpha}\left(1 + \sqrt{1 - \frac{4\alpha\gamma}{\beta^2}}\right), \quad \lambda_2^2 = -\frac{\beta}{2\alpha}\left(1 - \sqrt{1 - \frac{4\alpha\gamma}{\beta^2}}\right) \quad (6.65)$$

In a similar way μ_1^2 and μ_2^2 can be found to be

$$\mu_1^2 = \frac{\beta}{2\alpha}\left(1 + \sqrt{1 - \frac{4\alpha\gamma}{\beta^2}}\right), \quad \mu_2^2 = \frac{\beta}{2\alpha}\left(1 - \sqrt{1 - \frac{4\alpha\gamma}{\beta^2}}\right) \quad (6.66)$$

From Eq. (6.62)

$$\left(\frac{d^2}{dx^2} - \mu^2\right)X = 0, \quad \left(\frac{d^2}{dx^2} + \lambda^2\right)Y = 0 \quad (6.67)$$

and thus

$$X(x) = \cosh(\mu x), \quad Y(x) = \cos(\lambda x) \quad (6.68)$$

Since

$$\phi(x) = A \cosh(\mu x) + C \cos(\lambda x) \quad (6.69)$$

the following equations can be obtained from the Marshak boundary conditions (i.e., Eqs. (6.50) and (6.52))

$$\left\{ \left[\frac{9\mu^2}{70\Sigma_t^2} + \left(2 - \frac{11\Sigma_a - v\Sigma_f}{14\Sigma_t} \right) \right] \cosh(\mu a) + \frac{24\mu}{25\Sigma_t} \sinh(\mu a) \right\} \\ + C \left\{ \left[-\frac{9\lambda^2}{70\Sigma_t^2} + \left(2 - \frac{11\Sigma_a - v\Sigma_f}{14\Sigma_t} \right) \right] \cos(\lambda a) - \frac{24\lambda}{25\Sigma_t} \sin(\lambda a) \right\} = 0 \quad (6.70)$$

$$\left\{ \left[\frac{9\mu^3}{70\Sigma_t^2} - \left(\frac{7}{5} + \frac{11\Sigma_a - v\Sigma_f}{14\Sigma_t} \right) \mu \right] \sinh(\mu a) - \frac{21\Sigma_t}{8} \cosh(\mu a) \right\} \\ + C \left\{ \left[\frac{9\lambda^3}{70\Sigma_t^2} + \left(\frac{7}{5} + \frac{11\Sigma_a - v\Sigma_f}{14\Sigma_t} \right) \lambda \right] \sin(\lambda a) - \frac{21\Sigma_t}{8} \cos(\lambda a) \right\} = 0 \quad (6.71)$$

By defining

$$a_1 = \frac{9}{70\Sigma_t^2}, \quad a_2 = \frac{11\Sigma_a - v\Sigma_f}{14\Sigma_t}, \quad a_3 = \frac{21\Sigma_t}{8}, \quad a_4 = \frac{24}{25\Sigma_t} \quad (6.72)$$

a relation between the constants A and C can be found from Eqs. (6.70) and (6.71)

$$\frac{C}{A} = - \frac{\mu \left[a_1 \mu^2 - \left(\frac{7}{5} + a_2 \right) \right] \sinh(\mu a) - a_3 \cosh(\mu a)}{\lambda \left[a_1 \lambda^2 + \left(\frac{7}{5} + a_2 \right) \right] \sin(\lambda a) - a_3 \cos(\lambda a)} \quad (6.73)$$

In a similar way, using the reflective boundary conditions one can show that

$$\frac{C}{A} = - \frac{[a_1 \mu^2 + (2 - a_2)] \cosh(\mu a) + a_4 \mu \sinh(\mu a)}{[-a_1 \lambda^2 + (2 - a_2)] \cos(\lambda a) - a_4 \lambda \sin(\lambda a)} \quad (6.74)$$

Combining Eqs. (6.73) and (6.74) yields

$$f(\mu a) - g(\mu a) = 0 \quad (6.75)$$

where

$$f(\mu a) = \frac{\mu \left[a_1 \mu^2 - \left(\frac{7}{5} + a_2 \right) \right] \sinh(\mu a) - a_3 \cosh(\mu a)}{\lambda \left[a_1 \lambda^2 + \left(\frac{7}{5} + a_2 \right) \right] \sin(\lambda a) - a_3 \cos(\lambda a)} \quad (6.76)$$

$$g(\mu a) = \frac{[a_1 \mu^2 + (2 - a_2)] \cosh(\mu a) + a_4 \mu \sinh(\mu a)}{[-a_1 \lambda^2 + (2 - a_2)] \cos(\lambda a) - a_4 \lambda \sin(\lambda a)} \quad (6.77)$$

The solution of Eq. (6.75) provides the value of a which sustains a critical system. As an example if $\Sigma_a = 0.2\Sigma_t$ and $v\Sigma_f = 0.246\Sigma_t$ then the critical thickness can be found numerically to be $a = 4.102640972417\Sigma_t$.

6.3 Numerical Formulations

6.3.1 P_3 equations

For ease of illustration an external source problem is considered with anisotropic scattering. In this case the P_N equations become

$$\begin{aligned} \frac{d\phi_1}{dx} + [\Sigma_t - \Sigma_{s,0}] \phi_0 &= s_0 \\ \frac{n+1}{2n+1} \frac{d\phi_{n+1}}{dx} + \frac{n}{2n+1} \frac{d\phi_{n-1}}{dx} + [\Sigma_t - \Sigma_{s,n}] \phi_n &= s_n, n = 1, 2, \dots, N-1 \\ \frac{N}{2N+1} \frac{d\phi_{N-1}}{dx} + [\Sigma_t - \Sigma_{s,N}] \phi_N &= s_N \end{aligned} \quad (6.78)$$

Then the P_3 equations are

$$\begin{aligned} \frac{d\phi_1(x)}{dx} + [\Sigma_t - \Sigma_{s,0}] \phi_0(x) &= s_0(x) \\ \frac{2}{3} \frac{d\phi_2(x)}{dx} + \frac{1}{3} \frac{d\phi_0(x)}{dx} + [\Sigma_t - \Sigma_{s,1}] \phi_1(x) &= s_1(x) \\ \frac{3}{5} \frac{d\phi_3(x)}{dx} + \frac{2}{5} \frac{d\phi_1(x)}{dx} + [\Sigma_t - \Sigma_{s,2}] \phi_2(x) &= s_2(x) \\ \frac{3}{7} \frac{d\phi_2(x)}{dx} + [\Sigma_t - \Sigma_{s,3}] \phi_3(x) &= s_3(x) \end{aligned} \quad (6.79)$$

The Marshak boundary conditions can be derived by substituting the Legendre expansion

$$\varphi(a, \mu) = \sum_{m=0}^3 (2m + 1)P_m(\mu)\phi_m(a) \quad (6.80)$$

into Eq. (6.12) and evaluating the integrals. The resultant equations are

$$\begin{aligned} -\frac{1}{2}\phi_0(a) + \phi_1(a) - \frac{5}{8}\phi_2(a) &= 0 \\ \frac{1}{8}\phi_0(a) - \frac{5}{8}\phi_2(a) + \phi_3(a) &= 0 \end{aligned} \quad (6.81)$$

Finally the reflective boundary conditions are

$$\begin{aligned} \phi_1(0) &= 0 \\ \phi_3(0) &= 0 \end{aligned} \quad (6.82)$$

The numerical formulation of the problem starts by discretizing the problem domain with M nodes and an external node to improve the accuracy. When this discretization is compared with those made for diffusion problems, it is seen that the external node is created on only one side of the domain. If external nodes are used on both sides the collocation matrix becomes underdetermined, and there will be no solution. On the other hand with the even-parity form this problem can be solved and external nodes can be chosen on both sides of the domain. A typical set of nodes with $M = 6$ is illustrated in Figure 6.1.



Figure 6.1: Discretization of the 1-D domain with $M = 6$.

Then the flux moments are approximated with M radial basis functions:

$$\phi_n(x) = \sum_{j=1}^M a_j \psi_j(x), \quad n = 0,1,2,3 \quad (6.83)$$

Substituting these approximations into the differential equations and boundary conditions results with:

$$\begin{aligned}
& \sum_{j=1}^M a_j [(\Sigma_t - \Sigma_{s,0})\psi_j] + \sum_{j=M+1}^{2M} a_j \frac{d\psi_j}{dx} = s_0 \\
& \sum_{j=1}^M a_j \left[\frac{1}{3} \frac{d\psi_j}{dx} \right] + \sum_{j=M+1}^{2M} a_j [(\Sigma_t - \Sigma_{s,1})\psi_j] + \sum_{j=2M+1}^{3M} a_j \left[\frac{2}{3} \frac{d\psi_j}{dx} \right] = s_1 \\
& \sum_{j=M+1}^{2M} a_j \left[\frac{2}{5} \frac{d\psi_j}{dx} \right] + \sum_{j=2M+1}^{3M} a_j [(\Sigma_t - \Sigma_{s,2})\psi_j] + \sum_{j=3M+1}^{4M} a_j \left[\frac{3}{5} \frac{d\psi_j}{dx} \right] = s_2 \\
& \sum_{j=2M+1}^{3M} a_j \left[\frac{3}{7} \frac{d\psi_j}{dx} \right] + \sum_{j=3M+1}^{4M} a_j [(\Sigma_t - \Sigma_{s,3})\psi_j] = s_3
\end{aligned} \tag{6.84}$$

$$\begin{aligned}
& \sum_{j=1}^M a_j \left[-\frac{1}{2} \psi_j \right] + \sum_{j=M+1}^{2M} a_j \psi_j + \sum_{j=2M+1}^{3M} a_j \left[-\frac{5}{8} \psi_j \right] = 0 \\
& \sum_{j=1}^M a_j \left[\frac{1}{8} \psi_j \right] + \sum_{j=2M+1}^{3M} a_j \left[-\frac{5}{8} \psi_j \right] + \sum_{j=3M+1}^{4M} a_j \psi_j = 0
\end{aligned} \tag{6.85}$$

$$\begin{aligned}
& \sum_{j=M+1}^{2M} a_j \psi_j = 0 \\
& \sum_{j=3M+1}^{4M} a_j \psi_j = 0
\end{aligned} \tag{6.86}$$

Then these equations are collocated at the discretization nodes

$$\begin{aligned}
& \sum_{j=1}^M a_j [(\Sigma_t - \Sigma_{s,0})\psi_{ij}] + \sum_{j=M+1}^{2M} a_j \frac{d\psi_{ij}}{dx} = s_{0,i}, \quad i = 1, \dots, M \\
& \sum_{j=1}^M a_j \left[\frac{1}{3} \frac{d\psi_{ij}}{dx} \right] + \sum_{j=M+1}^{2M} a_j [(\Sigma_t - \Sigma_{s,1})\psi_{ij}] + \sum_{j=2M+1}^{3M} a_j \left[\frac{2}{3} \frac{d\psi_{ij}}{dx} \right] = s_{1,i} \\
& i = M + 1, \dots, 2M \\
& \sum_{j=M+1}^{2M} a_j \left[\frac{2}{5} \frac{d\psi_{ij}}{dx} \right] + \sum_{j=2M+1}^{3M} a_j [(\Sigma_t - \Sigma_{s,2})\psi_{ij}] + \sum_{j=3M+1}^{4M} a_j \left[\frac{3}{5} \frac{d\psi_{ij}}{dx} \right] = s_{2,i} \\
& i = 2M + 1, \dots, 3M \\
& \sum_{j=2M+1}^{3M} a_j \left[\frac{3}{7} \frac{d\psi_{ij}}{dx} \right] + \sum_{j=3M+1}^{4M} a_j [(\Sigma_t - \Sigma_{s,3})\psi_{ij}] = s_{3,i}, \quad i = 3M + 1, \dots, 4M
\end{aligned}$$

$$\begin{aligned}
\sum_{j=1}^M a_j \left[-\frac{1}{2} \psi_{ij} \right] + \sum_{j=M+1}^{2M} a_j \psi_{ij} + \sum_{j=2M+1}^{3M} a_j \left[-\frac{5}{8} \psi_{ij} \right] &= 0, \quad i = M \\
\sum_{j=1}^M a_j \left[\frac{1}{8} \psi_{ij} \right] + \sum_{j=2M+1}^{3M} a_j \left[-\frac{5}{8} \psi_{ij} \right] + \sum_{j=3M+1}^{4M} a_j \psi_{ij} &= 0, \quad i = M \\
\sum_{j=M+1}^{2M} a_j \psi_{ij} &= 0, \quad i = 1 \\
\sum_{j=3M+1}^{4M} a_j \psi_{ij} &= 0, \quad i = 1
\end{aligned}$$

These collocation equations can be cast into a $(4 \times M) \times (4 \times M)$ system of algebraic equations:

$$\mathbf{K}\mathbf{a} = \mathbf{f} \quad (6.87)$$

Here the matrix \mathbf{K} contains the coefficients in Eqs. (6.84)-(6.86), \mathbf{a} is a $4 \times M$ vector of the coefficients a_j and \mathbf{f} is a $4 \times M$ vector of the right hand side of Eqs. (6.84)-(6.86). Solution of Eq. (6.87) yields the coefficients and hence the numerical solution.

6.3.2 Even-parity P_3 equations

There are two alternatives for the numerical formulation when the even-parity form of the P_3 approximation is considered. As seen earlier the two ordinary differential equations can be cast into a single fourth order equation, and compatible boundary conditions can be derived from the original Marshak and reflective boundary conditions.

In the first route, the coupled equations together with the boundary conditions will be approximated by the RBFs. Once again the first step is the discretization of the domain as observed in Figure 6.1 and to interpolate the flux moments by

$$\phi_n(x) = \sum_{j=1}^M a_j \psi_j(x), \quad n = 0, 2 \quad (6.88)$$

Next, these two series are substituted into the Eqs. (6.34), (6.36), (6.45), (6.46), (6.57) and (6.58) to give

$$\sum_{j=1}^M a_j \left[-\frac{1}{3\Sigma_t} \frac{d^2\psi_j}{dx^2} + \Sigma_a \psi_j \right] + \sum_{j=M+1}^{2M} a_j \left[-\frac{2}{3\Sigma_t} \frac{d^2\psi_j}{dx^2} \right] = s \quad (6.89)$$

$$\sum_{j=1}^M a_j \left[-\frac{2}{15\Sigma_t} \frac{d^2\psi_j}{dx^2} \right] + \sum_{j=M+1}^{2M} a_j \left[-\frac{11}{21\Sigma_t} \frac{d^2\psi_j}{dx^2} + \Sigma_t \psi_j \right] = 0$$

$$\sum_{j=1}^M a_j \left[\frac{1}{2} \psi_j + \frac{1}{3\Sigma_t} \frac{d\psi_j}{dx} \right] + \sum_{j=M+1}^{2M} a_j \left[\frac{5}{8} \psi_j + \frac{2}{3\Sigma_t} \frac{d\psi_j}{dx} \right] = 0 \quad (6.90)$$

$$\sum_{j=1}^M a_j \frac{1}{8} \psi_j + \sum_{j=M+1}^{2M} a_j \left[-\frac{5}{8} \psi_j - \frac{3}{7\Sigma_t} \frac{d\psi_j}{dx} \right] = 0$$

$$\sum_{j=1}^M a_j \frac{d\psi_j}{dx} = 0 \quad (6.91)$$

$$\sum_{j=M+1}^{2M} a_j \frac{d\psi_j}{dx} = 0$$

These equations can be cast into a matrix form similar to Eq. (6.87). Notice that with the even parity form, the resulting system of equations has a dimension of $(2 \times M) \times (2 \times M)$.

The second alternative for the numerical solution of the even parity P_3 equations is to deal with the fourth order equation, Eq. (6.40). In this case there is only one flux moment to be approximated:

$$\phi_0(x) = \sum_{j=1}^M a_j \psi_j(x) \quad (6.92)$$

Substituting Eq. (6.92) into Eqs. (6.40), (6.50), (6.52), (6.58) and (6.59) gives the following:

$$\begin{aligned} & \sum_{j=1}^M a_j \left[\frac{d^4\psi_j}{dx^4} - \frac{5}{9} \Sigma_t (11\Sigma_a + 7\Sigma_t) \frac{d^2\psi_j}{dx^2} + \frac{35}{3} \Sigma_t^3 \Sigma_a \psi_j \right] \\ & = \frac{\Sigma_t}{3} \left[35\Sigma_t^2 s - \frac{55}{3} \frac{d^2s}{dx^2} \right] \end{aligned} \quad (6.93)$$

$$\sum_{j=1}^M a_j \left[\frac{9}{70\Sigma_t^2} \frac{d^2\psi_j}{dx^2} + \frac{24}{25\Sigma_t} \frac{d\psi_j}{dx} + \left(2 - \frac{11\Sigma_a}{14\Sigma_t} \right) \psi_j \right] = -\frac{11s}{14\Sigma_t} \quad (6.94)$$

$$\sum_{j=1}^M a_j \left[-\frac{9}{70\Sigma_t^2} \frac{d^3\psi_j}{dx^3} + \left(\frac{7}{5} + \frac{11\Sigma_a}{14\Sigma_t} \right) \frac{d\psi_j}{dx} + \frac{21}{8} \Sigma_t \psi_j \right] = -\frac{11}{14\Sigma_t} \frac{ds}{dx}$$

$$\sum_{j=1}^M a_j \frac{d\psi_j}{dx} = 0$$

$$\sum_{j=1}^M a_j \frac{d^3\psi_j}{dx^3} = 0 \quad (6.95)$$

Once again the fission source terms are replaced by external source terms. Final step of the formulation is the collocation of Eqs. (6.93)-(6.95)

$$\sum_{j=1}^M a_j \left[\frac{d^4\psi_{ij}}{dx^4} - \frac{5}{9} \Sigma_t (11\Sigma_a + 7\Sigma_t) \frac{d^2\psi_{ij}}{dx^2} + \frac{35}{3} \Sigma_t^3 \Sigma_a \psi_{ij} \right] = \frac{\Sigma_t}{3} \left[35\Sigma_t^2 s_i - \frac{55}{3} \frac{d^2 s_i}{dx^2} \right]$$

$$i = 1, \dots, M$$

$$\sum_{j=1}^M a_j \left[\frac{9}{70\Sigma_t^2} \frac{d^2\psi_{ij}}{dx^2} + \frac{24}{25\Sigma_t} \frac{d\psi_{ij}}{dx} + \left(2 - \frac{11\Sigma_a}{14\Sigma_t} \right) \psi_{ij} \right] = -\frac{11s_i}{14\Sigma_t}, \quad i = M$$

$$\sum_{j=1}^M a_j \left[-\frac{9}{70\Sigma_t^2} \frac{d^3\psi_{ij}}{dx^3} + \left(\frac{7}{5} + \frac{11\Sigma_a}{14\Sigma_t} \right) \frac{d\psi_{ij}}{dx} + \frac{21}{8} \Sigma_t \psi_{ij} \right] = -\frac{11}{14\Sigma_t} \frac{ds_i}{dx}, \quad i = M$$

$$\sum_{j=1}^M a_j \frac{d\psi_{ij}}{dx} = 0, \quad i = 1$$

$$\sum_{j=1}^M a_j \frac{d^3\psi_{ij}}{dx^3} = 0, \quad i = 1$$

These collocation equations can be cast into a $(1 \times M) \times (1 \times M)$ matrix equation. When this dimension size is compared with those of the previous formulations, it is seen that this last method is advantageous to the previous ones in terms of the CPU time. But, in the next section, it will be observed that, approximating the fourth order derivatives with RBFs directly is an important price to pay when accuracy is considered.

6.4 Results

To test the accuracy and stability of the RBF collocation method four problems are considered. All calculations are performed with MATHEMATICA 7 on a 2.7 GHz computer. Depending on the type of problem two error criteria, root mean square error in flux and relative percent error in the multiplication factor are used to assess the performance of the numerical scheme. Multiquadric is chosen as the RBF.

6.4.1 External source problem

The first problem is an external source case where a constant source term, $s(x) = 1 \text{ n/cm}^3\text{s}$, is chosen. This problem is solved within the even-parity P_3 context, and as mentioned in the previous section two algorithms are possible with this form of the transport equation. The cross sections are taken as $\Sigma_t = 1 \text{ cm}^{-1}$, $\Sigma_a = 0.2 \text{ cm}^{-1}$ and the size of the domain is $a = 5 \text{ cm}$. With these parameters the flux distribution is

$$\begin{aligned} \phi_0(x) = & 5 - 0.000014215 \exp(-2.14577x) - 0.077749 \exp(-0.71188x) \\ & - 0.077749 \exp(0.71188x) - 0.000014215 \exp(2.14577x) \end{aligned}$$

As the first approach, the coupled equations are chosen to tackle the problem. The effect of the shape parameter, $c = a\sqrt{m}$ on the RMS error in flux is illustrated in Figure 6.2. It is observed from this figure for all values of the shape parameter, a high level of accuracy is achieved. Also, the accuracy and convergence rate of the method improves when c takes on higher values.

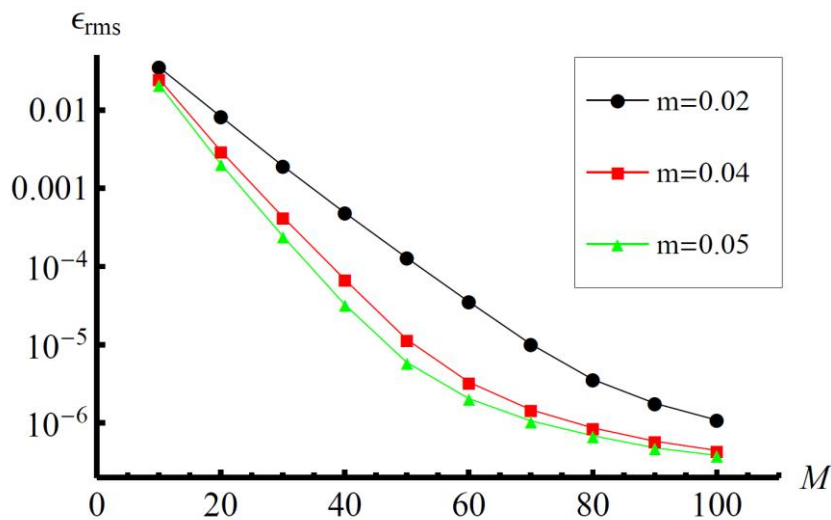


Figure 6.2: Effect of the shape parameter on the RMS error for the external source problem.

It is possible to get better accuracies by increasing the number of collocation nodes. In this case the collocation matrix becomes overdetermined, and the system of equations has to be solved by the least-squares method. In Figure 6.3 the RMS error is plotted with respect to M in semi-log scale for three sets of collocation nodes. The shape parameter is chosen as $c = \alpha\sqrt{0.08}$ for these calculations. As seen from this figure the accuracy of the method gets better by increasing the number of collocation nodes. Also, the method converges faster when M is low. This effect is significant when $h_{int} = 2h_{col}$ is utilized instead of $h_{int} = h_{col}$. Although better approximations are obtained with lower h_{col} , one should be careful on choosing the value of the shape parameter when dense set of collocation nodes are used. The method becomes unstable when a high value of c is chosen together with these types of node distributions.

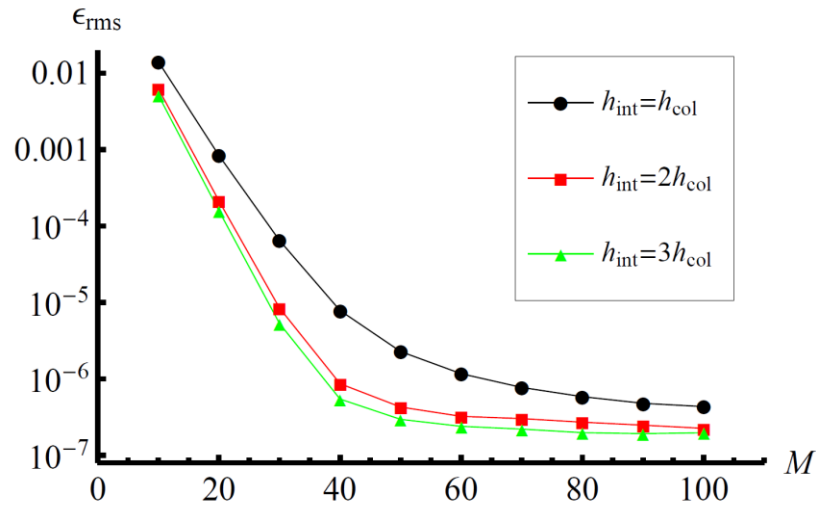


Figure 6.3: Effect of the number of collocation nodes on the RMS error for the external source problem.

Instead of a constant shape parameter strategy, a node number dependent approach can be used in calculations. As discussed earlier, one of them is to use a variable shape parameter strategy where $c = m \times h^{1/4}$. This approach has been adopted here and the results are shown in Figure 6.4 for three values of m . It is clear from this figure that high levels of accuracies can be achieved even with sparse sets of nodes, especially when $m = 3$. When the results are compared with the constant shape parameter strategy same convergence rate characteristics are observed and an RMS error around 10^{-7} is achieved with both schemes.

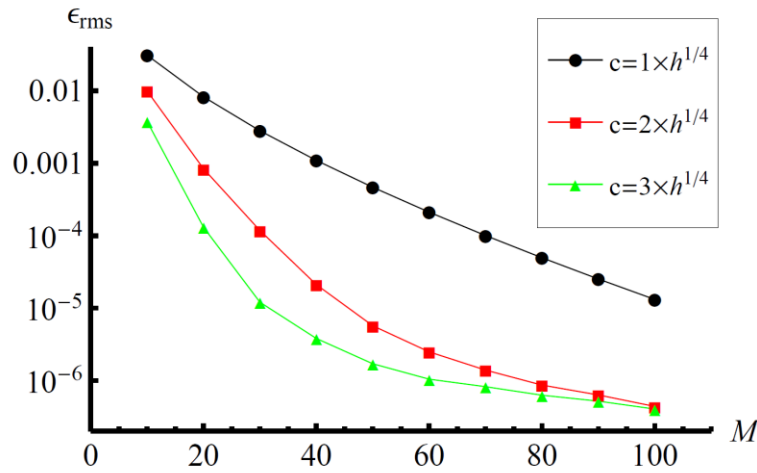


Figure 6.4: RMS errors for the external source problem when a variable shape parameter is utilized.

The external source problem can also be solved by directly approximating the fourth order differential equation (i.e., the second alternative of subsection 6.3.2). The RMS errors of this route are presented in Figure 6.5 for three values of the shape parameter. For these calculations a constant shape parameter strategy with $h_{col} = h_{int}$ is chosen. Comparison of Figures 6.2 and 6.5 reveals that there are two major problems when the second alternative is used. First, the method becomes unstable for sparse sets of nodes. The RMS errors are high and oscillation is observed below a threshold value of M which depends on the shape parameter. The second problem is the poor accuracy of the algorithm. The accuracy of the first alternative is better than the latter one by at least two orders of magnitude for all M values. This problem of approximating higher order derivatives is also pointed out in [93].

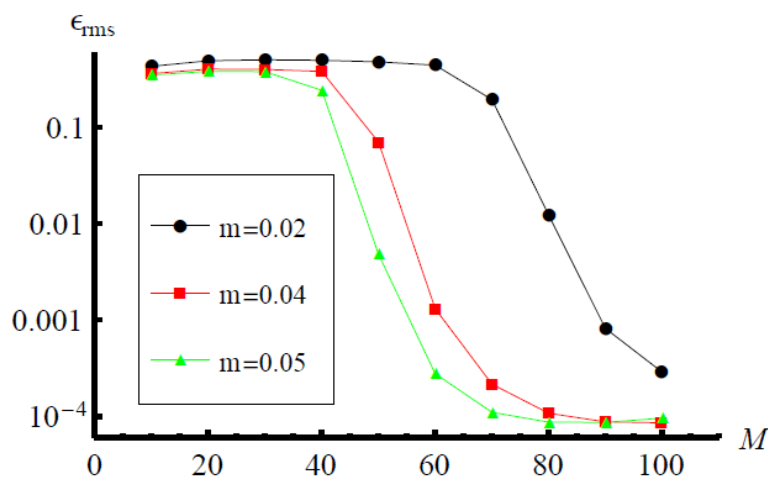


Figure 6.5: RMS error behavior of the external source problem when the fourth order equation is directly approximated with RBFs.

6.4.2 Fission source problems

The second problem solved with the even-parity P_3 approach is a fission source case. The nuclear constants are chosen to be $\Sigma_t = 1 \text{ cm}^{-1}$, $\Sigma_a = 0.2 \text{ cm}^{-1}$, $\Sigma_f = 0.1 \text{ cm}^{-1}$ and $\nu = 2.46$. With these parameters the value of a that makes the system critical is 3.4795925 cm . For the calculation of RMS error, the neutron flux is normalized to unity i.e. $\phi_0(0) = 1$ so that the following analytical form is obtained

$$\phi_0(x) = \frac{1}{1 - (a_1/a_2)} \left[\text{Cosh}(\mu x) - \frac{a_1}{a_2} \text{Cos}(\lambda x) \right]$$

where

$$a_1 = \left[\frac{9\mu^2}{70\Sigma_t^2} + \left(2 - \frac{11\Sigma_a - \nu\Sigma_f}{14\Sigma_t} \right) \right] \cosh(\mu a_{crit}) + \frac{24\mu}{25\Sigma_t} \sinh(\mu a_{crit})$$

$$a_2 = \left[-\frac{9\lambda^2}{70\Sigma_t^2} + \left(2 - \frac{11\Sigma_a - \nu\Sigma_f}{14\Sigma_t} \right) \right] \cos(\lambda a_{crit}) - \frac{24\lambda}{25\Sigma_t} \sin(\lambda a_{crit})$$

The relative percent error in the multiplication factor and the RMS error in neutron flux are presented in Figures 6.6a and 6.6b, respectively, where a variable shape parameter approach is chosen. High level of accuracies are achieved for both λ and ϕ . Similar to the previous problem the convergence rate of the RBF collocation method increases with a higher value of the shape parameter.

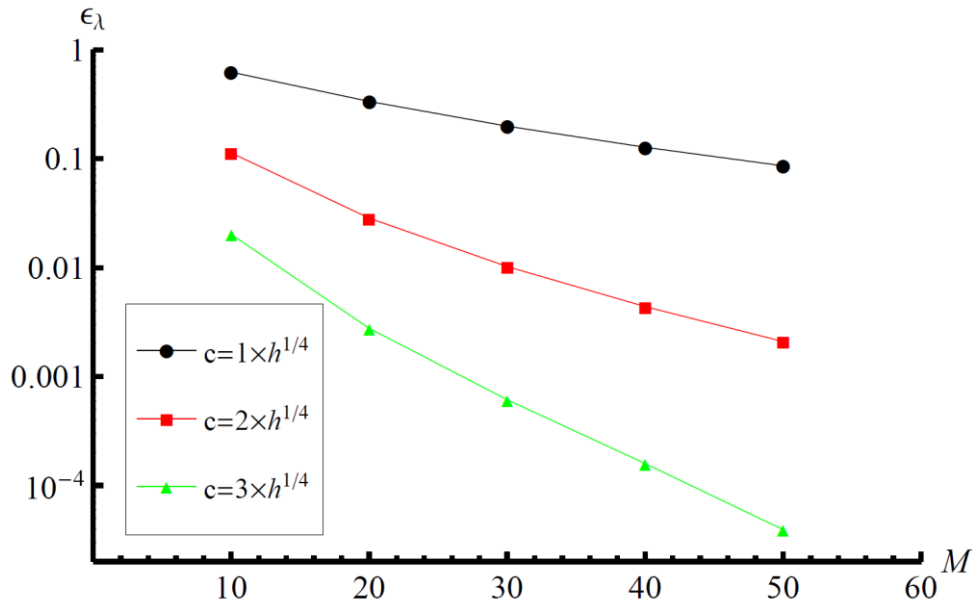


Figure 6.6a: Error in the multiplication factor for the fission source problem for three values of the shape parameter.

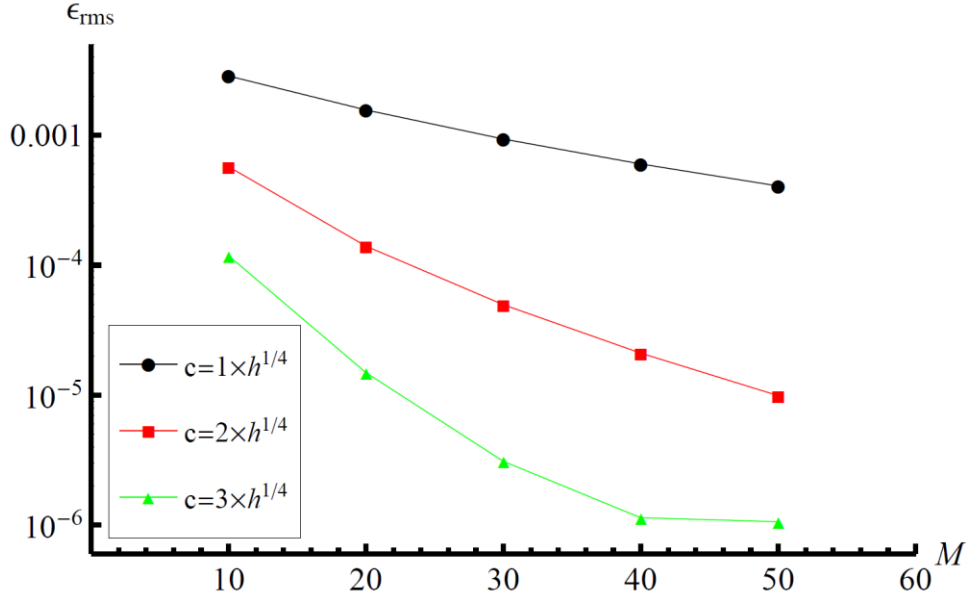


Figure 6.6b: RMS error in the neutron flux for the fission source problem for three values of the shape parameter.

The third example is a Pu-239 benchmark problem with isotropic scattering. The nuclear constants of this problem are $\Sigma_t = 0.3264 \text{ cm}^{-1}$, $\Sigma_a = 0.101184 \text{ cm}^{-1}$, $\Sigma_f = 0.0816 \text{ cm}^{-1}$ and $\nu = 3.24$, and the benchmark value of a_{crit} is 1.853722 cm [94]. Since the scattering is isotropic, this problem is solved with both conventional and even-parity forms of the transport equation with P_3 and P_5 approximations. Also, the discrete ordinates solutions are given for the purpose of comparison between the two angular approximations.

But before presenting these results, the accuracy and stability of the method will be tested by considering the analytical solution given in section 6.2, which produces an a_{crit} value of 1.927538 cm for the cross sections given above. In Figure 6.7, the relative percent error in λ with respect to the number of interpolation nodes is illustrated. A constant shape parameter strategy is utilized in these calculations. This figure shows that it is possible to obtain highly accurate values for the multiplication factor. The relative percent error is found to be 1.89816×10^{-6} at $M = 100$ when $m = 0.06$.

The value of the multiplication factor corresponding to the benchmark solution of $a_{crit} = 1.853722 \text{ cm}$ is plotted in Figures 6.8a and 6.8b for even-parity and conventional forms of the transport equation, respectively. The shape parameter is chosen to be $c = a\sqrt{0.05}$. Numerical results of the S_N approximation for the angular

flux are given in Tables 6.1-6.3 upto $N = 64$ where a diamond difference (finite difference), discontinuous linear finite element and discontinuous quadratic finite element is used for treatment of the spatial variable, respectively. It is obvious from Figure 6.8 that the RBF collocation method produces stable solutions for both even-parity and conventional form of the neutron transport equation. The results are almost identical, that P_3 and P_5 approximations converge to approximately 0.9717 and 0.9918, respectively. When the results are compared with the S_N approach, it is observed that the P_5 approach with RBF approximation for the spatial variable is equivalent to the results of S_8 finite difference and finite element solutions.

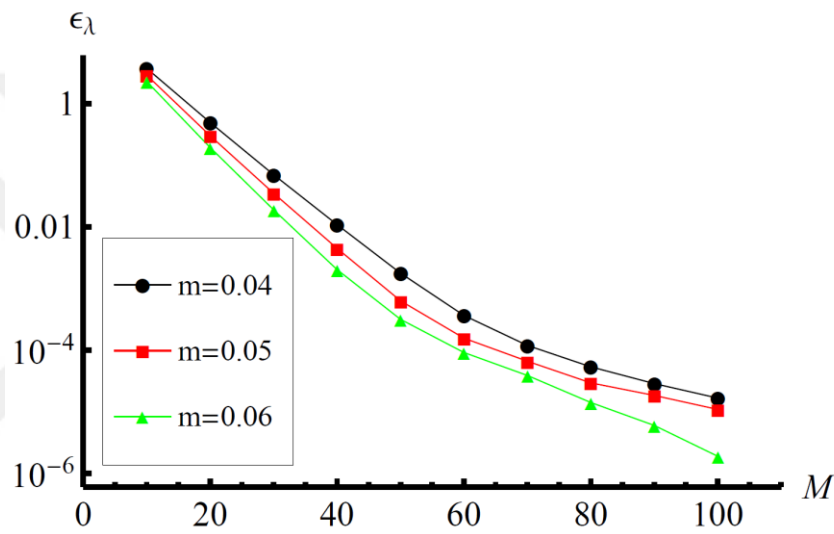


Figure 6.7: Percent error in λ for the plutonium benchmark problem with isotropic scattering when $a_{crit} = 1.927538$.

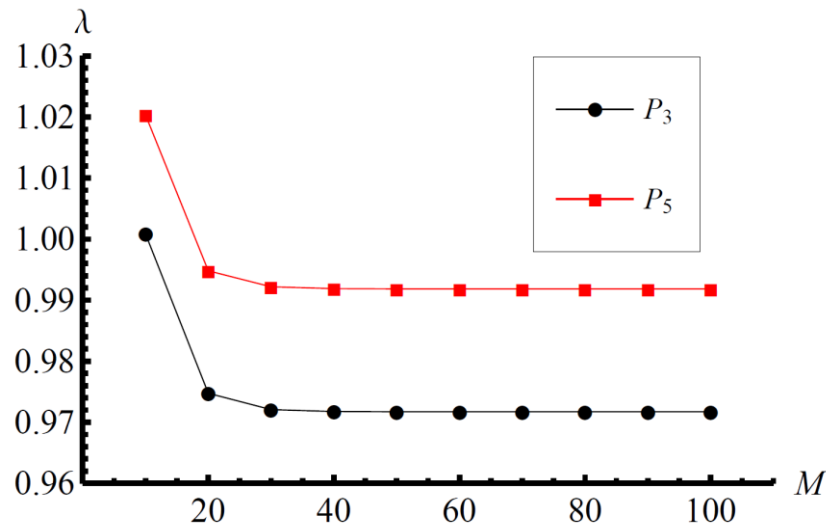


Figure 6.8a: The value of λ for the plutonium benchmark problem when $a_{crit} = 1.853722$ and even-parity form is considered.

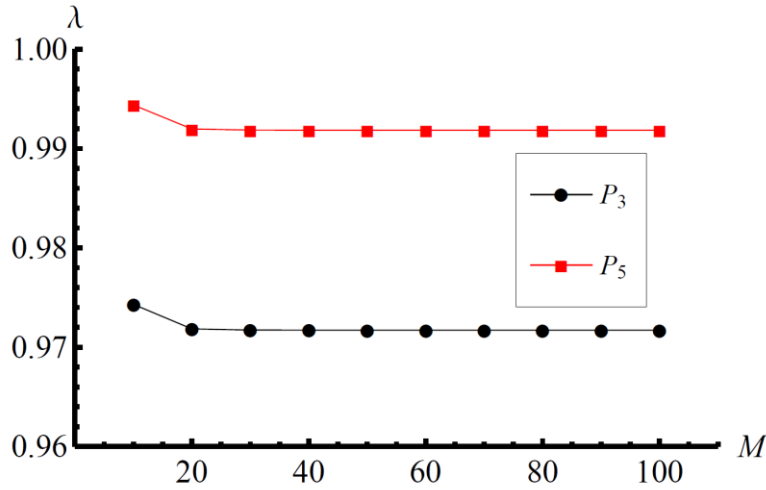


Figure 6.8b: The value of λ for the plutonium benchmark problem when $a_{crit} = 1.853722$ and conventional form is considered.

Table 6.1: S_N solutions of the Pu-239 benchmark problem with diamond difference approximation for the spatial variable.

M	S_2	S_4	S_8	S_{16}	S_{32}	S_{64}
10	0.803729	0.946616	0.991290	0.998012	0.999187	0.999459
20	0.804070	0.947008	0.991641	0.998352	0.999526	0.999798
30	0.804133	0.947081	0.991706	0.998415	0.999589	0.999860
40	0.804155	0.947106	0.991728	0.998437	0.999611	0.999882
50	0.804166	0.947118	0.991739	0.998448	0.999621	0.999892
60	0.804171	0.947124	0.991745	0.998453	0.999626	0.999898
70	0.804174	0.947128	0.991748	0.998457	0.999630	0.999901
80	0.804176	0.947131	0.991750	0.998459	0.999632	0.999903
90	0.804178	0.947132	0.991752	0.998460	0.999633	0.999905
100	0.804179	0.947134	0.991753	0.998461	0.999635	0.999906

Table 6.2: S_N solutions of the Pu-239 benchmark problem with discontinuous linear finite element approximation for the spatial variable.

M	S_2	S_4	S_8	S_{16}	S_{32}	S_{64}
10	0.8041789	0.9471308	0.9917496	0.9984574	0.9996297	0.9999007
20	0.8041832	0.9471378	0.9917567	0.9984648	0.9996379	0.9999092
30	0.8041836	0.9471385	0.9917574	0.9984656	0.9996387	0.9999102
40	0.8041837	0.9471387	0.9917576	0.9984658	0.9996390	0.9999104
50	0.8041838	0.9471388	0.9917577	0.9984658	0.9996390	0.9999105
60	0.8041838	0.9471388	0.9917577	0.9984659	0.9996391	0.9999106
70	0.8041838	0.9471388	0.9917577	0.9984659	0.9996391	0.9999106
80	0.8041838	0.9471388	0.9917577	0.9984659	0.9996391	0.9999106
90	0.8041838	0.9471388	0.9917577	0.9984659	0.9996391	0.9999106
100	0.8041838	0.9471388	0.9917577	0.9984659	0.9996391	0.9999106

Table 6.3: S_N solutions of the Pu-239 benchmark problem with discontinuous quadratic finite element approximation for the spatial variable.

M	S_2	S_4	S_8	S_{16}	S_{32}	S_{64}
10	0.8041838	0.9471388	0.9917577	0.9984658	0.9996390	0.9999105
20	0.8041838	0.9471388	0.9917577	0.9984658	0.9996391	0.9999106
30	0.8041838	0.9471388	0.9917577	0.9984658	0.9996391	0.9999106
40	0.8041838	0.9471388	0.9917577	0.9984658	0.9996391	0.9999106
50	0.8041838	0.9471388	0.9917577	0.9984658	0.9996391	0.9999106
60	0.8041838	0.9471388	0.9917577	0.9984658	0.9996391	0.9999106
70	0.8041838	0.9471388	0.9917577	0.9984658	0.9996391	0.9999106
80	0.8041838	0.9471388	0.9917577	0.9984658	0.9996391	0.9999106
90	0.8041838	0.9471388	0.9917577	0.9984658	0.9996391	0.9999106
100	0.8041838	0.9471388	0.9917577	0.9984658	0.9996391	0.9999106

The fourth and final problem is a Pu-239 benchmark with anisotropic scattering. Two levels of anisotropy in the scattering, P_1 and P_2 , are considered within this context. The benchmark solutions corresponding to these levels are $a_{crit} = 0.77032 \text{ cm}$ and $a_{crit} = 0.76378 \text{ cm}$, respectively. This problem is solved with conventional form of the transport equation with P_3 and P_5 approximations.

The variation of the multiplication factor with the number of interpolation nodes is illustrated in Figures 6.9a and 6.9b for P_1 and P_2 scattering cases, respectively. The shape parameter is chosen to be $c = \alpha\sqrt{0.05}$, and the number of interpolation and collocations nodes are the same in these calculations. The results show that for both problems the RBF collocation scheme is highly stable and with an increase in the degree of angular approximation a good accuracy is achievable. When a P_5 solution is performed, a multiplication value of approximately 0.995 is obtained which means that the percent error in λ is less than 1% even with this low level of angular approximation.

The numerical approximation of plutonium benchmark problems with isotropic and anisotropic scattering via RBFs are also done with variable shape parameter strategy, $c = mh^{-1/4}$. The results are similar to that of constant shape parameter route that a highly stable algorithm with a good accuracy is obtained with the meshless collocation method.

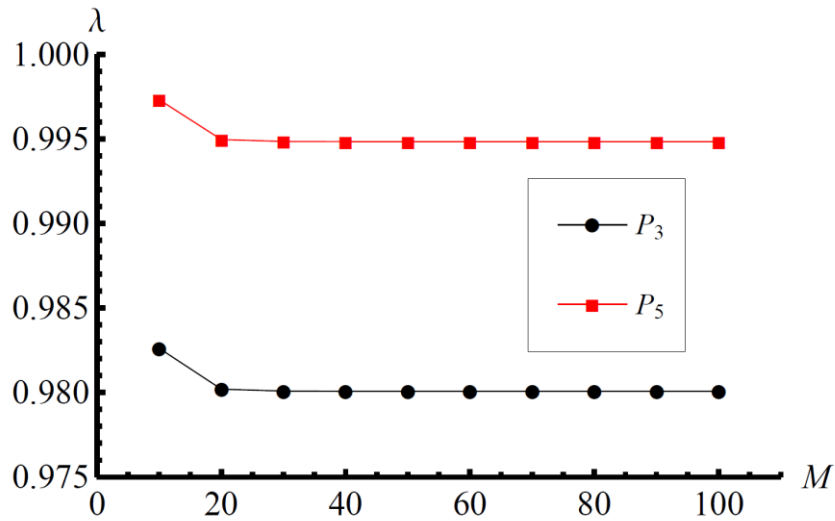


Figure 6.9a: The value of λ for the plutonium benchmark problem with anisotropic P_1 scattering.

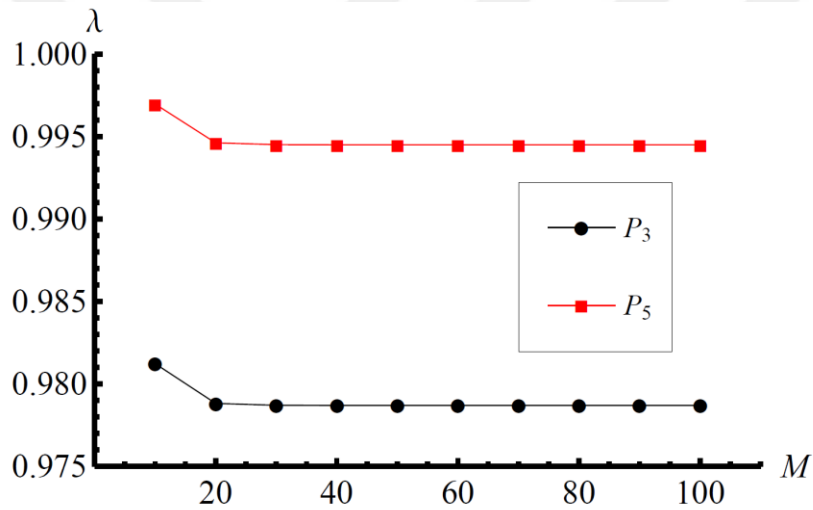


Figure 6.9b: The value of λ for the plutonium benchmark problem with anisotropic P_2 scattering.

7. CONCLUSIONS

In this study the time-independent neutron diffusion and transport equations are numerically solved by the meshless radial basis function collocation method. For the neutron diffusion case two-dimensional, multigroup homogeneous and heterogeneous problems are considered, while one-dimensional single region and energy cases with isotropic and anisotropic scattering are dealt within the transport approach.

For homogeneous problems two types of neutron sources are studied, and five examples, the external source problem, one-, two-, three- and four-group fission source problems are solved with the RBF collocation technique. Among these problems, the external source and four-energy group fission source cases are examined in detail (one-, two-, and three-energy group results are similar to those of the four-energy group problem). In this context a comparison is made between the meshless radial basis function collocation method and mesh-based finite and boundary element methods. For the collocation technique multiquadric, inverse multiquadric and Gaussian are used as the basis functions, while FEM and BEM are employed with linear shape functions. Since both examples have Cauchy boundary conditions external nodes are utilized to enhance the accuracy of the collocation method. The effect of shape parameter on the accuracy, convergence rate and stability of the collocation method is also investigated.

The external source problem was essentially the Helmholtz equation. Performance of the numerical methods is compared by calculating the root mean square and maximum pointwise errors for constant, trigonometric and linear sources. Numerical experiments showed that for all source types there is an optimum shape parameter value which yields the least RMS error, and MQ and IMQ have performed better than the GA in terms of both accuracy and stability. This optimization of the shape parameter is important; it provides a chance to obtain high levels of accuracy with just a few nodes. Another function of the shape parameter is its effect on the convergence rate of the collocation method. RBF collocation converges faster with

an increase in this parameter. It was found that the collocation method converges exponentially, which is better than the algebraic rates of FEM and BEM. Gaussian has the best convergence rate, but it has the disadvantage of being less stable and performing poorly for large fill distances. When CPU times are considered, the FEM is superior to other methods while RBF collocation is more efficient than the BEM. For the collocation technique, the distribution of pointwise errors has revealed that the error tends to have the maximum near the boundaries of the problem domain.

In the four-group fission source case accuracy of the methods is tested via calculating the relative percent errors in the multiplication factor and group fluxes. When the shape parameter dependence of the collocation method is investigated, an unusual behavior was observed. Depending on the choice of RBF, fill distance and criticality of the system, the error in multiplication factor may have a maximum value in the stable computation range of the shape parameter. The results have shown that, when the shape parameter is carefully selected, it is almost possible to produce analytical multiplication factors. A comparison among the three RBFs has showed that MQ is the best choice for fission source problems. Exponentially convergent MQ collocation has outperformed both FEM and BEM in the determination of the multiplication factor. On the contrary BEM gave the best solutions for the group fluxes. If the computation time is considered, the FEM is the most effective choice.

Although FEM and BEM have slow algebraic convergence rates, they have the significant advantage of being more stable than the RBF collocation method. This stability is a result of local approximation and weak-form characteristics of these methods. If the shape parameter is fixed, to preserve stability of the collocation method, algorithms such as domain decomposition and matrix preconditioning should be preferred. However, if the shape parameter is optimized very good accuracies can be obtained without encountering ill-conditioning problems.

Before tackling multiregion neutron diffusion problems four strategies are tested to improve the performance of the RBF collocation method via performing numerical experiments on the external source problem. First the effect of increasing the precision is investigated, and it is found that the stability of the algorithm can be improved significantly in price of computation time. Next the exponent of the generalized multiquadric is taken into account, and it is shown that it has a similar effect to that of the shape parameter on the characteristics of the RBF collocation.

The third approach is to use a variable shape parameter which decreases with the number of the interpolation nodes. Although accurate and stable results are obtained, this strategy generally did not improve the performance of the collocation method. The final technique is to use the singular value decomposition filtering method to achieve a better result, and it was found that the accuracy can be enhanced in both stable and unstable computation regions.

Next topic of this work is to model the multiregion neutron diffusion problems with the RBF collocation method. These problems are solved with the conventional and weighted forms of the RBF collocation method. The accuracy and stability of these two approaches are investigated by working on five problems. First a one-dimensional two-region external source configuration is studied. This problem is solved with the conventional form of the RBF collocation method. Since it is a 1-D problem the arbitrary precision computation of MATHEMATICA is employed in calculations, and highly accurate and stable results are observed. It is also found that by increasing the number of collocation nodes it is possible to obtain extraordinary accuracy in neutron flux values. The second problem is a two-dimensional, two-group fission source case for which an analytical solution exists, and it is solved with both RBF collocation and weighted RBF collocation methods. These two methods yield highly accurate results for this problem, and a comparison with the linear boundary element method has shown that with their fast convergence rates, a much better solution is possible with the collocation technique.

After treating the two analytically solvable problems, more complex multiregion configurations are considered. The third case is a two-region system containing a corner singularity. The numerical results have shown that when overcollocation is utilized, the numerical scheme underestimates the value of the multiplication factor unlike the situation where the number of interpolation and collocation nodes is the same. A comparison of the two methods has revealed that the conventional form of the RBF collocation method is better in terms of both accuracy and stability. As the fourth problem, the corner singularity problem is modified so that a high level of heterogeneity is present. The aim of this alteration is to assess the robustness of the two collocation schemes, and it was found that the no-weight collocation method is more reliable than the weighted collocation alternative. The last problem is a five-region IAEA benchmark. This problem is modelled with the conventional form of

the RBF collocation technique, and the numerical results show that the meshless collocation method is effective in the approximation of multiregion neutron diffusion problems.

The numerical solution of the neutron transport equation with the RBF collocation method is the final task of this study. In this regard, the spatial variable of the one-dimensional transport equation is approximated with RBFs. For the angular variable the P_N approach is chosen, and both conventional and even-parity forms of this equation are considered. The assessment of the RBF collocation method is done by solving four problems. The first example is an external source case, and it is solved within the even-parity framework. Two solution routes are possible for this problem, and it is found that using the coupled equations instead of directly solving the fourth order differential equation results in a much better accuracy and stability. The numerical results also show that, similar to the diffusion case, the accuracy and convergence rate of the method can be improved by adjusting the shape parameter. As the second problem a fission source case is solved again within the even-parity form, and it is shown that very good accuracies are possible for both the multiplication factor and neutron flux distribution. The third problem is a Pu-239 benchmark with isotropic scattering, and it is approached with both conventional and even-parity forms of the transport equation. It is found that the numerical solution resulting from these two alternatives is almost identical. Also a comparison with the discrete ordinates finite difference and finite element solutions revealed that the P_5 meshless collocation solution is equivalent to the S_8 finite difference and finite element approaches. The fourth and final problem is again a Pu-239 benchmark, this time with anisotropic scattering, and it is dealt with the conventional form of the transport equation. The RBF collocation method has produced a highly stable algorithm, and the accuracy of the method is good even with a low order approximation for the angular variable of the flux.

Although an extensive study is performed on the numerical modelling of neutron diffusion and transport processes with the meshless RBF collocation method, there are still a lot of things to do in this research area. As explained in the third chapter, and demonstrated in the following three chapters, the shape parameter of the radial basis functions has a significant effect on the properties of the collocation scheme. In this work, constant and node number dependent shape parameters are used, but one

can find optimization techniques in the literature that focus on the ideal choice of this important parameter. Another topic of interest in RBF collocation is the domain decomposition technique, which is employed to enhance the stability of the collocation method. The solution of the multiregion diffusion problems has shown the positive effect of splitting the problem domain into subdomains, especially when corner singularities are present in the configuration. Hence, the use of domain decomposition techniques in heterogeneous problems can be done as a further study. Another subject in multiregion problems is the improvement of the weighted RBF collocation method by adding local shape functions to better capture the local behavior near the interfaces of different regions. As for the neutron transport equation, the radial basis functions can also be used together with the discrete ordinates approach for the angular variable of the neutron flux, and a comparison can be made with the results of this thesis. Finally, other weak-form, strong-form or hybrid meshless methods can also be used for the numerical solution of problems in nuclear reactor physics.



REFERENCES

- [1] **Lewis, E.E. and Miller Jr., W.F.** (1993). *Computational Methods of Neutron Transport*. La Grange Park, IL: American Nuclear Society.
- [2] **Marchuk, G.I. and Lebedev, V.I.** (1986). *Numerical Methods In The Theory of Neutron Transport* (2nd ed). Glasgow: Bell and Bain Ltd.
- [3] **Cacuci, D.G. (Ed.)** (2010). *Handbook of Nuclear Engineering*. New York, NY: Springer.
- [4] **Duderstadt, J.J. and Hamilton L.J.** (1976). *Nuclear Reactor Analysis*. New York, NY: John Wiley and Sons Inc.
- [5] **Stacey, W.M.** (2001). *Nuclear Reactor Physics*. New York, NY: John Wiley and Sons Inc.
- [6] **Ackroyd, R.T.** (1997). *Finite Element Methods for Particle Transport: Applications to Reactor and Radiation Physics*. Somerset: Research Studies Press.
- [7] **Yildiz, C. and Alcan, E.** (1995). The effect of strong anisotropic scattering on the critical sphere problem in neutron transport theory using a synthetic kernel, *Annals of Nuclear Energy*, 22, 671-679.
- [8] **Yildiz, C.** (1998). Variation of the critical slab thickness with the degree of strongly anisotropic scattering in one-speed neutron transport theory, *Annals of Nuclear Energy*, 25, 529-540.
- [9] **Goffin, M.A., Baker, C.M.J., Buchan, A.G., Pain, C.C., Eaton M.D. and Smith, P.N.** (2013). Minimising the error in eigenvalue calculations involving the Boltzmann transport equation using goal-based adaptivity on unstructured meshes, *Journal of Computational Physics*, 242, 726-752.
- [10] **Barbarino, A., Dulla, S., Mund, E.H. and Ravetto, P.** (2014). Assessment of the performance of the spectral element method applied to neutron transport problems, *Annals of Nuclear Energy*, 65, 190-198.
- [11] **Buchan, A.G., Calloo, A.A., Goffin, M.G., Dargaville, S., Fang, F., Pain, C.C. and Navon, I.M.** (2015). A POD reduced order model for resolving angular direction in neutron/photon transport problems, *Journal of Computational Physics*, 296, 138-157.
- [12] **Williams, M.M.R., Welch, J. and Eaton, M.D.** (2015). Relationship of the SPN_{A_N} method to the even-parity transport equation, *Annals of Nuclear Energy*, 81, 342-353.
- [13] **Tan, J.Y., Zhao, J.M., Liu, L.H. and Wang, Y.Y.** (2009). Comparative study on accuracy and solution cost of the first/second order radiative transfer equations using the meshless method, *Numerical Heat Transfer, Part B: Fundamentals*, 55, 324-337.

- [14] **Kindelan, M., Bernal, F., Rodriguez, P.G. and Moscoso, M.** (2010). Application of the RBF meshless method to the solution of the radiative transport equation, *Journal of Computational Physics*, 229, 1897-1908.
- [15] **Zhao, J.M., Tan, J.Y. and Liu, L.H.** (2013). A second order radiative transfer equation and its solution by meshless method with application to strongly inhomogeneous media, *Journal of Computational Physics*, 232, 431-455.
- [16] **Rokrok, B., Minucmehr, H. and Zolfaghari, A.** (2012). Element-free Galerkin modeling of neutron diffusion equation in $X - Y$ geometry, *Annals of Nuclear Energy*, 43, 39-48.
- [17] **Liu, G.R. and Gu, Y.T.** (2005). *An Introduction to Meshfree Methods and Their Programming*. Dordrecht: Springer.
- [18] **Liu, G.R.** (2009). *Meshfree Methods: Moving Beyond The Finite Element Method* (2nd ed.). Boca Raton, FL: CRC Press.
- [19] **Fasshauer, G.E.** (2007). *Meshfree Approximation Methods with MATLAB*. Singapore: World Scientific Publishing.
- [20] **Atluri, S.N. and Shen, S.** (2002). *The Meshless Local Petrov-Galerkin (MLPG) Method*. Los Angeles, CA: Tech Science Press.
- [21] **Liu, G.R. and Liu, M.B.** (2003). *Smoothed Particle Hydrodynamics: A Meshfree Particle Method*. Singapore: World Scientific Publishing.
- [22] **Roque, C.M.C., Ferreira, A.J.M. and Reddy, J.N.** (2011). Analysis of Timoshenko nanobeams with a nonlocal formulation and meshless method, *International Journal of Engineering Science*, 49, 976-984.
- [23] **Singh, J. and Shukla, K.K.** (2012). Nonlinear flexural analysis of laminated composite plates using RBF based meshless method, *Composite Structures*, 94, 1714-1720.
- [24] **Al-Gahtani, H.J. and Mukhtar, F.M.** (2014). RBF-based meshless method for the free vibration of beams on elastic foundations, *Applied Mathematics and Computation*, 249, 198-208.
- [25] **Bourantas, G.C., Petsi, A.J., Skouras, E.D. and Burganos, V.N.** (2012). Meshless point collocation for the numerical solution of Navier–Stokes flow equations inside an evaporating sessile droplet, *Engineering Analysis with Boundary Elements*, 36, 240-247.
- [26] **Ooi, E.H. and Popov, V.** (2013). Meshless solution of two-dimensional incompressible flow problems using the radial basis integral equation method, *Applied Mathematical Modelling*, 37, 8985-8998.
- [27] **Zheng, X., Ma, Q.W. and Duan, W.Y.** (2014). Incompressible SPH method based on Rankine source solution for violent water wave simulation, *Journal of Computational Physics*, 276, 291-314.
- [28] **Rossi, E., Colagrossi, A. and Graziani, G.** (2015). Numerical simulation of 2D-vorticity dynamics using particle methods, *Computers and Mathematics with Applications*, 69, 1484-1503.

- [29] **Prax, C. and Sadat, H.** (2011). A low-order meshless model for multidimensional heat conduction problems, *Applied Mathematical Modelling*, 35, 4926-4933.
- [30] **Johansson, B.T., Lesnic, D. and Reeve, T.** (2014). A meshless method for an inverse two-phase one-dimensional nonlinear Stefan problem, *Mathematics and Computers in Simulation*, 101, 61-77.
- [31] **Gerace, S., Erhart, K., Kassab, A. and Divo, E.** (2014). A model-integrated localized collocation meshless method for large scale three-dimensional heat transfer problems, *Engineering Analysis with Boundary Elements*, 45, 2-19.
- [32] **Wang, H., Zeng, X. and Chen, L.** (2013). Calculation of sound fields in small enclosures using a meshless model, *Applied Acoustics*, 74, 459-466.
- [33] **Cai, X., Sun, X., Li, Z., Ji, G. and Lu, J.** (2012). The Element-Free Galerkin Method for Two-dimensional Schrödinger Equation, *Procedia Engineering*, 31, 1108-1114.
- [34] **Lucy, L.B.** (1977). A numerical approach to the testing of fission hypothesis, *The Astronomical Journal*, 82, 1013-1024.
- [35] **Nayroles, B., Touzot, G. and Villon, P.** (1992). Generalizing the finite element method: Diffuse approximation and diffuse elements, *Computational Mechanics*, 10, 307-318.
- [36] **Belytschko, T., Lu, Y.Y. and Gu, L.** (1994). Element-free Galerkin methods, *International Journal for Numerical Methods in Engineering*, 37, 229-256.
- [37] **Atluri, S.N. and Zhu, T.** (1998). A new meshless local Petrov-Galerkin (MLPG) approach in computational mechanics, *Computational Mechanics*, 22, 117-127.
- [38] **Kansa, E.J.** (1990). Multiquadrics – A scattered data approximation scheme with application to computational fluid dynamics-I, *Computers and Mathematics with Applications*, 19, 127-145.
- [39] **Oñate, E., Idelsohn, S., Zienkiewicz, O.Z. and Taylor, R.L.** (1996). A finite point method in computational mechanics. Applications to convective transport and fluid flow, *International Journal for Numerical Methods in Engineering*, 39, 3839-3866.
- [40] **Liu, G.R. and Gu, Y.T.** (2003). A meshfree method: Meshfree Weak-Strong (MWS) form method, *Computational Mechanics*, 33, 2-14.
- [41] **Fasshauer, G.E.** (1996). Solving partial differential equations by collocation with radial basis functions. In: A. Le Mechaute, C. Rabut and L.L. Schumaker (Eds.), *Surface Fitting and Multiresolution Methods* (pp. 1-8). Nashville, TN: Vanderbilt University Press.
- [42] **Ling, L. and Hon, Y.C.** (2005). Improved numerical solver for Kansa's method based on affine space decomposition, *Engineering Analysis with Boundary Elements*, 29, 1077-1085.

- [43] **Ling, L. and Kansa, E.J.** (2005). A least-squares preconditioner for radial basis functions collocation methods, *Advances in Computational Mathematics*, 23, 31-54.
- [44] **Roque, C.M.C and Ferreira, A.J.M.** (2009). Numerical experiments on optimal shape parameters for radial basis functions, *Numerical Methods for Partial Differential Equations*, 26, 675-689.
- [45] **Hon, Y.C. and Schaback R.** (2001). On unsymmetric collocation by radial basis functions, *Applied Mathematics and Computation*, 119, 177-186.
- [46] **Duan Y.** (2008). A note on the meshless method using radial basis functions, *Computers and Mathematics with Applications*, 55, 66-75.
- [47] **Cheng, A.H.D., Golberg, M.A., Kansa, E.J. and Zамmito, G.** (2003). Exponential convergence and h-c multiquadric collocation method for partial differential equations, *Numerical Methods for Partial Differential Equations*, 19, 571-594.
- [48] **Larsson, E. and Fornberg B.** (2003). A numerical study of some radial basis function based solution methods for elliptic PDEs, *Computers and Mathematics with Applications*, 46, 891-902.
- [49] **Li, J., Cheng, A.H.D. and Chen, C.S.** (2003). A comparison of efficiency and error convergence of multiquadric collocation method and finite element method, *Engineering Analysis with Boundary Elements*, 27, 251-257.
- [50] **Wendland, H.** (2005). *Scattered data approximation*. New York, NY: Cambridge University Press.
- [51] **Buhmann, M.D.** (2003). *Radial basis functions: Theory and implementations*. United Kingdom: Cambridge University Press.
- [52] **Madych, W.R.** (1992). Miscellaneous error bounds for multiquadric and related interpolators, *Computers and Mathematics with Applications*, 24, 121-138.
- [53] **Schaback, R.** (1995). Error estimates and condition numbers for radial basis function interpolation, *Advances in Computational Mathematics*, 3, 251-264.
- [54] **Kansa, E.J. and Hon, Y.C.** (2000). Circumventing the ill-conditioning problem with multiquadric radial basis functions-Applications to elliptic partial differential equations, *Computers and Mathematics with Applications*, 39, 123-137.
- [55] **Fornberg, B. and Zuev, J.** (2007). The Runge phenomenon and spatially variable shape parameters in RBF interpolation, *Computers and Mathematics with Applications*, 54, 379-398.
- [56] **Fornberg, B. and Wright, G.** (2004). Stable computation of multiquadric interpolants for all values of the shape parameter, *Computers and Mathematics with Applications*, 48, 853-867.
- [57] **Micchelli, C.A.** (1986). Interpolation of scattered data-distance matrices and conditionally positive definite functions, *Constructive Approximation*, 2, 11-22.

- [58] **Cheng, A.H.D.** (2012). Multiquadric and its shape parameter-A numerical investigation of error estimate, condition number, and round-off error by arbitrary precision computation, *Engineering Analysis with Boundary Elements*, 36, 220-239.
- [59] **Zhang, X., Song, K.Z., Lu, M.W. and Liu, X.** (2000). Meshless methods based on collocation with radial basis functions, *Computational Mechanics*, 26, 333-343.
- [60] **Fedoseyev, A.I., Friedman, M.J. and Kansa, E.J.** (2002). Improved multiquadric method for elliptic partial differential equations via PDE collocation on the boundary, *Computers and Mathematics with Applications*, 43, 439-455.
- [61] **Chen, J.S., Wang, L., Hu, H.Y. and Chi, S.W.** (2009). Subdomain radial basis collocation method for heterogeneous media, *International Journal for Numerical Methods in Engineering*, 80, 163-190.
- [62] **Hu, H.Y., Chen, J.S. and Hu, W.** (2007). Weighted radial basis collocation method for boundary value problems, *International Journal for Numerical Methods in Engineering*, 69, 2736-2757.
- [63] **Jamil, M. and Ng, E.Y.K.** (2013). Evaluation of meshless radial basis collocation method (RBCM) for heterogeneous conduction and simulation of temperature inside the biological tissues, *International Journal of Thermal Sciences*, 68, 42-52.
- [64] **Jiang, B.N.** (1998). On the least-squares method, *Computer Methods in Applied Mechanics and Engineering*, 152, 239-257.
- [65] **Li, Z.C.** (1998). *Combined Methods for Elliptic Equations with Singularities, Interfaces and Infinities*. Dordrecht: Kluwer Academic Publishers.
- [66] **Zienkiewicz, O.C., Taylor, R.L. and Zhu, J.Z.** (2005). *The Finite Element Method: Its Basis and Fundamentals* (6th ed.). United Kingdom: Butterworth Heinemann.
- [67] **Hu, H.Y., Li, Z.C. and Cheng, A.H.D.** (2005). Radial basis collocation methods for elliptic boundary value problems, *Computers and Mathematics with Applications*, 50, 289-320.
- [68] **Hu, H.Y. and Li, Z.C.** (2006). Collocation methods for Poisson's equation, *Computer Methods in Applied Mechanics and Engineering*, 195, 4139-4160.
- [69] **Chen, J.S., Hu, W. and Hu, H.Y.** (2009). Localized radial basis functions with partition of unity properties. In A.J.M. Ferreira, E.J. Kansa, G.E. Fasshauer and V.M.A. Leitao (Eds.), *Progress on Meshless Methods* (Vol. 11 pp.37-56). Berlin: Springer.
- [70] **Quarteroni, A. and Valli, A.** (1994). *Numerical Approximation of Partial Differential Equations*. Berlin: Springer.
- [71] **Ozgener, B. and Kabadayi, Y.** (1996). The acceleration of the finite element solutions of the diffusion theory criticality eigenvalue problems by Chebyshev polynomial extrapolation (in Turkish), *Proceedings of the 7th national meeting on nuclear science and technology* (pp.190-197), Istanbul: Çekmece Nuclear Research and Training Center.

- [72] **Ozgener, B.** (1998). A boundary integral equation for boundary element applications in multigroup neutron diffusion theory, *Annals of Nuclear Energy*, 25, 347-357.
- [73] **Ozgener, B. and Ozgener, H.A.** (1994). The application of the multiple reciprocity method to the boundary element formulation of the neutron diffusion equation, *Annals of Nuclear Energy*, 21, 711-723.
- [74] **Carlson, R.E. and Foley, T.A.** (1991). The parameter R^2 in multiquadric interpolation, *Computers and Mathematics with Applications*, 21, 29-42.
- [75] **Huang, C.S., Lee, C.F. and Cheng, A.H.D.** (2007). Error estimate, optimal shape factor, and high precision computation of multiquadric collocation method, *Engineering Analysis with Boundary Elements*, 31, 614-623.
- [76] **Boyd, J.P.** (2010). Six strategies for defeating the Runge phenomenon in Gaussian radial basis functions on a finite interval, *Computers and Mathematics with Applications*, 60, 3108-3122.
- [77] **Golub, G.H. and Van Loan, C.F.** (2013). *Matrix Computations* (4th ed.). Baltimore, MD: The John Hopkins University Press.
- [78] **Akritas, A.G. and Malaschonok, G.I.** (2004). Applications of singular value decomposition (SVD), *Mathematics and Computers in Simulation*, 67, 15-31.
- [79] **Ozgener, H.A. and Ozgener, B.** (2001). A multi-region boundary element method for multigroup neutron diffusion calculations, *Annals of Nuclear Energy*, 28, 585-616.
- [80] **Marin, L.** (2010). Treatment of singularities in the method of fundamental solutions for two-dimensional Helmholtz type equations, *Applied Mathematical Modelling*, 34, 1615-1633.
- [81] **Li, Z.C., Chu, P.C., Young, L.J. and Lee, M.G.** (2010). Models of corner and crack singularity of linear elastostatics and their numerical solutions, *Engineering Analysis with Boundary Elements*, 34, 533-548.
- [82] **Lee, M.G. and Li, Z.C.** (2012). Corner and crack singularity of different boundary conditions for linear elastostatics and their numerical solutions, *Engineering Analysis with Boundary Elements*, 36, 1125-1137.
- [83] **Smith, K.S.** (1979). *An analytical nodal method for solving the two-group, multidimensional, static and transient neutron diffusion equations* (Master's Thesis). Retrieved from: <https://dspace.mit.edu/>
- [84] **Abramowitz, M. and Stegun, I.** (Eds.) (1965). *Handbook of Mathematical Functions*. New York, NY: Dover.
- [85] **Eddington, A.** (1926). *The internal constitution of stars*. New York, NY: Dover.
- [86] **Gelbard, E.M.** (1968). Spherical harmonics methods: P_L and double P_L approximations, In: H. Greenspan, C.K. Kelber and D. Okrent (Eds.) *Computing Methods in Reactor Physics* (pp.271-358). New York, NY: Gordon and Breach.

- [87] **Chandrasekhar, S.** (1960). *Radiative Transfer*. New York, NY: Dover.
- [88] **Carlson, B.G. and Bell, G.I.** (1958). Solution of the transport equation by the S_N method, *Proc. U.N. International Conference on Peaceful Uses of Atomic Energy*, Geneva.
- [89] **Bell, G.I. and Glasstone, S.** (1970). *Nuclear Reactor Theory*. Florida, FL: Robert E. Krieger Publishing.
- [90] **Davison, B.** (1957). *Neutron Transport Theory*. London: Oxford University Press.
- [91] **Gast, R.** (1958). *On the equivalence of the spherical harmonics method and the discrete ordinates method using Gauss quadrature for the Boltzmann equation*, (Report No:118), Pittsburg, PA: Westinghouse Electric Corp. Bettis Plant.
- [92] **Lillie, R.A. and Robinson, J.C.** (1976). *A linear triangle finite element formulation for multigroup neutron transport analysis with anisotropic scattering*, (Report No: 5281), Tennessee, TN: Oak Ridge National Laboratory.
- [93] **Mai-Duy, N.** (2005). Solving high order ordinary differential equations with radial basis function networks, *International Journal for Numerical Methods in Engineering*, 62, 824-852.
- [94] **Sood, A., Forster, R.A. and Parsons, D.K.** (1999). *Analytical benchmark test set for criticality code verification*, (Report No: 13511), New Mexico, NM: Los Alamos National Laboratory.



CURRICULUM VITAE



Name Surname: Tayfun Tanbay

Place and Date of Birth: Istanbul – 13/07/1984

E-Mail: ttanbay@itu.edu.tr

EDUCATION:

B.Sc.: Istanbul University – Mechanical and chemical engineering

M.Sc.: Istanbul Technical University – Energy Science and Technology

PROFESSIONAL EXPERIENCE:

2009 – Present: Istanbul Technical University – Energy Institute

2008 – 2009: Turkish Atomic Energy Authority – Çekmece Nuclear Research and Training Center, Nuclear Fuel Department

PUBLICATIONS ON THE THESIS:

- **Tanbay, T.** and Ozgener, B. (2014). A comparison of the meshless RBF collocation method with finite element and boundary element methods in neutron diffusion calculations, *Engineering Analysis with Boundary Elements*, 46, 30-40.
- **Tanbay, T.** and Ozgener, B. (2013). Numerical Solution of the Multigroup Neutron Diffusion Equation by the Meshless RBF Collocation Method, *Mathematical and Computational Applications*, 18, 399-407. (Presented in 4th International Conference on Mathematical and Computational Applications, 11-13 June 2013, Manisa, Turkey).

OTHER PUBLICATIONS:

- **Tanbay, T.** and Ozgener, B. (2013). A Numerical Method for Resonance Integral Calculations, *Kerntechnik*, 78, 220-228.
- Hacıyakupoglu, S., Esen, A.N., Erenturk, S., Okka, M., Genceli, M., Mercimek, M., Genceli, E., Yusan, S., Filiz, F.G., Olgen, K., Camtakan, Z., Kiziltas, S. and **Tanbay, T.** (2015). Determining distribution of heavy metal pollution in terms of ecological risk levels in soil of industrially intensive areas around Istanbul, *Toxicological and Environmental Chemistry*, 97, 62-75.

